



**UNIVERSIDAD DE INVESTIGACIÓN DE TECNOLOGÍA
EXPERIMENTAL YACHAY**

Escuela de Ciencias de la Tierra, Energía y Ambiente

**TÍTULO: SOIL CO₂ EMISSIONS AT CHILES VOLCANO, ECUADOR:
SURVEY FROM AGUAS HEDIONDAS AND LAGUNAS VERDES**

Trabajo de titulación presentado como requisito para la
obtención de título de Geóloga

Autor:

Villarroel Barreno Zulay Micaela

Tutor:

PhD. Weller Dereck

Co-tutor:

PhD. Mandon Celine

PhD. Viveiros Fátima

Urcuquí, Noviembre 2022

SECRETARÍA GENERAL
ESCUELA DE CIENCIAS DE LA TIERRA, ENERGÍA Y AMBIENTE
CARRERA DE GEOLOGÍA
ACTA DE DEFENSA No. UITEY-GEO-2022-00011-AD

En la ciudad de San Miguel de Urucuquí, Provincia de Imbabura, a los 13 días del mes de septiembre de 2022, a las 11:00 horas, en el Aula S_CAN de la Universidad de Investigación de Tecnología Experimental Yachay y ante el Tribunal Calificador, integrado por los docentes:

Presidente Tribunal de Defensa	Mgs. RODRIGUEZ CALVOPÍÑA, MARIELA FERNANDA
Miembro No Tutor	Dr. TORO ALAVA, JORGE EDUARDO , Ph.D.
Tutor	Dr. WELLER DEREK JAMES , Ph.D.

Se presenta el(la) señor(ita) estudiante **VILLARROEL BARRENO, ZULAY MICAELA**, con cédula de identidad No. **1805347950**, de la **ESCUELA DE CIENCIAS DE LA TIERRA, ENERGÍA Y AMBIENTE**, de la Carrera de **GEOLOGÍA**, aprobada por el Consejo de Educación Superior (CES), mediante Resolución **RPC-SE-10-No.031-2016**, con el objeto de rendir la sustentación de su trabajo de titulación denominado: **Soil CO2 emissions at Chiles volcano, Ecuador: Survey from Aguas Hediondas and Lagunas Verdes** , previa a la obtención del título de **GEÓLOGO/A**.

El citado trabajo de titulación, fue debidamente aprobado por el(los) docente(s):

Tutor	Dr. WELLER DEREK JAMES , Ph.D.
--------------	--------------------------------

Y recibió las observaciones de los otros miembros del Tribunal Calificador, las mismas que han sido incorporadas por el(la) estudiante.

Previamente cumplidos los requisitos legales y reglamentarios, el trabajo de titulación fue sustentado por el(la) estudiante y examinado por los miembros del Tribunal Calificador. Escuchada la sustentación del trabajo de titulación, que integró la exposición de el(la) estudiante sobre el contenido de la misma y las preguntas formuladas por los miembros del Tribunal, se califica la sustentación del trabajo de titulación con las siguientes calificaciones:

Tipo	Docente	Calificación
Tutor	Dr. WELLER DEREK JAMES , Ph.D.	9,2
Presidente Tribunal De Defensa	Mgs. RODRIGUEZ CALVOPÍÑA, MARIELA FERNANDA	9,5
Miembro Tribunal De Defensa	Dr. TORO ALAVA, JORGE EDUARDO , Ph.D.	9,3

Lo que da un promedio de: **9.3 (Nueve punto Tres)**, sobre 10 (diez), equivalente a: **APROBADO**

Para constancia de lo actuado, firman los miembros del Tribunal Calificador, el/la estudiante y el/la secretario ad-hoc.

VILLARROEL BARRENO, ZULAY MICAELA
Estudiante

Mgs. RODRIGUEZ CALVOPÍÑA, MARIELA FERNANDA
Presidente Tribunal de Defensa



Firmado electrónicamente por:
MARIELA FERNANDA
RODRIGUEZ
CALVOPÍÑA

Dr. WELLER DEREK JAMES , Ph.D.
Tutor

Dr. TORO ALAVA, JORGE EDUARDO , Ph.D.
Miembro No Tutor

TERÁN ROSALES, ANDREA YOLANDA
Secretario Ad-hoc



Firmado electrónicamente por:
ANDREA YOLANDA
TERAN ROSALES

AUTORÍA

Yo, **Zulay Micaela Villarroel Barreno**, con cédula de identidad 1805347950, declaro que las ideas, juicios, valoraciones, interpretaciones, consultas bibliográficas, definiciones y conceptualizaciones expuestas en el presente trabajo; así como, los procedimientos y herramientas utilizadas en la investigación, son de absoluta responsabilidad de el/la autora (a) del trabajo de integración curricular. Así mismo, me acojo a los reglamentos internos de la Universidad de Investigación de Tecnología Experimental Yachay.

Urququí, Noviembre 2022

Zulay Micaela Villarroel Barreno

CI: 1805347950

AUTORIZACIÓN DE PUBLICACIÓN

Yo, **Zulay Micaela Villarroel Barreno**, con cédula de identidad 1805347950, cedo a la Universidad de Investigación de Tecnología Experimental Yachay, los derechos de publicación de la presente obra, sin que deba haber un reconocimiento económico por este concepto. Declaro además que el texto del presente trabajo de titulación no podrá ser cedido a ninguna empresa editorial para su publicación u otros fines, sin contar previamente con la autorización escrita de la Universidad.

Asimismo, autorizo a la Universidad que realice la digitalización y publicación de este trabajo de integración curricular en el repositorio virtual, de conformidad a lo dispuesto en el Art. 144 de la Ley Orgánica de Educación Superior.

Urququí, Noviembre del 2022.

Zulay Micaela Villarroel Barreno

CI: 1805347950

DEDICATION

To my mom, she told me once, 'don't worry, you will make it.' And guess what, mom, I did it.
Thanks for always believing in me, your unconditional support, and the infinite love you give me.

With all my love, this is for you.

Zulay Micaela Villarroel Barreno

ACKNOWLEDGMENTS

First of all, I would like to start by giving a huge thank you to Ph.D. Celine Mandon, Ph.D. Elisa Piispa, M.Sc. Domenica Guillén, and M.Sc. Katie Nelson. Without any of them, this thesis project would not have been possible. I am eternally grateful to have had the incredible experience we shared during this project fieldwork. I am really thankful to them for their unconditional help and mentorship throughout this learning journey. This thesis is thanks to you. Also, thank Ph.D. Fatima Viveiros, who was a fundamental pillar of this work. Fatima had the patience to teach us and explain all the necessary concepts for this investigation. Indeed, each of these incredible women represents an inspiration for what I would like to become one day.

Thanks again to Ph.D. Celine Mandon for having me as her thesis student. Her passion for volcanology is an inspiration to me. Thank you for sharing with me as a teacher and as a friend. For all the advice, support, and encouragement she gave me throughout this arduous process of writing the thesis. I am truly grateful to live for having had the opportunity to coincide with her in this life.

A special thanks to Prefectura del Carchi, who gave us permission to perform the survey on the area of Aguas Hediondas. Thanks to Edwin Fraga, who helped us by giving us access to the Tourist complex every day of the survey.

Thank you to all the teachers from whom I had the privilege of learning. I am eternally grateful to have had unconditional teachers from whom, more than learning academic things, I realized what vocation is and how to make things with love. Thanks to Yaniel, Germán, Rafael, Anna, Jorge, Luis, Luis Felipe, Alejandra, Celine, and Elissa, for sharing their infinite passion for science and geology with me and, above all, for always giving more than what we expected as students. All my training as a Geologist, person, and friend is thanks to you. I promise to follow in your footsteps and spread the passion for science.

I want to thank my family, my mother Elena, my father Tito, my sister Gabriela, my brothers Justin, Tito, and my niece Mabel. They play a fundamental role in my life, they have been my support since I was born, and this would not be possible without their efforts.

A sincere thanks to Nicolas, one of the most beautiful people I have ever met. Literally, this work would not have seen the light without him since he lent me the computer on which this thesis was done. Thank you for the constant support and motivation he has given me since I met him.

Thanks to 'my girls' Jhuliana, Paola, and Sahori, for being my partners on this trip to called university. Thanks to them for teaching me about true unbelievable friendship and for all the beautiful experiences I have thanks to them. Thanks to 'los geoamigos,' the best career companions you may have had. I have kept with great affection all those incredible experiences, shared beers, and endless talks that we had on field trips. Thank you for being a representation of what camaraderie is.

Thanks to my alma mater, Yachay Tech University, which gave me the best experience of my life, coincided with the best people I have ever met, and made me who I am. Last but not least, thanks to me. For forcing me to get out of bed despite the intense anxiety that gripped my body. For the strength, I have gained and for allowing me to cry but not give up. You are powerful.

Zulay Micaela Villarroel Barreno

RESUMEN

La desgasificación difusa de CO₂ en volcanes inactivos es un proceso bien conocido, pero se desconocen las emisiones de CO₂ en muchos volcanes. Este estudio presenta los resultados de la desgasificación difusa de CO₂ del volcán Chiles. El Complejo Volcánico Chiles-Cerro Negro está ubicado en la frontera entre Colombia y Ecuador. A pesar de su potencial geotérmico, el volcán de Chile ha sido muy poco estudiado debido a su ubicación geográfica y discrepancias políticas. Las termas son un atractivo turístico a ambos lados de la frontera, con notorias emisiones de gases. Sin embargo, este último nunca ha sido cuantificado. Presentamos los resultados de un estudio de emisiones de CO₂ en suelo en dos lugares estratégicos del entorno del volcán Chiles: Aguas Hediondas y Lagunas Verdes. En Aguas Hediondas, medimos en 303 puntos de flujo de CO₂ en una grilla de 5 metros cubriendo un área de 6 000 m², junto con 14 muestras para análisis de $\delta^{13}\text{C}_{\text{CO}_2}$. Tomamos otras 76 mediciones de flujo de CO₂ y cuatro muestras para $\delta^{13}\text{C}_{\text{CO}_2}$ en el área más pequeña de Lagunas Verdes, cubriendo un área de 5 000 m².

Presentamos mapas de desgasificación difusa para las dos áreas de estudio, donde ubicamos áreas de flujo de anomalías de CO₂ e interpretamos su distribución espacial con estructuras tectónicas del complejo volcánico. Además, para comprender mejor el comportamiento hidrotermal del área, realizamos mapas de distribución de la temperatura del suelo para identificar las anomalías de calor relacionadas con las estructuras de desgasificación difusa. Utilizando un enfoque estadístico y datos isotópicos, estimamos los flujos de CO₂ derivados de las profundidades. Gracias al análisis de $\delta^{13}\text{C}_{\text{CO}_2}$, discriminamos entre dos fuentes de CO₂: CO₂ biogénico y CO₂ hidrotermal profundo. En resumen, en Aguas Hediondas obtuvimos una desgasificación difusa de CO₂ total de 0,11 t d⁻¹ de las cuales 0,06 t d⁻¹ presentan aporte hidrotermal profundo de CO₂. En el caso de Lagunas Verdes, la emisión total es más significativa, siendo de 1,66 t d⁻¹, de las cuales más del 80% (1,49 t d⁻¹) presenta aporte de CO₂ de fuente volcánica.

La estimación de las emisiones totales contribuirá a nuestra comprensión de la contribución natural de CO₂ de los volcanes a la atmósfera durante la desgasificación difusa. Por lo tanto, este estudio es significativo, llenando los vacíos de conocimiento sobre el volcán Chiles a pesar de su alto potencial geotérmico. Además, aporta conocimientos esenciales sobre el peligro que suponen las elevadas emisiones de CO₂ en una zona turística.

Palabras clave: desgasificación de CO₂ del suelo, flujo de CO₂, dióxido de carbono, isótopos de carbono, sistema hidrotermal, temperatura del suelo, volcán Chiles.

ABSTRACT

Diffuse CO₂ degassing at dormant volcanoes is a well-known process, yet CO₂ emissions are unknown at many volcanoes. This study presents results of CO₂ diffuse degassing from Chiles volcano. Chiles-Cerro Negro Volcanic Complex is located on the border between Colombia and Ecuador. Despite its geothermal potential, Chiles volcano has been very seldom studied due to its geographical location and political discrepancies. Hot springs are a tourist attraction on both sides of the border, with well-known gas emissions. Yet, the latter has never been quantified. We present results from a CO₂ soil emission survey in two strategic places in the surroundings of Chiles volcano: Aguas Hediondas and Lagunas Verdes. In Aguas Hediondas, we measured in 303 CO₂ flux points in a 5-meter grid covering an area of 6 000 m², along with 14 samples for δ¹³C_{CO2} analysis. We took another 76 CO₂ flux measurements and four samples for δ¹³C_{CO2} in the smaller area of Lagunas Verdes, covering an area of 5 000m².

We present diffuse degassing maps for the two survey areas, where we located CO₂-anomalies flux areas and interpreted their spatial distribution with tectonic structures of the volcanic complex. Moreover, to understand better the hydrothermal behavior of the area, we performed maps of the soil temperature distribution to identify the heat anomalies related to diffuse degassing structures. Using a statistical approach and isotopic data, we estimated the deep-derived CO₂ fluxes. Thanks to the δ¹³C_{CO2} analysis, we discriminate between two CO₂ sources: biogenic CO₂ and deep hydrothermal CO₂. In summary, in Aguas Hediondas, we obtained a total CO₂ diffuse degassing of 0.11 t d⁻¹ of which 0.06 t d⁻¹ presents a deep CO₂ hydrothermal contribution. In the case of Lagunas Verdes, the total emission is more significant, being 1.66 t d⁻¹, of which more than the 80% (1.49 t d⁻¹) presents a volcanic source CO₂ contribution.

Estimation of total emissions will contribute to our understanding of the natural contribution of CO₂ from volcanoes to the atmosphere during diffuse degassing. Therefore, this study is significant, filling the gaps in knowledge on the Chiles volcano despite its high geothermal potential. Moreover, it brings essential knowledge regarding the hazard posed by elevated CO₂ emissions in a touristic area.

Keywords: CO₂ soil degassing, CO₂ flux, carbon dioxide, carbon isotopes, hydrothermal system, soil temperature, Chiles volcano.

TABLE OF CONTENTS

AUTORÍA	I
AUTORIZACIÓN DE PUBLICACIÓN	II
DEDICATION	III
ACKNOWLEDGMENTS	IV
ABSTRACT	V
CHAPTER 1: INTRODUCTION	1
1.1 The contribution of volcanic systems to the Carbon cycle.....	1
1.2 Volcanic Hydrothermal Systems	1
1.3 Diffuse Degassing.....	2
1.4 Biogenic carbon dioxide.....	3
1.5 Distinction between CO ₂ sources	4
1.6 Chiles Volcano.....	5
1.7 Statement of the problem	5
1.8 Objectives	6
CHAPTER 2: CHILES VOLCANO	7
2.1 Geological Background	7
2.1.1 The Andes Cordillera.....	7
2.1.2 Chiles Volcano.....	8
2.2 Survey Areas	12
2.2.1 Aguas Hediondas	12
2.2.2 Lagunas Verdes.....	13
2.3 Vegetation of Chiles Volcano.....	14
2.3.1 Types of plants in the area	14
CHAPTER 3: METHODOLOGY	16
3.1 CO ₂ flux measurements	16
3.2 Other measurements.....	19
3.3 Isotopic Samples	20
3.3.1 Sampling strategy and collection.....	20
3.3.2 Isotopic analysis.....	22
3.3.3 Mapping strategy.....	23

3.4	Data processing.....	24
3.4.1	Preparation and correction of the data.....	24
3.4.2	Sequential Gaussian Simulation (sGs)	25
3.4.3	Variograms.....	27
CHAPTER 4:	RESULTS	29
4.1	CO ₂ fluxes.....	29
4.1.1	Aguas Hediondas	29
4.1.2	Lagunas Verdes.....	32
4.2	Isotopic Data	34
4.3	Soil Temperature	36
4.3.1	Aguas Hediondas	36
4.3.2	Lagunas Verdes.....	38
CHAPTER 5:	DISCUSSION.....	41
5.1	Control points	41
5.1.1	The role of barometric pressure	42
5.1.2	The role of soil moisture	43
5.1.3	The roll of air temperature	43
5.1.4	The roll of soil temperature.....	44
5.2	Soil Temperature Distribution	45
5.3	Volcanic CO ₂ contribution to the Diffuse Degassing.....	47
5.3.1	Mixing model with isotopes	47
5.3.2	Probability maps for soil CO ₂ flux	48
5.3.3	CO ₂ total emission	49
5.3.4	CO ₂ diffuse degassing around the world	50
5.3.5	Diffuse Degassing Structures.....	52
CHAPTER 6:	CONCLUSIONS AND FUTURE WORK.....	54
REFERENCES	56

CHAPTER 1: INTRODUCTION

1.1 The contribution of volcanic systems to the Carbon cycle

Nowadays, climate change is one of the biggest challenges for human beings. CO₂ emissions are responsible for 60% of greenhouse gas effects, therefore, understanding the Carbon cycle is one of the main priorities for researchers (Rastogi et al., 2002). The CO₂ input into the atmosphere from non-anthropogenic sources has been detected as a factor that controls the long-term climate of Earth (Marty & Tolstikhin, 1998; Rogie et al., 2001). Non-anthropogenic sources mean sources related to geological processes like geochemical cycles of rocks and igneous/metamorphic activity. Calculating the contribution from igneous and metamorphic processes is one of the biggest challenges for researchers who have been working on models of the global carbon cycle (Bernier & Lasaga, 1989; Franck et al., 1999; Johansson et al., 2018).

Volcanic activity contributes to CO₂ emissions into the atmosphere, during eruptions and quiescent periods. During eruptions, we can have direct and diffuse degassing from active volcanoes. Direct degassing refers to CO₂ discharges directly from the crater, known as a “volcanic plume” (Kerrick, 2001). However, most of the measurements related to CO₂ degassing have been taken during quiescent periods. Quiescent periods refer to degassing during a non-eruptive process of a volcano (Kerrick, 2001).

1.2 Volcanic Hydrothermal Systems

Hydrothermal systems are defined as the sum of a permeable porous layer, an aquifer, and a heat source. In this system each component is fundamental, the permeable soil allows the infiltration of water to the aquifer; the aquifer as the groundwater reserve and the heat source would be the main energy source for the system (U.S. DOE, 2012). The heat source heats up the aquifer, changing the physicochemical water properties' before it comes to the surface such as altering the water composition with the addition of hydrothermal gases. Volcanic hydrothermal system refers to systems in which the heat source is a magmatic body, related with an active or dormant volcano (Delmelle & Stix, 2000). The interaction of groundwater reservoirs and the heat released by an active magma chamber results in hot hydrothermal fluids contaminated with magmatic volatiles (Branney & Acocella, 2015).

Figure 1 illustrates a general view of the dynamic of a volcanic hydrothermal system. The recharge zone is on the volcano's flanks, with meteoric water being the main source. The magma chamber represents

the heat source . Fumaroles, CO₂ diffuse degassing, and hydrothermal springs are the surface expressions of volcanic hydrothermal systems. The hydrothermal springs represent the discharge area where faults and cracks play a fundamental role in this superficial expression of volcanic hydrothermal systems, allowing fluids to seep to the surface.

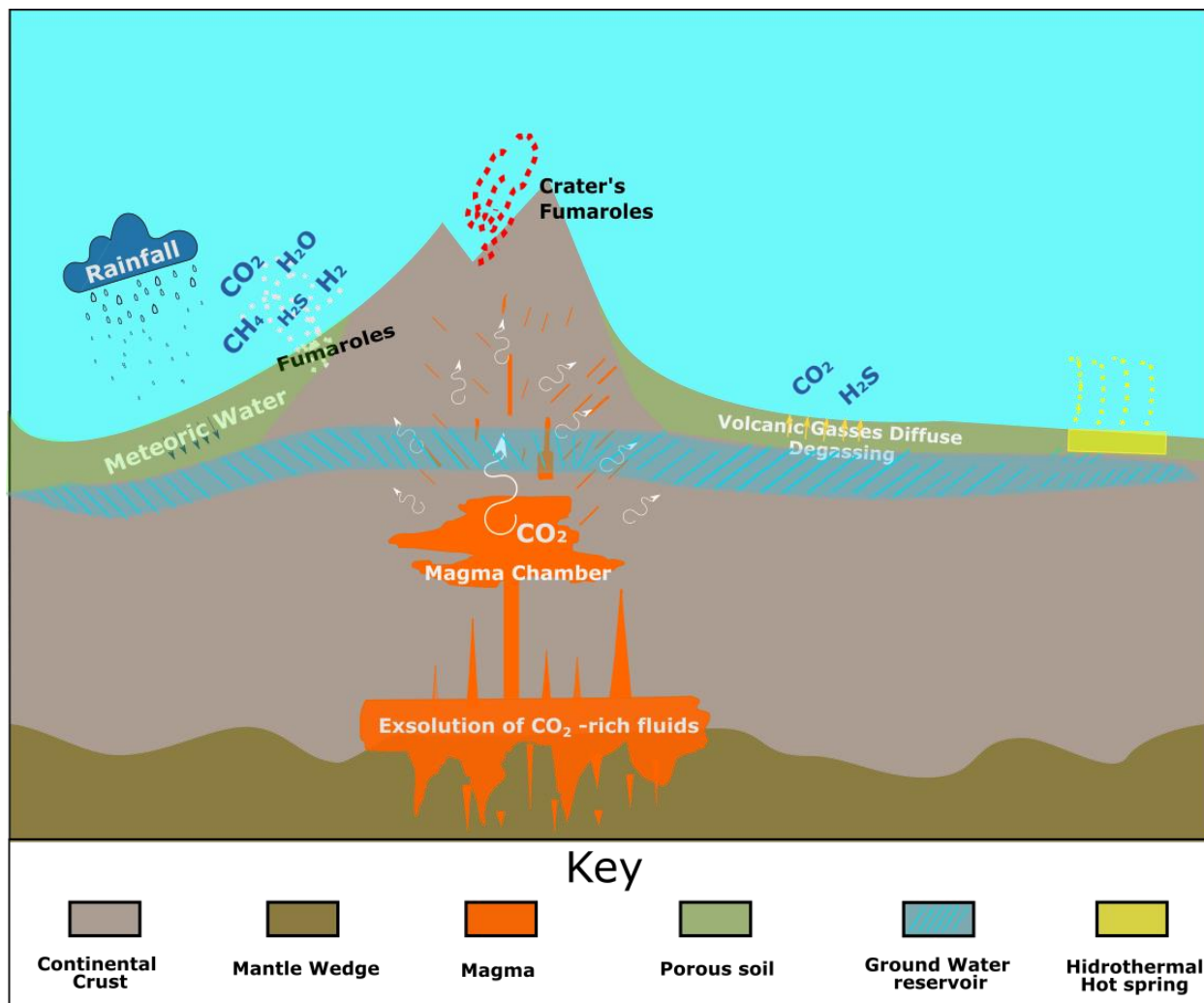


Figure 1. General Sketch of a Volcanic Hydrothermal System.

1.3 Diffuse Degassing

Hydrothermal gases result from the interaction between magmatic gas and a liquid phase (Stix, 2015). Magmatic gases are released by the magma stored at depth in the crust. The main gases released by magma are H₂O and CO₂, with lower amounts of other gases such as SO₂ and halogens. In the case of hydrothermal gases, the other main gases that we can find despite H₂O and CO₂ are H₂S and CH₄. Although

SO₂ is a gas that can be found at high concentrations in magmatic gases, can't be found in hydrothermal gasses. When H₂O comes to the surface, it condenses, releasing thermal energy. On the other hand, CO₂ is less condensable, so it is released through the soil as diffuse degassing along diffuse degassing structures (Fischer & Chiodini, 2015).

As Fischer & Chiodini (2015) describe, diffuse degassing refers to the volatile exsolution to the surface from the magma degassing. Diffuse degassing starts with the magma vesiculation leading to the separation of the gas phase from the melt and, as a result, the gas emission enters into the atmosphere or hydrosphere. The composition of the exsolved gas depends on several physicochemical parameters, such as the magma composition, the volatile solubility, pressure and temperature. Diffuse degassing is a permanent and non-observable process that needs specific instruments to detect the gas emission in volcanically active regions. It is important also to mention that CO₂ is the main gas released in these kinds of areas (Allard, 1992). The most common way in which the gases get to the surface is through diffuse degassing structures (DDS) producing what is better known as soil diffuse degassing.

The most common diffuse degassing structures are small vents, tectonic structures (faults), and steaming ground (Stix, 2015). Several authors have concluded that the degassing patterns could correlate with hidden tectonic structures such as faults and fractures (Chiodini et al., 2001; Werner & Cardellini, 2006; Viveiros et al., 2010). Faults and fractures can represent a weak zone creating an easy path for deep gases to the surface (Viveiros et al., 2010). Therefore, identifying tectonic structures is essential in soil degassing studies.

Soil CO₂ fluxes (the rate of CO₂ flowing per area unit) are measured using the accumulation chamber method (Chiodini et al., 1998). The accumulation chamber method uses an inverted circular chamber to catch the CO₂ gas that comes up from the soil. Maintaining an isolated system between the chamber and the soil is essential. Inside the accumulation chamber, the gas is mixed with a fan. Finally, the gas is analyzed, read, computed, and recorded in the field (Chiodini et al., 2008).

1.4 Biogenic carbon dioxide

Aside from hydrothermal and magmatic sources, CO₂ can be from a biogenic origin. The biogenic source refers to the CO₂ emitted by a living organism's activity. The most usual way of biogenic CO₂ release is through soil respiration, representing 20% of total CO₂ emissions to the atmosphere (Smith et al., 1997) and could represent more than the 16% of the total urban carbon emissions of a city over the course of one year (Bezyk et al., 2021). Soil respiration comprises three biological processes: root respiration, faunal

respiration and microbial respiration (Jong et al., 1974; Edwards, 1975). Soil microflora decomposition is another source of CO₂ soil respiration (Bunt & Rovira, 1954) which depends on the soil conditions, such as temperature, water content and alternate wetting (Agehara & Warncke, 2005; Lee et al., 2006; Rahman, 2013).

1.5 Distinction between CO₂ sources

Carbon comprises two stable isotopes: ¹²C (abundance of 98.93%) and ¹³C (abundance of 1.07%) (Rosman & Taylor, 1998). Analyzing the carbon isotopic composition of CO₂ can be a more precise way to study the gas origin and discriminate between different CO₂ sources found in nature (Chiodini et al., 2008). This technique has been used successfully in recent studies (Chiodini et al., 2008; Viveiros et al., 2010; Lamberti et al., 2020). The most commonly used geochemical terminology for isotopic composition is in terms of delta (δ) values. Delta represents the difference between a standard value and a mean value (Hoefs, 2004). In the case of carbon isotopes, the most frequent standard used is the Vienna Pee Dee Belemnite (VPDB) which is an international isotopic reference material (Coplen, 1996). Following these terminologies, which was applied in the isotopic data along this study, the isotopic composition is defined by Equation [1]:

$$\delta^{13}C = \left[\frac{\left(\frac{^{13}C}{^{12}C}\right)_{muestra}}{\left(\frac{^{13}C}{^{12}C}\right)_{VPDB}} - 1 \right] \times 1000 \quad [1]$$

In general, δ¹³C_{CO₂} value differs depending on how CO₂ was formed, through exsolution from the magma at depth or by biological processes in the soil. The typical value of δ¹³C_{CO₂} for volcanic-hydrothermal CO₂ is between -10‰ to -3‰ vs. VPDB (Pineau & Javoy, 1983; Javoy et al., 1986) (Figure 2). The δ¹³C_{CO₂} composition for biogenic CO₂ ranges from -34‰ to -12‰ vs. VPDB (Hoefs, 1980; O'Leary, 1988). Plants can be classified based on each plant's process of photosynthesis. C³ and C⁴ plants are examples of this classification. Both types of plants differ in their δ¹³C_{CO₂} composition. Studies such as the one performed by Smith & Epstein (1971) have demonstrated that each type of plant has its own isotopic signature range value (Figure 2). Flux values and isotopic compositions are therefore useful to distinguish CO₂ soil diffuse degassing origin, which is crucial to understand the degassing behavior of the area, the tectonic structures, and the volcanic-hydrothermal system.

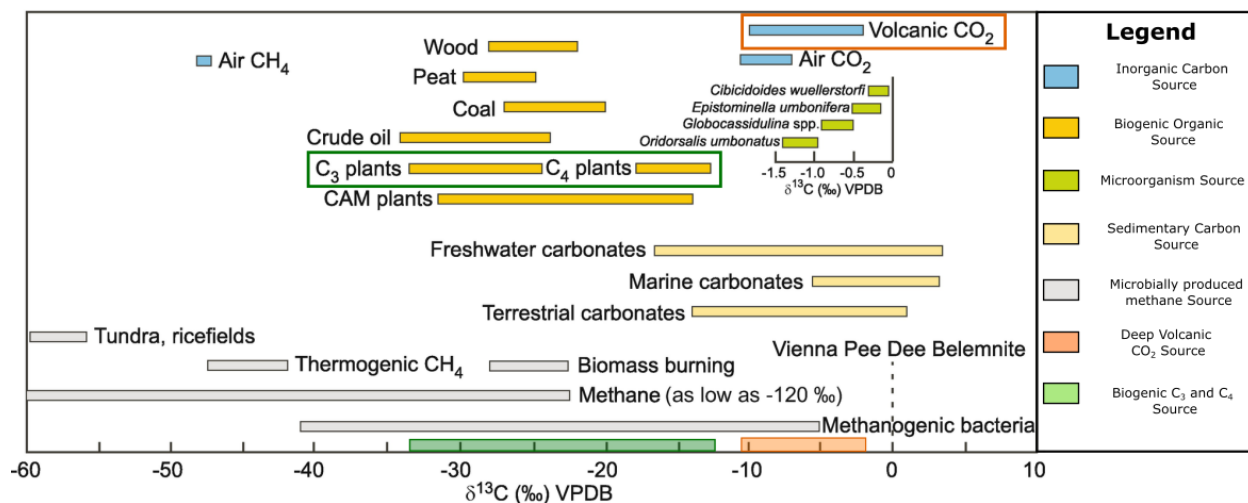


Figure 2. Summarized data of carbon 13 isotope signatures for different sources. It is remarked with orange and green rectangles the sources of interest for this study, Volcanic and Biogenic (C_3 and C_4 plants) sources, respectively. (Source: Wefer & Berger, 1991; Schidlowski & Aharon, 1992; Wagner et al., 2018).

1.6 Chiles Volcano

The volcanic-hydrothermal system of interest in this study is the one related to Chiles volcano. Chiles is a stratovolcano located on the border between Colombia and Ecuador, belonging to the Chiles-Cerro Negro Volcanic Complex. In Ecuador, it is located in the Northern part of the Western Cordillera in the Andes Cordillera. The nearest town to the volcano in Ecuador is Tufiño, in the Carchi province, 9 km to the west of the summit. Chiles is the nearest town in Colombia, located 10 km west of the volcano. Chiles volcano is known due to its geothermal potential. A binational project called 'Tufiño-Chiles-Cerro Negro' was carried out (CELEC & ISAGEN, 2015). The presence of hot springs, gas emissions, and some old fumarolic fields in the area make it an ideal location for a diffuse degassing study.

1.7 Statement of the problem

Despite the fact that Chiles volcano has a high geothermal potential, there are few studies carried out in the area. There is very little information about gas emissions, and there is no previous work related to CO_2 diffuse degassing. Approximately 2300 people live nearby the volcano and many tourists visit this rare high-altitude landscape and its hot springs. CO_2 is an odorless and colorless gas, and if concentrated (>15 vol%) can cause asphyxia (NIOSH/OSHA, 1981; Blong RJ, 1984). Hazardous conditions can be produced when the gas flux increases due to changes in meteorological variables such as pressure and rainfall (Viveiros et al., 2009) or if CO_2 accumulates in a depression. Better knowledge on CO_2 diffuse degassing is therefore critical to better understand the risk associated with the Chiles volcano, as well as to help in

the global quantification of volcanic CO₂ emissions and increase our knowledge on the Chiles magmatic-hydrothermal system.

1.8 Objectives

The main objective of this study is to provide the first CO₂ diffuse degassing quantification of the Chiles volcano and to contribute to the challenge of understanding the carbon input of non-anthropogenic CO₂ into the atmosphere. This study's specific objectives are as follows:

- Realize a CO₂ soil emission survey at Aguas Hediondas and Lagunas Verdes and collect samples for carbon isotope analysis to differentiate between biogenic and volcanic-hydrothermal CO₂ sources.
- Estimate the total flux of deep volcanic CO₂ using a statistical approach combined with isotopic composition of the gases.
- Create a map of the soil degassing flux in relation to tectonic structures using statistical analysis to interpolate the data.
- Compare CO₂ degassing with degassing at other volcanoes to have a better context of the CO₂ input from volcanoes to the atmosphere.

CHAPTER 2: CHILES VOLCANO

2.1 Geological Background

2.1.1 The Andes Cordillera

Chiles volcano is located in Ecuador, on the Northern end of the Andes Cordillera. The Andes Cordillera represents the most outstanding geological feature in South America. The Andean volcanic belt was formed due to the subduction of the Nazca plate beneath the South American Plate. The beginning of this plate tectonic convergence has been dated during the late Triassic - Early Jurassic (James, 1971; Aspden et al., 1987). Nowadays, the convergence rate between the two plates has been estimated around 8 cm/y (Larson et al., 1997; Norabuena et al., 1998; Angermann et al., 1999). Researchers have defined that the Nazca plate has a subduction angle of 25-35° plunging until a depth around 200 km (Guillier et al., 2001). The Cordillera extends along the western border of Chile to Venezuela, getting an extension of 8000 km (Jaillard et al., 2000). Due to the different orientations and structural characteristics, this mountain chain has been divided into three segments. Gansser (1973) defines these subdivisions as the Southern or Patagonian Andes, The Central Andes, and the Northern Andes (Figure 3). The Southern Andes extends from the continent southern tip in the Chilean and Argentine territory to the Gulf of Penas, Chile. The Central Andes extends from the Gulf of Penas, Chile, to the Peruvian – Ecuadorian border. Finally, the Northern Andes starts from southern Ecuador until the northern part of Venezuela.

Two parallel mountain ranges compose the Andes in the Ecuadorian territory. The westernmost range is called 'Cordillera Occidental' and the easternmost mountain range called 'Cordillera Real'. The two cordilleras are divided by a well-defined topographic depression called 'Inter-Andean Valley' (Goossens et al., 1970) (Figure 4). Both cordilleras harbor several dormant and active volcanoes. The volcanoes in Ecuador present an extensive variability in their geochemical composition, morphology, and eruptive styles (Hall & Beate, 1991). Bernard & Andrade (2011) defined 84 Quaternary volcanoes in continental Ecuador, classified according to their last eruption. For dormant volcanoes, the last eruption was older than 10 000 years. Potentially active volcanoes had their last eruption in the last 1 000 years, while active volcanoes had an eruption in the last 500 years.

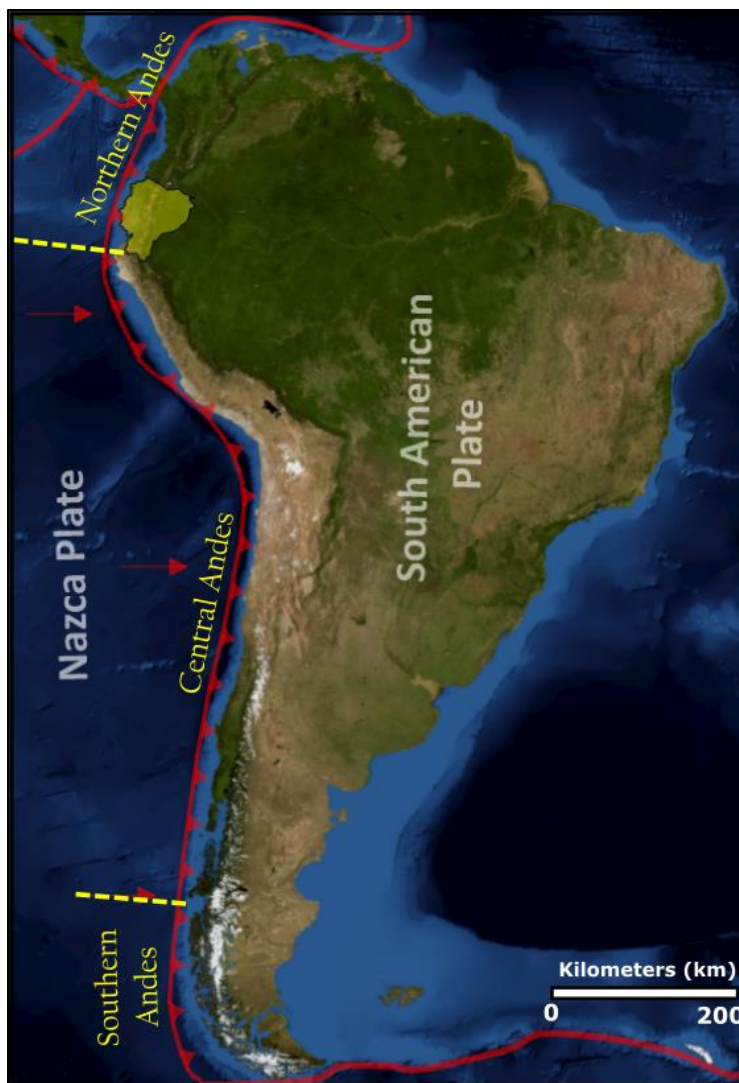


Figure 3. The Andes Cordillera. Map showing the subduction of the Nazca plate underneath the South American plate. In yellow are drawn the cordillera subdivisions proposed by Gansser (1973). Ecuador is shaded in yellow.

2.1.2 Chiles Volcano

The Chiles volcano ($0^{\circ} 49' 0''$ N, $77^{\circ} 56' 05''$ W) is located on the border between Ecuador and Colombia (Figure 5A). The Chiles volcano forms part of the Chiles - Cerro Negro Volcanic Complex. It is located in the Carchi province, 24 km from Tulcán, and 130 km north of the Ecuadorian capital, Quito. Chiles is part of the Western Cordillera (Figure 4). It covers an area of 36.44 km^2 and its summit lies at 4748 meters above sea level (masl). Chiles is a stratovolcano formed mainly by lava flows distributed radially around the crater. After the lava flow deposition, they were eroded by glaciation periods creating glacial deposits more commonly known as moraines (Telenchana, 2017). Besides, the volcano exhibits a 1 km diameter collapse scar on the northern flank (Figure 5B) (Cortés & Calvache, 1997).

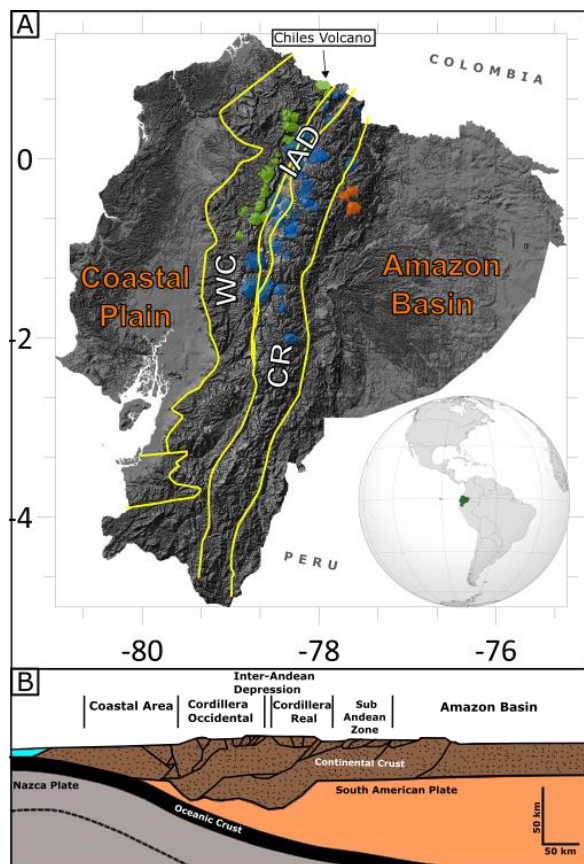


Figure 4. Tectonic setting of Ecuador. A: Digital Elevation Model (DEM from SIGTIERRAS) showing the structural subdivisions of the Andes Cordillera in Ecuador: Western Cordillera (WC), Intern Andean Depression (IAD), Cordillera Real (CR), Coastal Plain and Amazon Basin. Quaternary volcanoes are shown in green for the volcanic front, blue for the main arc and orange for the back arc. B: Structural W-E sketch of the subduction of the Nazca plate beneath the South American plate and the main orogenic structures in Ecuador (After Mégard, 1987).

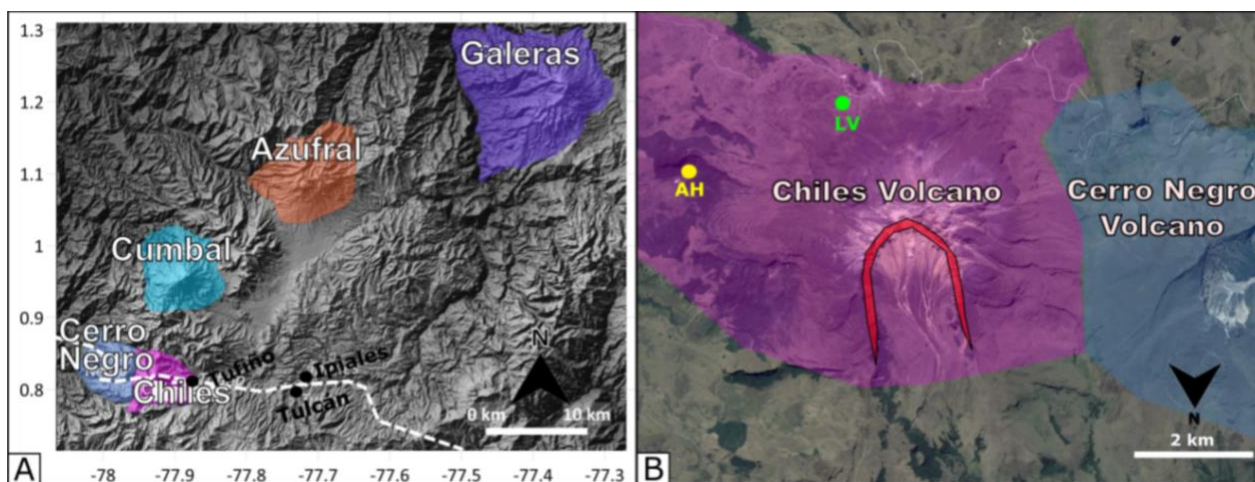


Figure 5. Geographical Location of Chiles Volcano. A: Location of Chiles volcano and the nearest volcanoes. The dashed white line represents the borderline between Ecuador and Colombia. The map coordinates are in decimal degrees. B: Collapse scar on the northern flank of Chiles Volcano (red) and location of the two surveyed areas: Aguas Hediondas (AH) and Lagunas Verdes (LV). Image taken from Google Earth.

Chiles volcano was classified by Instituto Geofísico - EPN (2014) as a potentially active volcano based on the assumption that its last eruption happened in the course of the last 10 000 years. There is however no record of its last eruption. The oldest lava flow is dated at around 572 ka BP while the youngest is dated around 42 ka BP (Telenchana, 2017). The lava flows vary between basaltic-andesite and rhyodacite compositions ($\text{SiO}_2 = 55\text{-}70$ wt%) (Cortés & Calvache, 1997). Telenchana (2017) has defined two units that form the structure of Chiles volcano: CHILES I and CHILES II. Both units are similar in their geochemical rock composition, calc-alkaline, a typical rock composition at subduction-related volcanoes.

Structural and tectonic features have been described around Chiles. It is located on a chevron fold in the West direction. The main fault system has a preferred direction of N20E (Bocanegra & Sánchez, 2017). Perdomo et al. (1986) defined the main structural faults in the area. The most outstanding faults are Chiles – Cumbal, Chiles-Norte, Chiles – Cerro Negro, Cerro Negro – Nasate, Tufiño, and Nasate (Figure 6).

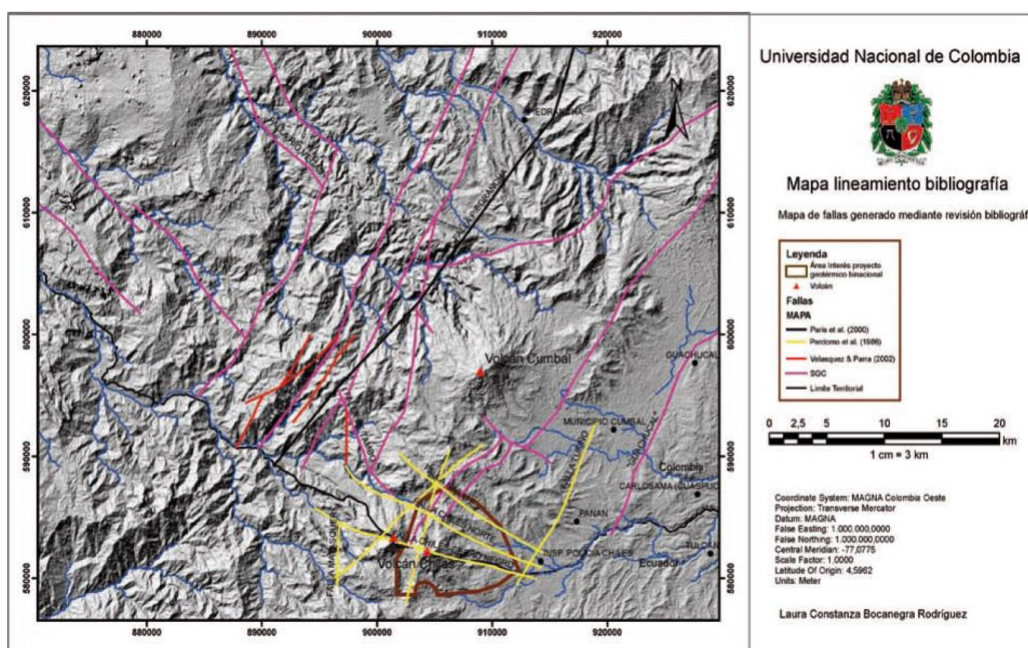


Figure 6. Fault Map in Chiles volcano area. It is a bibliographic compilation of different sources showing the main faults identified in the area. Source: Bocanegra and Sánchez (2017).

As a result of its location and structural setting, the surrounding area of Chiles volcano is susceptible to suffer a high seismic activity. The internal activity of the volcano could also lead to seismic swarms in the area, more commonly known as Volcano Tectonic Seismicity. Volcano Tectonic Seismicity can be an effect of hydrothermal fluids and magma movement (Ebmeier et al., 2016). Chiles volcano did not have a historical seismic activity until 2013. In October 2013, seismic activity started around 2-6 km south of the

volcano with a seismic swarm with more than 1000 recorded events per day. A couple of months later, in February-May and September-December 2014, two more swarm events occurred in the area with an incidence of events per day varying between 10 to 100. The largest registered earthquake had a magnitude of 5.6 M_{LV} (local magnitude calculated with the vertical component of the whole seismic record of the area) and happened at 13 km of depth. It occurred on the 20th of October 2014 at 19:33 UTC. It was felt in Tulcán and Tufiño in Ecuador and, consequently, several damages in the surrounding towns to Chiles Volcano were registered (IG - EPN, 2014). The last seismic episode was during September 2018 and July 2019, where more than 147 000 events were registered. The earthquake magnitude, in general, is less than 3.6 M_{LV} . The most significant earthquake during this period was of M_{LV} 4.0 at 4 km depth that happened on the 25th of July 2019 (IG - EPN & SGC - OSVP, 2019).

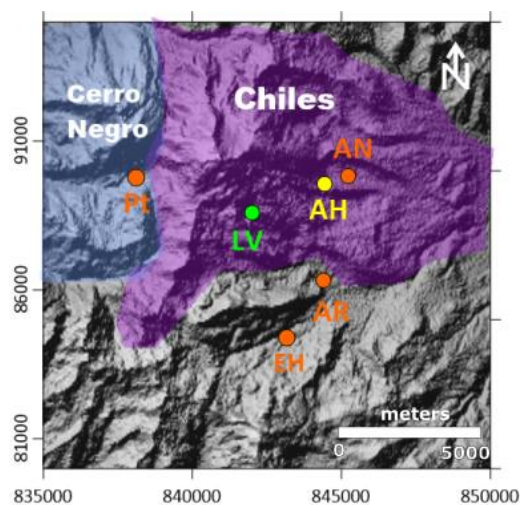


Figure 7. Location of the Hydrothermal hot springs and fumarolic fields monitored by IG-EPN. The hot springs and fumarolic fields are: Potrerillos (Pt), El Hondón (EH), Artezón (AR), Aguas Negras (AN). This study's surveyed areas are green and yellow, corresponding to Lagunas Verdes (LV) and Aguas Hedionds (AH), respectively. The map coordinates are in meters, UTM – WGS84, 18N.

IG-EPN and SGC-OSVP (Servicio Geológico de Colombia- observatorio Sismológico y Volcanológico de Pasto) are the two institutions in charge of monitoring Chiles volcano. IG-EPN monitors the volcano in the Ecuadorian territory and SGC in the Colombian territory. The monitoring network is based on seismicity, deformation, geochemistry and temperature of hydrothermal hot springs (Instituto Geofísico - EPN, 2014; SGC, 2021). The seismicity is monitored thanks to two broadband seismic stations, and in 2014 new stations were installed due to the increases in the Chiles's volcano seismic activity (IG-EPN, 2015). The deformation is mainly tracked with inclinometers and GNSS (Global Navigation Satellite System). The geochemistry and temperature of hydrothermal hot springs monitoring are performed in 6 sites of interest in the Ecuadorian territory: Potrerillos, Lagunas Verdes, Artezón, Aguas Negras, El Hondón and

Aguas Hediondas (Figure 7). where the main physico-chemical parameters measured are temperature, pH and conductivity. Besides, gases are measured in the hydrothermal areas using a multi-GAS instrument. Moreover, samples of the water are taken for major element analysis (IG-EPN, 2020).

2.2 Survey Areas

2.2.1 Aguas Hediondas

Aguas Hediondas ($0^{\circ}48'35''$ N, $77^{\circ}54'22''$ W) is a hot spring located on the eastern flank of Chiles (Figure 7). A tourism complex with pools was built few meters to the South East of the hot spring, preventing people to access the spring area where gas emanations have caused casualties in the past. It is located 4 km East of Chiles summit. The hot spring is in a restricted area due to the known gas emissions of CO_2 and H_2S (IG - EPN, 2020) (Figure 8B). During the last measurements made by IG-EPN (2020), the water temperature ranged from 57 to 59 $^{\circ}\text{C}$, as is shown in Table 1. The emission of H_2S provides to the area a characteristic smell of rotten eggs, which gave its name to the place 'Aguas Hediondas' meaning 'stinking waters'. In the area, there is evidence of hydrothermal alteration (Figure 8D). The survey area around the hot spring is covered mainly by paramo vegetation in the upper part, and all around is an extensive paramo forest. However, inside the restricted area, there is no vegetation; the soil is predominantly loose soil and rocks. A landslide occurred in the beginning of the 20th century, covering the location of the hot spring which re-emerged lower down.



Figure 8. Photos of Aguas Hediondas survey area A: Entrance to the tourist complex 'Aguas Hediondas'. B: The entrance to the restricted hot spring area marked with warning signals. Photo Credits: Celine Mandon. C: Photo showing the hot spring and survey area, as well as the pools built lower down in the tourist complex. Photo Credits: Celine Mandon. D: An active fumarole surrounded by hydrothermally altered rock. It is located right next to the spring.

Table 1. Physico-chemical parameters of water and gas measurement in Aguas Hediondas. Source: IG - EPN, 2020.

Date	Temperature (°C)	pH	H ₂ O/CO ₂	CO ₂ /H ₂ S
Jul-31-2019	58	3.64	21.55	4.85
Oct-23-2019	59.1	3.6	1	4.45
Dec-12-2019	57.8	3.7	0.25	5.89

2.2.2 Lagunas Verdes

Lagunas Verdes (0°48'10" N, 77°55'36" W) is the name given to little lakes on the southern flank of Chiles (Figure 9A), next to which sits an old fumarolic field (Figure 9B). Like Aguas Hediondas, the fumarolic field above Lagunas Verdes presents hydrothermal alteration (Figure 9C) and the characteristic smell of rotten eggs. The survey area is mainly covered by little consolidated rocks and very little vegetation. Lagunas Verdes also is known for the emission of CO₂ and H₂S. Since 2014 IG-EPN has measured the physical and chemical properties of the released gas using mainly a Multi-Gas instrument. Besides, they measure the temperature and pH of the water of the lagoons, as is shown in Table 2.

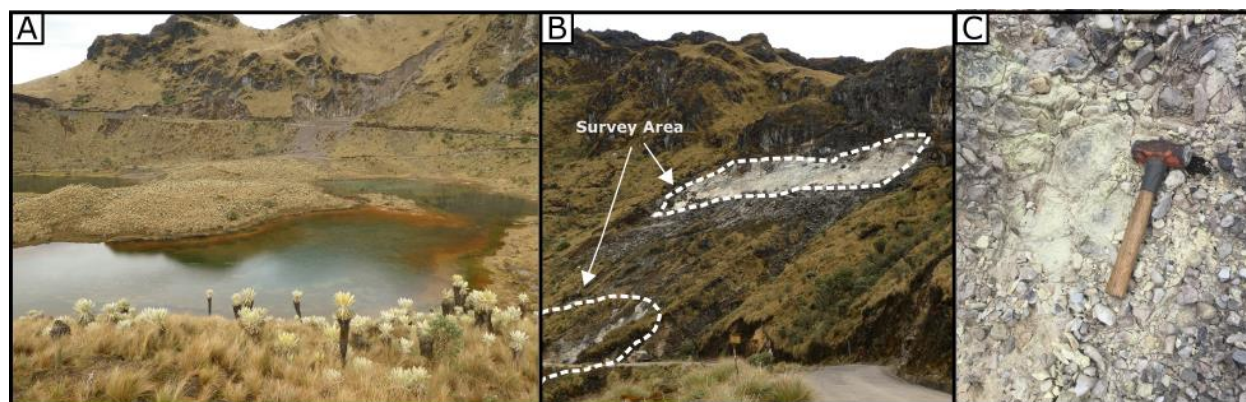


Figure 9. Lagunas Verdes survey area. A: The touristic zone of 'Lagunas Verdes'. B: The two survey areas. C: Hydrothermal alterations in the rocks of the survey area. Photos Credits: Celine Mandon.

Table 2. Physico-chemical parameters of water and gas measurement in Lagunas Verdes. Source: IG - EPN, 2020.

Date	Temperature °C	pH	H ₂ O/CO ₂	CO ₂ /H ₂ S
Jul-31-2019	9.1	5.58	1.2	71.2
Oct-22-2019	9.4	6.42	4.77	66.5

2.3 Vegetation of Chiles Volcano

2.3.1 Types of plants in the area

In Chiles volcano, the climate is the typical climate of the high mountain paramo. According to the Ecuadorian Institute of Meteorology and Hydrology (INAMHI), the climate in Chiles volcano is mainly cold, with mean temperatures ranging between 9 and 11 °C (INAMHI, 1994). However, it can reach 22 °C during the day, and be below zero degree during the night. The precipitation reaches on average 1500 mm per year, but the precipitation varies from day to day. The vegetation in the area is characterized by the protected giant rosette plant whose scientific name is *Espeletia pycnophylla ssp. angelensis*, better known by the community as Frailejón (Figure 10 & Figure 11L). This particular plant grows at altitudes of about 3 200 to 4 200 masl (Ramsay, 2001).



Figure 10. Picture of Chiles volcano with the surrounding vegetation formed mainly by Frailejones.

In general, the vegetation in Chiles volcano area is constituted by paramo vegetation. Paramo vegetation is distinguished by tree-less vegetation. A study recorded 569 plant species of 90 families in Chiles surroundings, where the most considerable families are Asteraceae with 75 species, Poaceae with 45 species, and Orchidaceae with 35 species (Ramsay, 2001).

These plants cover mainly the area of Aguas Hediondas, where the surrounding area is a paramo forest, and some parts of the soil are covered with small shrub vegetation and moss. On the other hand, there is not too much vegetation in the survey area of Aguas Verdes. The soil is mainly formed by rock debris and unconsolidated soil. The most abundant plants in the survey area, following the work of Ramsay (2001) and Chimbolema et al. (2013) are showed in Figure 11.

Different types of plants exist according to the photosynthetic pathway composition (Still et al., 2003), out of which C3 and C4 are the most common. In the case of Chile's volcano vegetation, most of the plants are C3 plants due to the paramo environment, climate, and soil type. According to the study performed by Smith & Epstein (1971) the mean isotopic $\delta^{13}\text{C}_{\text{CO}_2}$ composition in C3 plants is -27‰. This mean value agrees with the isotopic analyses of the study by Chapela et al. (2001). These authors focused on the paramo grasslands of Ecuador and concluded that the isotopic mean value of paramo soil for $\delta^{13}\text{C}_{\text{CO}_2}$ is -24‰.

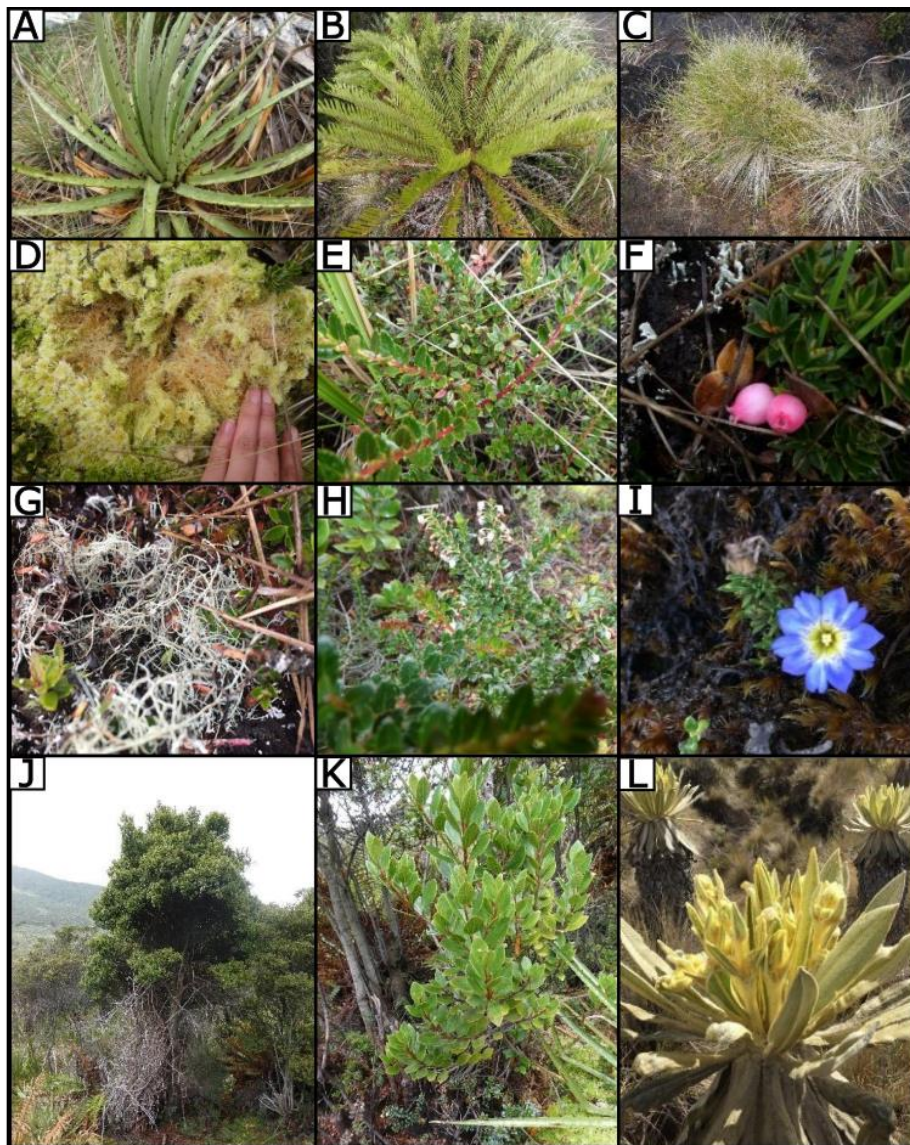


Figure 11. Compilation of the vegetation found in Aguas Hediondas and Lagunas verdes. A: 'Achupalla' *Puya Hamata* L.B. Sm. B: *Blechnum auratum* (Fée) R.M. Tryon & Stolze. C: "Sigse" *Cortaderia nitida* (Kunth) Pilg. D: 'Mosses' *Breutelia*. E: "Flor del andinista" "*chuquiragua*" *jussieui* Hieron. F: "Pasinu chirimote" *Disterigma empetrifolium* (Kunth) Drude. G: *Cladina* (Nyl.) Nyl. H: "Ashpa mortiño" *Pernettya prostrata* (Cav.) Sleumer. I: "Kuyana yuyo" "amor sachá" *Gentiana sedifolia* Kunth. J: *Polylepis incana* KUNTH. K: "Aretes" *Brachyotum lindenii* Cogn. L: "Frailejón" *Espeletia pycnophylla* subsp. *angelensis* Cuatrec

CHAPTER 3: METHODOLOGY

3.1 CO₂ flux measurements

Direct and indirect methods can be used for measuring the CO₂ soil diffuse degassing. The direct method is an in-situ methodology based on directly measuring the flux from the soil and seeing the values in real-time. The indirect methods are based on estimating the CO₂ concentrations at different depths applying a theoretical gas flow in a porous media model (Fick's first law). The latter has some limitations because it is necessary to know the soil porosity properties and transport mechanism. Moreover, it must be applied only in steady-state diffusive fluxes (Chiodini et al., 1998).

The accumulation chamber method is a direct measuring method. This method was initially applied successfully to determine soil respiration in agricultural science (Parkinson, 1981). Then, this method was used in volcanological-geothermal studies in different places around the world (Chiodini et al., 1996; Padrón et al., 2008; Viveiros et al., 2010; Lamberti et al., 2020).

We chose the accumulation chamber method to perform the survey in this study. As the name suggests, this method is based on an inverted chamber that is pressed against the soil to create a closed-system with the atmosphere. A spectrometer measures the CO₂ concentration inside the chamber during a particular time. A constant or decreasing concentration signifies that there is no CO₂ soil degassing, i.e., the concentration in the chamber is that of the atmosphere and does not vary. On the contrary, if the concentration increases, it highlights CO₂ diffuse emission coming from the soil and trapped inside the chamber (Chiodini et al., 1998). The flux value (Φ_{CO_2}) is calculated after the next equation:

$$\Phi_{CO_2} = cf \times \frac{d[CO_2]}{dt} \quad [2]$$

where Φ_{CO_2} is soil CO₂ flux, and *cf* is the proportional factor and dC_{CO_2}/dt is the variation in CO₂ concentration in the chamber as a function of time. The proportional factor was derived from a laboratory test by Chiodini et al. (1998). The equipment was tested emitting Φ_{CO_2} on a 'synthetic soil' made of 10 cm thick dry sand located in a box with an open top. As a result, *cf* was estimated as the dC_{CO_2}/dt and Φ_{CO_2} flux best-fit. It was showed that measuring the increasing concentration for a long enough time makes it reliable to determine the CO₂ flux from the soil with this mathematical relation (Chiodini et al., 1998).

The West System Classic Portable Fluxmeter (Figure 12A) was used for measuring the CO₂ diffuse degassing in this study. This equipment is composed of:

1. A LICOR® LI-840A CO₂/H₂O infrared gas analyzer with a range of 0 – 20000 ppm (parts per million) (Figure 12B)
2. An AD (analogue – digital) converter (Figure 12B)
3. A metallic circular accumulation chamber (West System model B) with an area of approximately 0.0314 m² and with a volume of 0.006231 m³ (Figure 12C)
4. A field computer with FluxManager software allowing for real-time concentration readings (Figure 12D)

The equipment was kindly provided by Michigan Technological University (MTU) and was calibrated in the same institution.



Figure 12. The West System Fluxmeter equipment used for the study. A: The Classic Portable Fluxmeter. B: The AD (analogue – digital) converter and the LICOR® infrared gas analyzer is located inside a box adapted as a backpack to be transported. C: The metallic accumulation chamber (model B). D: The field computer, connected via Bluetooth to the AD converter

The functioning of the Portable Fluxmeter is shown in Figure 13. The accumulation chamber is pressed against the soil, avoiding holes between the ground and the chamber to ensure a closed system with respect to the atmosphere. The diffusing gas that comes from the soil is emitted inside the chamber, where a fan allows for homogenization of the gas phase. The mixed gas is pumped to the infrared sensor. After analysis, the gas is returned to the chamber to not modify the natural gas flux of the soil. The results from the infrared gas analysis are converted by the AD converter and shared via Bluetooth with the computer. The FluxManager program allows seeing a real-time graph of C_{CO₂} vs. time and the

corresponding measuring values for each point (Figure 14). Additionally, this program saves the measured values at each survey point, which can later be revised and corrected if needed.

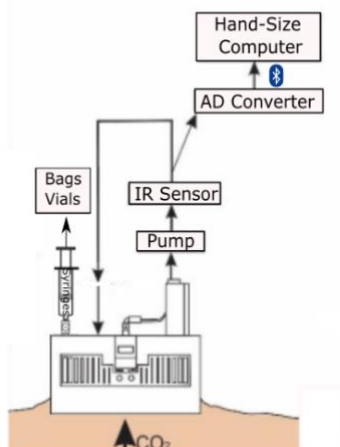


Figure 13. Sketch representing the steps followed by CO_2 gas to be measured using the accumulation chamber method. Modified from: Lamberti et al., 2020.

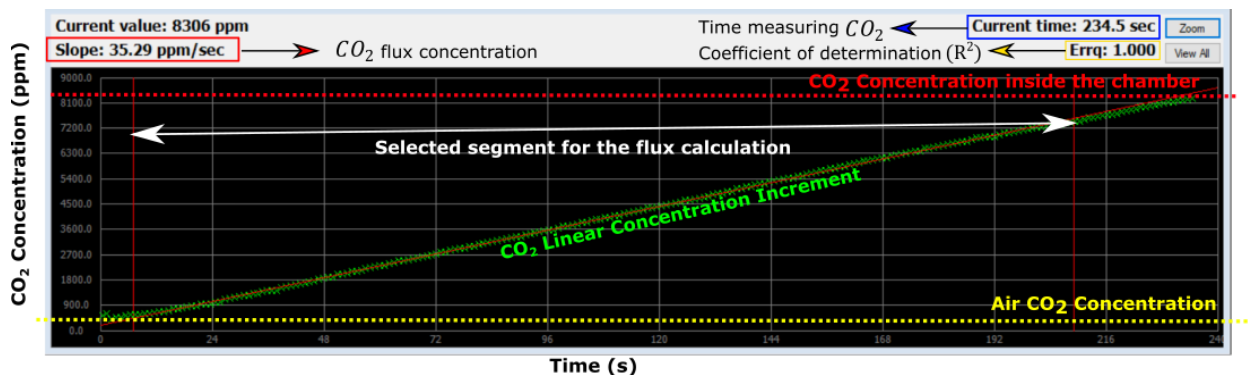


Figure 14. A screenshot of the FluxManager software, where the increase in CO_2 concentration in the accumulation chamber is plotted as a function of time. The initial concentration corresponds to the CO_2 concentration in the chamber at the beginning of the measurement, i.e. the atmospheric CO_2 concentration.

Figure 14 shows an example of CO_2 flux calculation. The CO_2 concentration at the beginning of each measurement is equal to the background value (i.e., the atmospheric CO_2 concentration). As soon as the chamber is pressed against the ground, the concentration increases inside the chamber due to diffuse soil degassing. In order to get the best CO_2 flux estimation, we need to choose the best fit line. The coefficient of determination (R^2) tells us about the quality of the linear relation between both variables, time and CO_2 concentration. R^2 values range from 0 to 1, with best fit being closer to 1. The program allows us to vary the beginning and end of the selected segment to compare the regression coefficients. To obtain the best estimate, we need to adjust the segment until the R^2 value is closest to 1.

3.2 Other measurements

Besides the CO₂ flux measurements, we took other measurements and observations (Figure 15). We measured soil moisture and soil temperature, and we took notes about soil cover, vegetation type, and soil type at each point. Soil moisture was measured with HydroSense II, a handheld Soil Moisture Sensor designed by Campbell Scientific® (Figure 16A). The measurement unit is Volumetric Water Content (VWC). Its water content accuracy is around 3%, and the measurement range is from 0 % to 50% VWC. Soil temperature was measured with a portable thermocouple thermometer patented by HANNA® (Figure 16B). The measurement unit was in Celsius degrees (°C). The resolution of this instrument is 0.1 in the range of -149.9 to 999.9 °C. The accuracy of the equipment is ±0.5°C. These measurements and observations were recorded directly in the ArcGIS collector program, along with the CO₂ flux for each survey point (Figure 17).

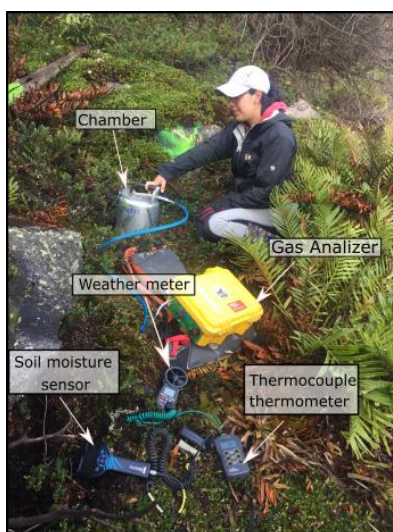


Figure 15. Photograph showing all the instruments used at each survey point to take the measurements during field work.

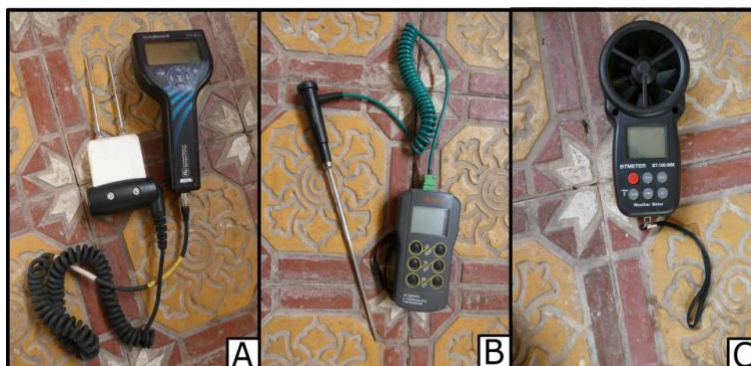


Figure 16. Instruments used in the field to take various measurements. A: handheld Soil Moisture Sensor. B: Portable thermocouple thermometer. C: Anemometer - weather meter.

We took measurements of atmospheric pressure, wind speed, air temperature and humidity during different times throughout the day. These measurements were taken by a BTMETER Anemometer Handheld Digital Barometer Weather Meter (Figure 16C). The atmospheric pressure was recorded in mbar, the wind speed in m/s, and the humidity in $\text{g}\cdot\text{m}^{-3}$. Besides, a sensor is built-in the accumulation chamber which measures the atmospheric pressure in KPa at each point and records it automatically in the FluxManager software.

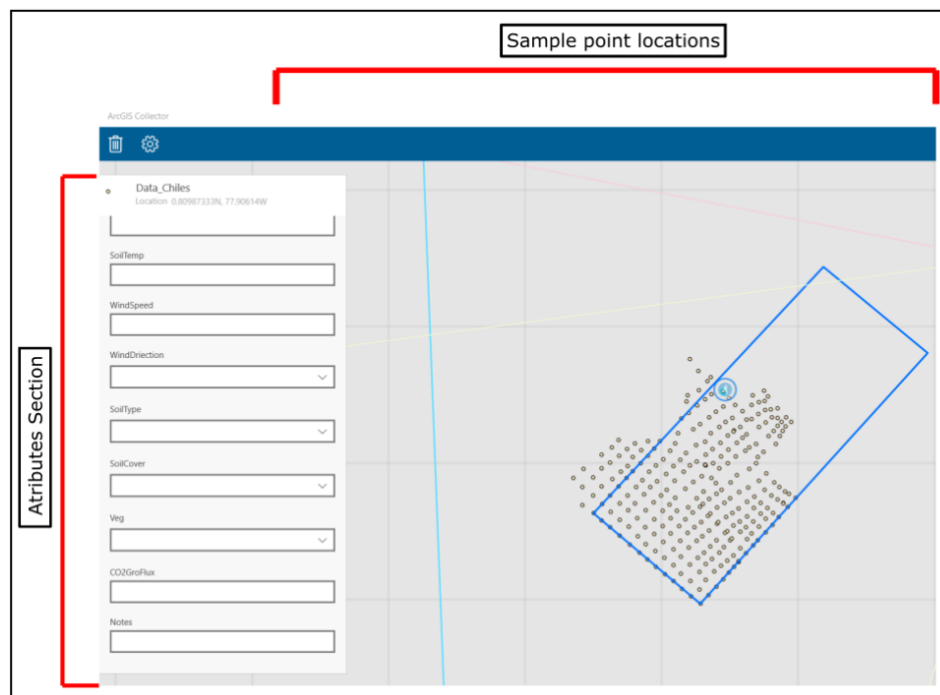


Figure 17. Screenshot from the ArcGIS collector program used to record flux values and observations in the field.

3.3 Isotopic Samples

3.3.1 Sampling strategy and collection

We obtained CO_2 gas samples for isotopic analysis. The gas samples were taken in 12 mL vials (for concentrated samples) and 500 mL bags (for diluted samples) (Figure 18). Gas for isotopic analysis is collected after the gas detector, using a syringe to fill 12 mL vials or directly filling bags from a three-way valve (Figure 19).



Figure 18. Gas sample collection instruments. A: bag used to take gas samples. B: Vials used to take gas samples.

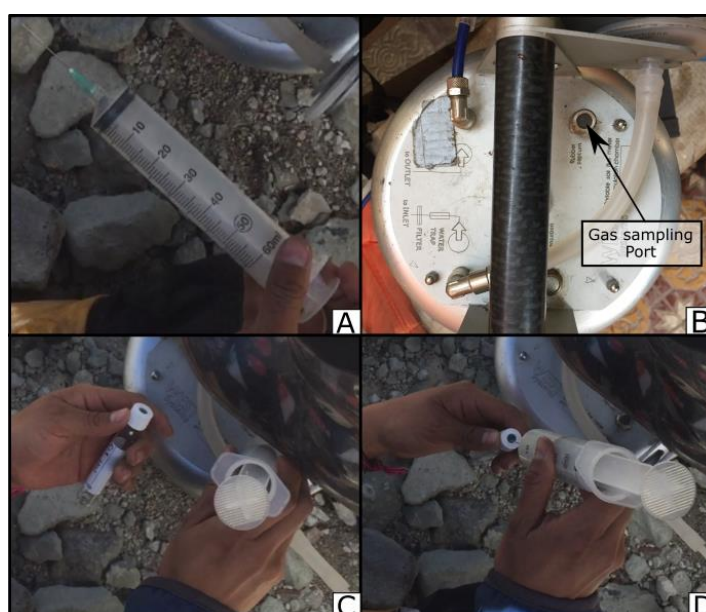


Figure 19. Collection of gas samples for isotope analysis. A: Photograph of the syringe used to take gas sample in the chamber through the gas sampling port. B: Photograph of the chamber showing the location of the gas sampling port. C: Photograph showing the syringe taking the gas sample. D: Photograph while reinjecting the gas sample into the vial.

Isotopic data is used to discriminate between various CO₂ sources. The collection method, developed by Chiodini et al. (2008), consists of collecting two gas samples at each survey point. The first sample (A) is taken at low CO₂ concentration in the chamber after a few seconds of starting the measurement, to allow the mixing of the gas. The second sample (B) is taken later during the flux measurement, when the CO₂ concentration in the chamber is higher. For most of the sites, we collected the second sample (B) when a value of 1000 ppm of CO₂ in the chamber was reached. For two survey points, the concentration was lower than this value due to a very low flux in the first case, and the pump battery dying in the second case. For sites with very high flux, the value of 1000 ppm CO₂ was reached too rapidly, and sample B was

collected at much higher CO₂ concentrations. The final isotopic composition for each survey point is calculated with the following equation:

$$\delta^{13}C_{CO_2} = \frac{\delta^{13}C_{CO_2,B} \times X_{CO_2,B} - \delta^{13}C_{CO_2,A} \times X_{CO_2,A}}{X_{CO_2,B} - X_{CO_2,A}} \quad [3]$$

Where $\delta^{13}C_{CO_2,A}$ and $\delta^{13}C_{CO_2,B}$ correspond to the isotopic composition of the low CO₂ concentration sample A and high CO₂ concentration sample B, respectively, and $X_{CO_2,A}$ and $X_{CO_2,B}$ represent the CO₂ concentrations of samples A and B, respectively, as measured by the accumulation chamber spectrometer.

3.3.2 Isotopic analysis

The gas samples, vials and bags, were sent to Arizona, United States, to be analyzed. The analysis was performed at the Arizona State University a month and a half after the survey using a Thermo Fisher Delta Ray Isotope Ratio Infrared Spectrometer (*Figure 20*). This instrument is based on direct absorption spectroscopy, simultaneously determining $\delta^{13}C$ and $\delta^{18}O$ in CO₂. It consists of a tunable near-infrared diode laser combined with a nonlinear crystal to produce a laser beam. Calibration is performed using a pure CO₂ calibration gas with known $\delta^{13}C$ signature. During analysis, the laser scans the absorption lines of the various CO₂ isotopologues. The isotope composition of the sample is obtained relative to a reference standard (Vienna Pee Dee Belemnite, VPDB) and expressed as delta (δ) per mil (‰) values.

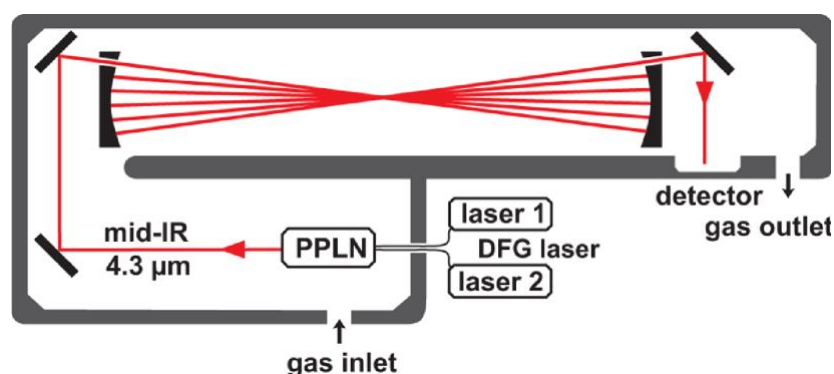


Figure 20. Basic diagram showing how Delta Ray method works for $\delta^{13}C_{CO_2}$ analysis. DFG indicates the difference frequency generation laser and PPLN represents the periodically poled lithium niobate. After: Van Geldern et al. (2014).

3.3.3 Mapping strategy

The survey was carried out from 6th to 12th of December in 2020. We chose two locations on the Chiles volcano flanks to execute the study, at Aguas Hediondas and Lagunas Verdes, both located on the Ecuadorian territory. They are known for their hydrothermal activity and gas emissions. We covered an area of 6 000 m², where we followed a 5-meter grid using a measuring tape as guidelines (Figure 21). We obtained a total of 339 CO₂ flux measurements and 14 samples for isotopic analysis at seven survey points (Figure 22). Furthermore, two locations, one with vegetation and one barren, were chosen as control points, where we repeatedly measured the CO₂ flux at the beginning and end of each workday.



Figure 21. Photographs showing the measuring tape used to perform the 5-meter grid in Aguas Hediondas. A: Measuring tape located in the Western part of the survey area. B: Measuring tape located across the hot spring's channel.

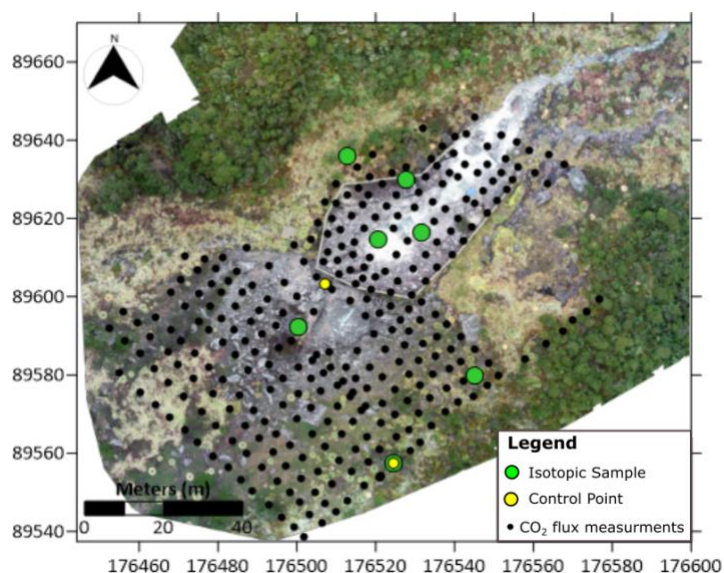


Figure 22. Survey points taken in Aguas Hediondas. Small black points represent the sites where we took CO₂ flux measurements. Green points are locations where we took gas samples for isotopic analysis. Yellow points are the two control points. Orthophoto from December 2020. The map coordinates are in meters UTM – WGS84, 18N.

In Lagunas Verdes, we worked on 6th, 9th, and 12th of December 2020. We covered an area of 5 000 m², where we took 76 CO₂ flux measurements and four samples for isotopic analysis at two survey points (Figure 23). In this case, we followed an irregular grid.

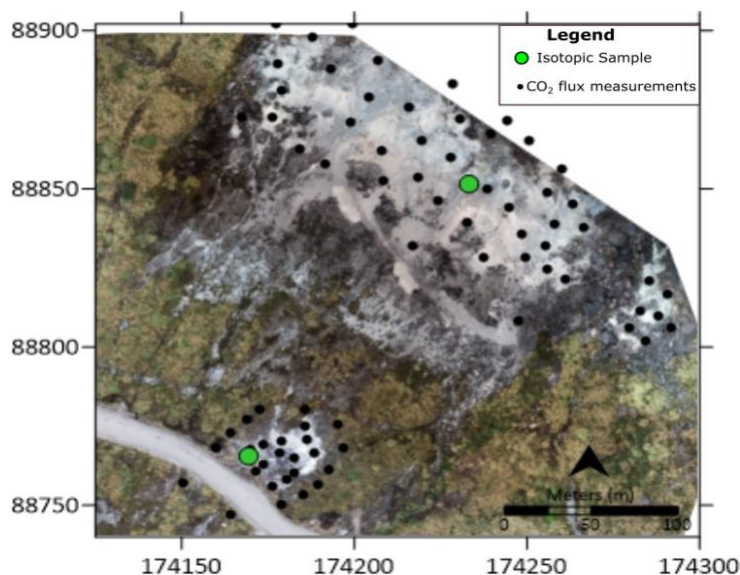


Figure 23. Survey points taken in Lagunas Verdes. Small black points represent the sites where we took CO₂ flux measurements. Green points are locations where we took gas samples for isotopic analysis. Orthophoto from June 2021. The map coordinates are in meters UTM – WGS84, 18N.

The location of the sampling points in both sites was recorded in the ArcGIS collector from a handheld GPS (Figure 17). However, we also used the orthophotos from the area to rectify each survey point location, minimizing the location error associated with the accuracy of the GPS. GPS accuracy was around ± 3 meters in good weather and ± 5 meters in a cloudy sky. Precise location of survey points for the 5-m grid at Aguas Hediondas is critical during spatial interpolation to create CO₂ flux maps.

3.4 Data processing

3.4.1 Preparation and correction of the data

Once the fieldwork is finished with all the data collected, the first step to process the data is to review the flux recorded at each point, to make sure the best CO₂ vs. time slope is chosen. The revision and correction of the data were made using the software developed by West, Flux revision 4.11. This program allows for reprocessing of the CO₂ concentration versus time data. It is mostly important to make sure the window chosen to interpolate the CO₂ flux is correct and representative of the survey point (small variations may happen with time). The CO₂ flux in ppm/s then needs to be converted into more convenient units for

analysis, i.e., grams per square meter per day ($\text{g m}^{-2} \text{d}^{-1}$). We applied the following formulas for the conversion:

$$F_g = F_{ppm} * K * C_{molec} \quad [4]$$

Where:

- F_g is the CO_2 flux in $\text{g m}^{-2} \text{d}^{-1}$.
- F_{ppm} is the CO_2 flux in ppm/s.
- C_{molec} is the molecular weight of CO_2 .

Finally, K needs to be calculated with the following formula:

$$k = \frac{86400 * P}{10^6 * R * T_k} * \frac{V}{A} \quad [5]$$

Where:

- P is the barometric pressure expressed in mbar (HPa).
- R is the gas constant $0.08314510 \text{ bar L K}^{-1} \text{ mol}^{-1}$.
- T_k is the air temperature expressed in Kelvin degrees.
- V is the chamber net volume in cubic meters.
- A is the chamber inlet area in square meters.

The following step is to correct the data using the calibration factor. The calibration was performed at Michigan Technological University. For the calibration tests, the equipment measured CO_2 gas at different concentrations and different flux rates. In this case, the calibration was applied with 99.9% CO_2 , 10% CO_2 , and 1% CO_2 concentrations with various flux rates into the sensor: 10, 8, 7, 5, 4, 2, 1 sccm (standard cubic centimeters) with each gas. The obtained values are converted to the units used in this study ($\text{g m}^{-2} \text{d}^{-1}$). Plotting the real values vs. the measured values create a calibration curve from which a total correction factor is obtained. The CO_2 fluxes measured during our survey are then corrected with this correction factor.

Once the CO_2 fluxes are converted and corrected, we rectified the location of points. We used the orthophotos to georeference the start and end of each grid line in the case of Aguas Hediondas. After this, we just measured the 5-meter distance to locate every sample point in a line. Finally, the coordinates had to be converted from geographic coordinates WGS 1984 to a projected one, WGS84 UTM zone 18N.

3.4.2 Sequential Gaussian Simulation (sGs)

The data obtained during the survey were processed using a geostatistical approach. Geostatistics is a branch of statistics used in geoscience, which basic concept is that there is a relation between the spatial

distribution of the values. It considers that two close points in space are more probable to be similar than two distant points (Isaaks et al., 1989). There are numerous geostatistical methods to create simulations of the variables. The technique used in this study is the Sequential Gaussian Simulation (sGs), defined by Cardellini et al. (2003), as the most appropriate method for diffuse degassing studies. sGs is based on an interpolation technique. The interpolations techniques are used to predict the values in unsampled locations based on the spatial correlation of the sampled data obtained during the fieldwork (Goovaerts, 1999).

The sGs method was applied following the algorithm described by Deutsch & Journel (1998). This algorithm was designed for the Geostatistical Software Library, GSLIB. This algorithm consists of creating a certain number of simulations of the spatial distribution of the variable, which in this case is the CO₂ flux. The algorithm followed is represented in Figure 24, and described below:

- Have the experimental data ready to be processed
- Looking if it is necessary to apply decluster weights or not. Decluster weights are used in the cases where the data is not spread evenly throughout the area, meaning that there is more concentration of data in certain parts than others. When this effect happens, it is necessary to apply a value to equalize the data.
- Transform the data to a normal distribution using a normal score.
- Create experimental variograms of the data normally distributed.
- Modelling the variogram previously created to have the best fit curve of the data.
- Execute sequential Gaussian simulation. In this step, we can apply different parameters according to the goal of each study. The kriging type used in this study was simple kriging.
- Back transform the normally distributed data into the initial data.
- Post-processing data is the final step that allows verifying the spatial distribution, adding the corresponding coordinates to the data, choosing the visualization map type (E-type and probability maps) and estimating the uncertainty.

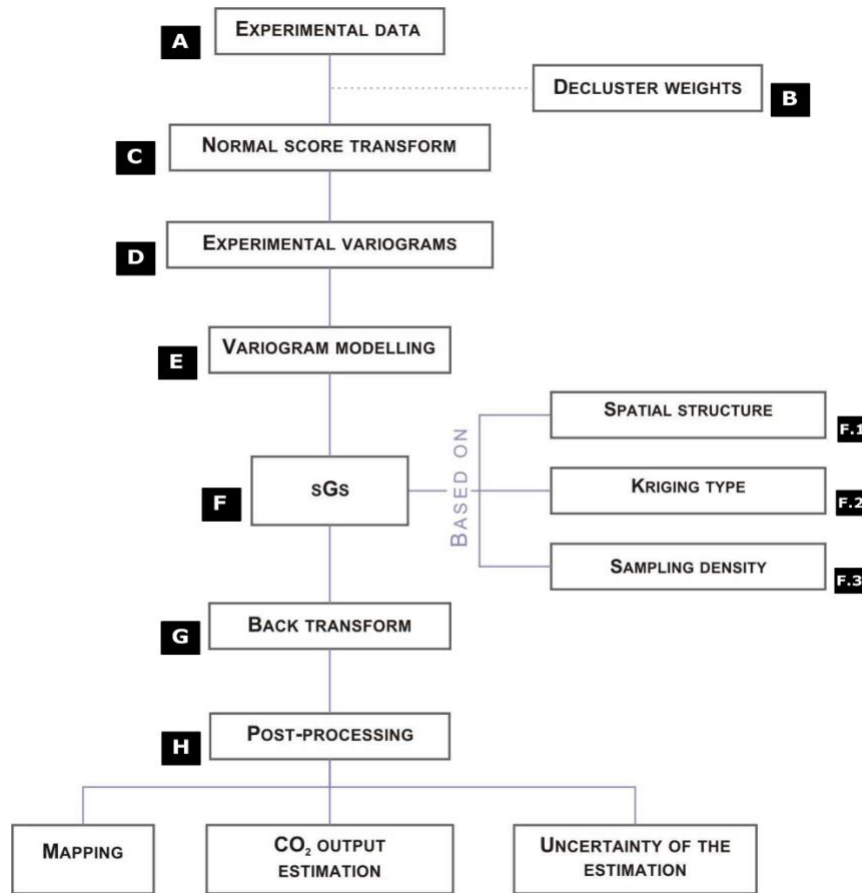


Figure 24. Procedure scheme of the sGs algorithm. Modified from Viveiros et al., (2020) from the original source of Frondini et al., (2004).

Once the sGs is successfully applied, one of the post-processing steps is to choose the map type in which we would like to perform the simulation. In this study, we decided to use two types of maps, E-type and probability maps. The E-type maps display predicted values for each location in the area based on an average of all the data simulations. This type of map is helpful to calculate an estimate of the total diffuse degassing of the area. Instead, the probability maps are beneficial to identify the DDS and estimate deep hydrothermal degassing only. It indicates the probability of the simulated values exceeding a selected threshold value (Cardellini et al., 2003).

3.4.3 Variograms

Step D in the algorithm showed in Figure 24 is about creating an experimental variogram that fits better with the data. Variograms are a statistical tool used to represent the correlation between the spatial data analyzed. It indicates the range within which two data points influence each other. An example of a variogram plot is given in Figure 25. It shows the distance lag vs. semi variance of the data. Sill, range, and

nugget are the values that define the variogram plot. The sill represents the value at which the semi variance reaches the plateau. When this curve attains a plateau, it means that the values are no more correlated. The range is the x-axis value where the sill is reached. The nugget represents the position at which the curve crosses the y-axis. These values are crucial to define the sequential Gaussian simulation for each data set.

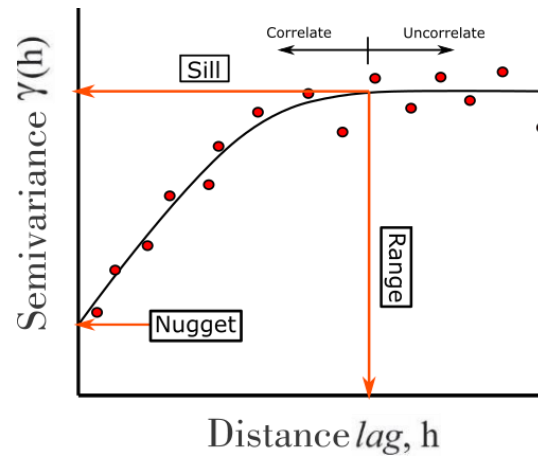


Figure 25. Example of a variogram plot showing its main features. The red circle represents the experimental variogram created from the normally distributed data. The black curve represents the model created to fit the variogram.

Step E is modeling the variogram to get the best fit curve to the experimental variogram. We have different options to model the variograms. The most common models are spherical, exponential, and gaussian (Figure 26).

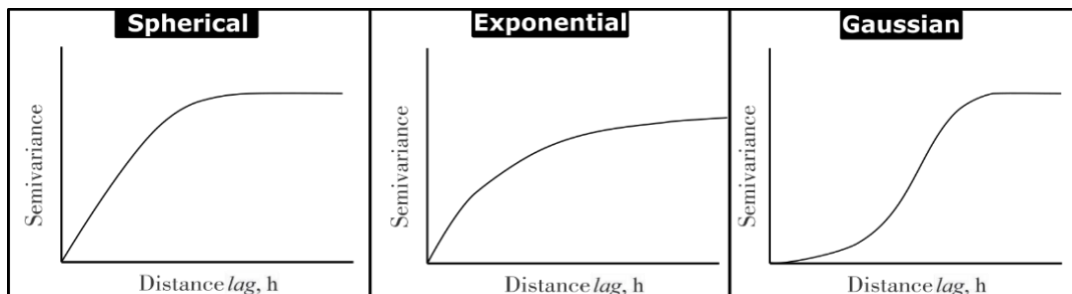


Figure 26. Example of the most used variogram models.

CHAPTER 4: RESULTS

4.1 CO₂ fluxes

4.1.1 Aguas Hediondas

In Aguas Hediondas at the end of the survey we took 303 CO₂ flux measurements, without taking into account the control points. The statistical parameters of the collected data are shown in Table 3. The map in Figure 27 shows the variation in the CO₂ flux measurements. We can observe that the highest values are located inside the restricted area (Figure 8B). We find the two highest values concentrated near the active fumarole and near the hot spring (Figure 8D) and medium values in the surrounding area. Inside the walls, in the restricted area, vegetation is absent. Otherwise, in the external area of the restricted area, the vegetation is more abundant, ranging from small plants and moss to paramo trees that create the surrounding paramo forest. In this part of the surveyed area, we find the lowest values that do not show significant variability.

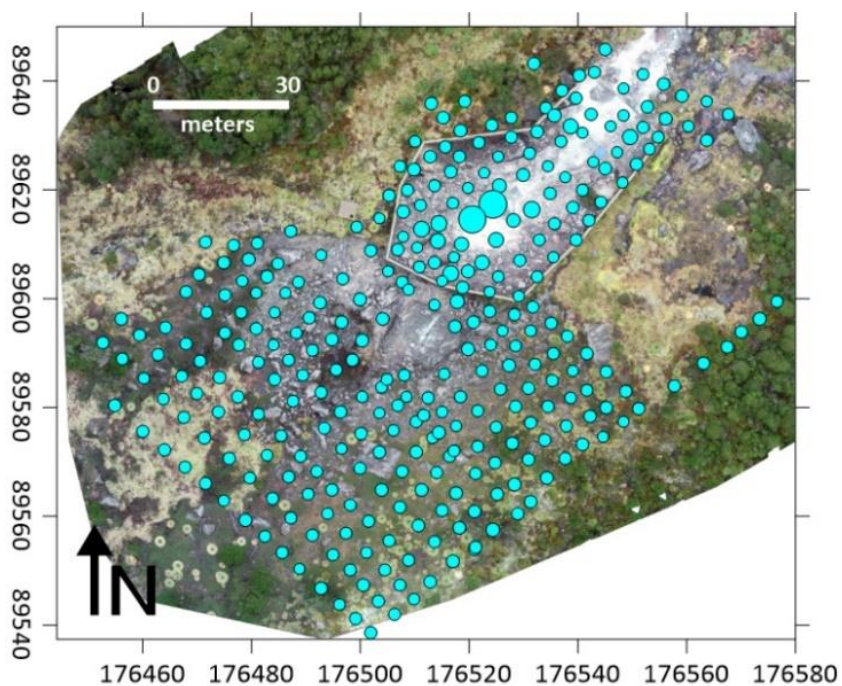


Figure 27. Map of the CO₂ flux measurements ($\text{g m}^{-2} \text{d}^{-1}$) from Aguas Hediondas. The dot sizes are proportional to the CO₂ flux, higher CO₂ fluxes correspond to bigger dots. The map coordinates are in meters, UTM – WGS84 18N.

Table 3. Statistical parameters of the measured CO₂ fluxes at Aguas Hediondas and Lagunas Verdes during December 2020.

Area	No. of measurements	Min.CO ₂ flux (g m ⁻² d ⁻¹)	Max.CO ₂ flux (g m ⁻² d ⁻¹)	Average CO ₂ flux (g m ⁻² d ⁻¹)
Aguas Hediondas	303	0.60	1263.32	17.36
Lagunas Verdes	76	1.59	3614.08	305.92

Following the process to apply the sGs described earlier, we first create the histogram of the collected data (Figure 28A). It is clear that the data does not follow a normal distribution as is usually in Earth sciences data. The histogram is very useful for visualizing the data distribution, which in this case shows the dominance of values around 0 to 100 g m⁻² d⁻¹. On the other hand, we see fewer higher values higher than 1000 g m⁻² d⁻¹. The minimum value besides background value (0 g m⁻² d⁻¹) is 0.60 g m⁻² d⁻¹.

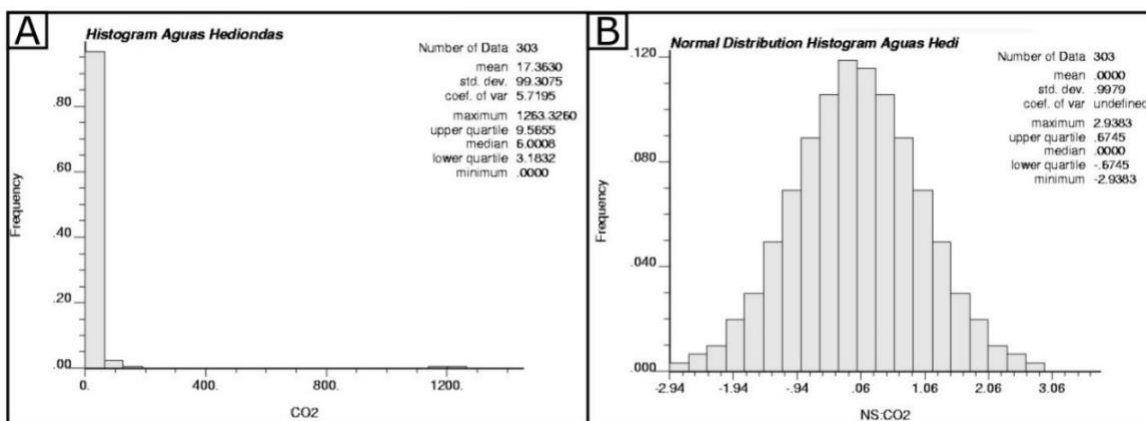


Figure 28. Histograms of the CO₂ flux measurements collected in Aguas Hediondas. A: Histogram of the original collected data of CO₂ flux (g m⁻² d⁻¹) in Aguas Hediondas. B: Histogram of the normal score transformed CO₂ flux data for Aguas Hediondas.

We performed a normal score transformation to convert the data to a normal distribution (Figure 28B). The next step is to create the variogram to be used in the sGs, using the normal score transformed CO₂ fluxes. Once a variogram is obtained, we need to find a model that best fits the variogram. For Aguas Hediondas, the parameters that best fit the data were a spherical model with a sill value of 1.1, a range of 12 meters and a nugget value of 0.7 (Figure 29).

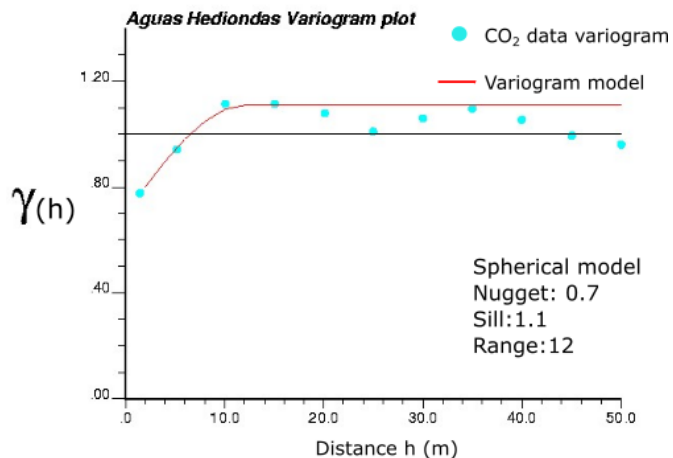


Figure 29. Experimental variogram and variogram model. The light blue dots show the variogram obtained from the normal score transformed Aguas Hediondas CO₂ fluxes. The red line represents the ideal variogram model that best fits the data.

To execute the sequential Gaussian simulation, it is crucial to define the spatial structure of the grid, the kriging type, and the sample density. The kriging type used was simple kriging. The other parameters were defined according to the data properties and the variogram model specifications. Using the results for the simulation, we can visualize the CO₂ flux distribution in the area using the E-type map.

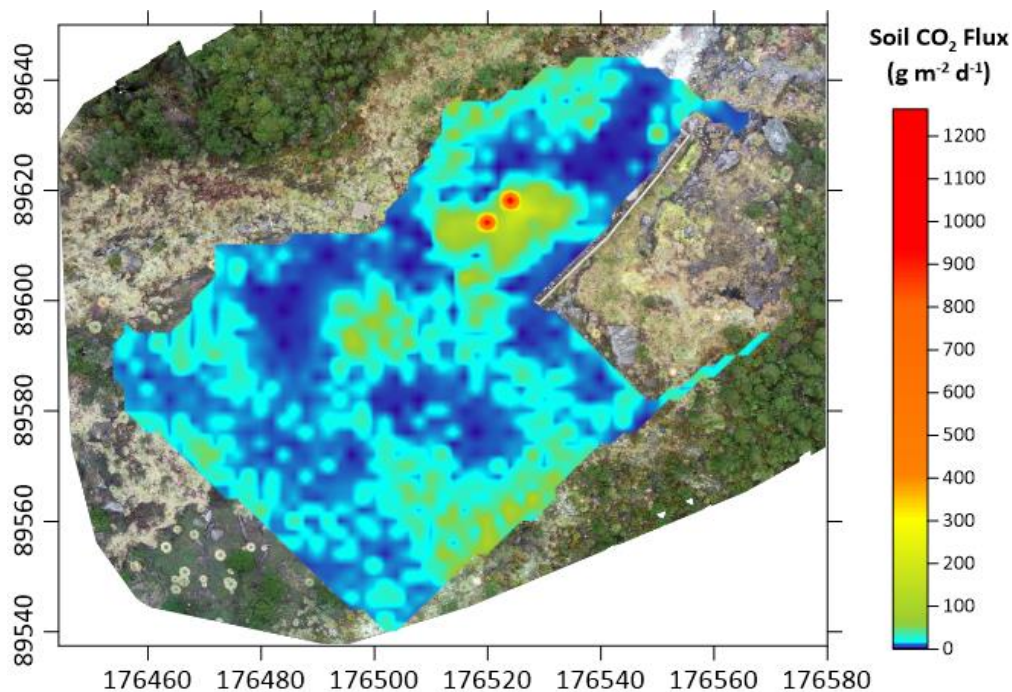


Figure 30. E-type map of the CO₂ diffuse degassing spatial distribution of the average of the 100 sequential Gaussian simulations obtained for Aguas Hediondas survey area. The map coordinates are in meters, UTM – WGS84 18N.

4.1.2 Lagunas Verdes

The total gas measurements in Lagunas Verdes were 76 without the bags/vial samples for isotope analysis. As we see in the statistics summary in Table 3, the maximum value measured in the area is $3614.08 \text{ g m}^{-2} \text{ d}^{-1}$. The average is $305.92 \text{ g m}^{-2} \text{ d}^{-1}$, and the minimum value in spite of the background value is $1.59 \text{ g m}^{-2} \text{ d}^{-1}$.

The map in Figure 31 shows the location of survey points and variation in CO_2 flux. We can observe that high values are located mainly in the lower part of the old fumarolic field. However, we find two high values in the upper part. It is essential to mention that the highest values are located in parts of the survey area where the vegetation was absent. The lowest values are evenly distributed in both parts of the area.

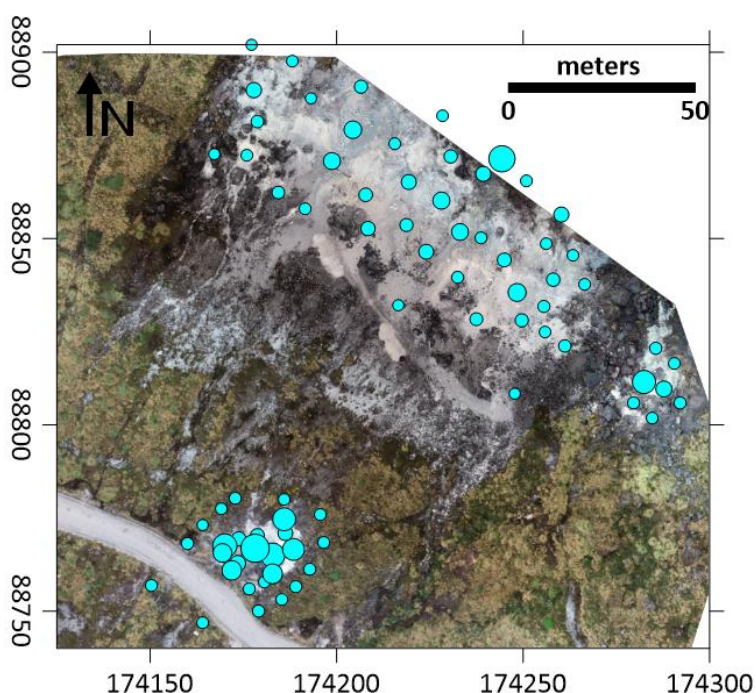


Figure 31. Map of the CO_2 flux measurements ($\text{g m}^{-2} \text{ d}^{-1}$) from Lagunas Verdes. The dot sizes are proportional to the CO_2 flux, higher CO_2 fluxes correspond to bigger dots. The map coordinates are in meters, UTM – WGS84 18N.

Similarly to Aguas Hediondas, the flux data did not follow a normal distribution and we had to apply a normal score transformation (Figure 32). Using the transformed data, we performed the variogram and created the variogram model that best fits the data (Figure 33). The variogram was created using a spherical model with a sill value of 0.97, a range of 22 meters and a nugget value of 0.4.

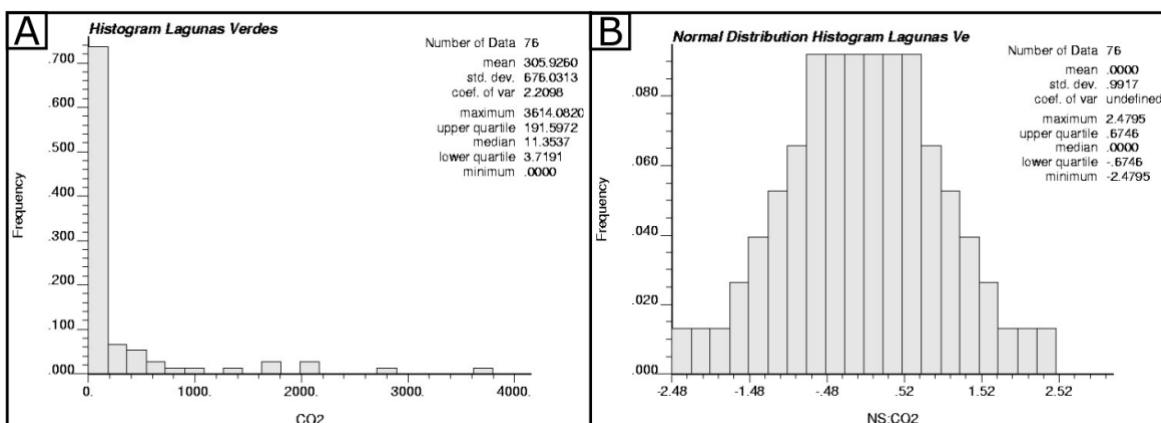


Figure 32. Histograms of the CO_2 flux measurements collected in Lagunas Verdes. A: Histogram of the collected data of CO_2 flux ($g\ m^{-2}\ d^{-1}$) in Lagunas Verdes. B: Histogram of the normal score transformed CO_2 flux data for Lagunas Verdes.

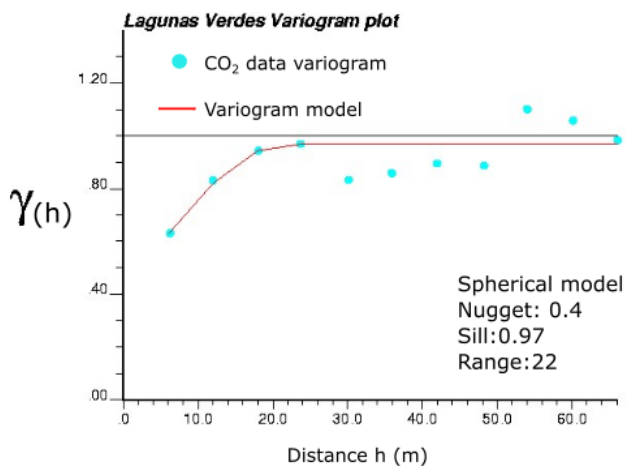


Figure 33. Experimental variogram and variogram model. The light blue dots show the variogram for the normal score transformed Lagunas Verdes CO_2 fluxes. The red line represents the ideal variogram model that better fits the data.

We applied the variogram to the normalized data to perform the 100 simulations. The E-type map resulting from the sGs is shown in Figure 34. As in Figure 31, the data follow the same tendency having high values in the lower part and some in the upper part of the area. Nevertheless, generally, the values in Lagunas Verdes are higher than at Aguas Hediondas.

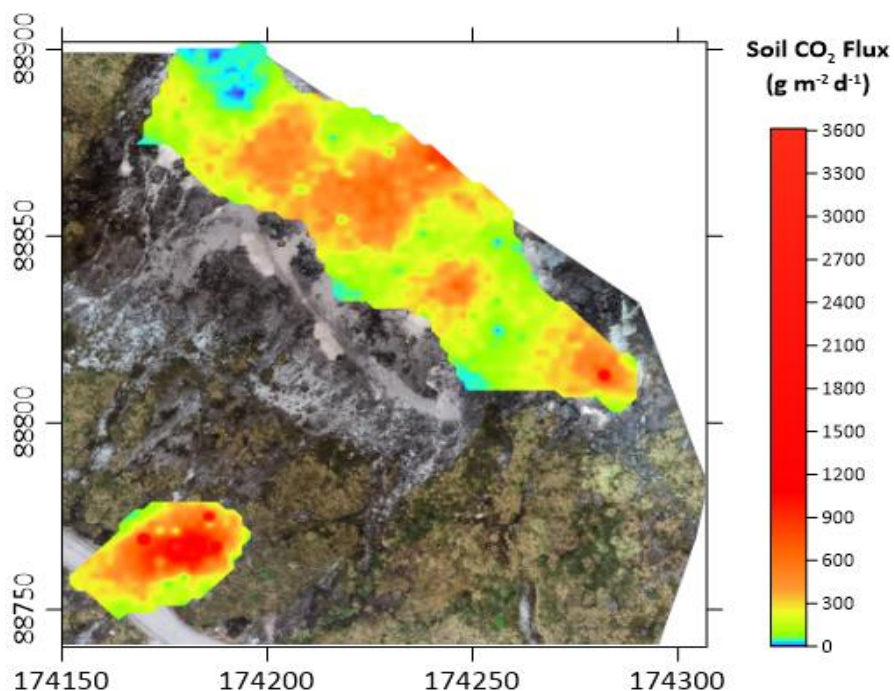


Figure 34. E-type map of the CO_2 diffuse degassing spatial distribution of the average of the 100 sequential Gaussian simulations obtained for Lagunas Verdes survey area. The map coordinates are in meters, UTM – WGS84 18N.

4.2 Isotopic Data

The isotopic analysis results are summarized in Table 4. In Aguas Hediondas, we took 12 samples at seven different survey points. On the other hand, we took four samples in Lagunas Verdes at two survey points. Column 5 in Table 4 contains the isotopic ^{13}C composition measured in the laboratory of each sample. On the other hand, the final $\delta^{13}\text{C}$ ‰ value (Column 8 Table 4) for each survey point was calculated using Equation [3] mentioned in the Methodology chapter, based on the procedure by Chiodini et al. (2008). This procedure is applied mainly to avoid uncertainty in the isotopic composition estimation due to the air pollution from different sources such as anthropogenic CO_2 . This final value was used for the further interpretation of the data.

Table 4. Isotopic $^{13}\text{C}_{\text{CO}_2}$ ($\delta^{13}\text{C}$ ‰) results for both areas, Aguas Hediondas and Lagunas Verdes.

Location	Sample	Sample type	CO_2 flux $\text{g m}^{-2}\text{d}^{-1}$	$\delta^{13}\text{C}$ ‰	\pm	CO_2 ppm (Instrument)	$\delta^{13}\text{C}$ ‰ Final
Aguas Hediondas	CI-2-78L	Bag	25.60	-10.26	0.02	600	-11.81
	CI-2-78H	Bag	18.01	-10.88	0.02	1000	
Aguas Hediondas	CI-3-53L	Bag	19.14	-9.87	0.03	600	-7.92
	CI-3-53H	Bag	12.97	-9.09	0.04	1000	
Aguas Hediondas	CI-5-12L	Bag	11.41	-9.92	0.04	600	-12.88
	CI-5-12H	Bag	8.10	-10.66	0.01	800	
Aguas Hediondas	CI-5-78L	Bag	8.79	-9.87	0.02	550	-13.93
	CI-5-78H	Bag	6.56	-10.08	0.04	580	
Aguas Hediondas	CI-6-9L	Bag	14.20	-10.48	0.01	600	-11.66
	CI-6-9H	Bag	9.91	-10.95	0.03	1000	
Aguas Hediondas	CI-5-49L	Vial	1220.81	-7.155		7000	-7.40
	CI-5-49H	Vial	1165.44	-7.27	0.01	13000	
Lagunas Verdes	CI-7-1L	Vial	412.57	-7.85		4500	-7.69
	CI-7-1H	Vial	408.62	-7.76	0.07	10000	
Lagunas Verdes	CI-7-2L	Vial	731.29	-7.58		5000	-7.00
	CI-7-2H	Vial	706.85	-7.29	0.04	10000	

The location of survey points where samples for isotopic analysis were taken is shown in Figure 35. As we can observe, the values for Aguas Hediondas range from -13.93 to -7.40 ‰, and from -7.69 to -7.00 ‰ in Lagunas Verdes.

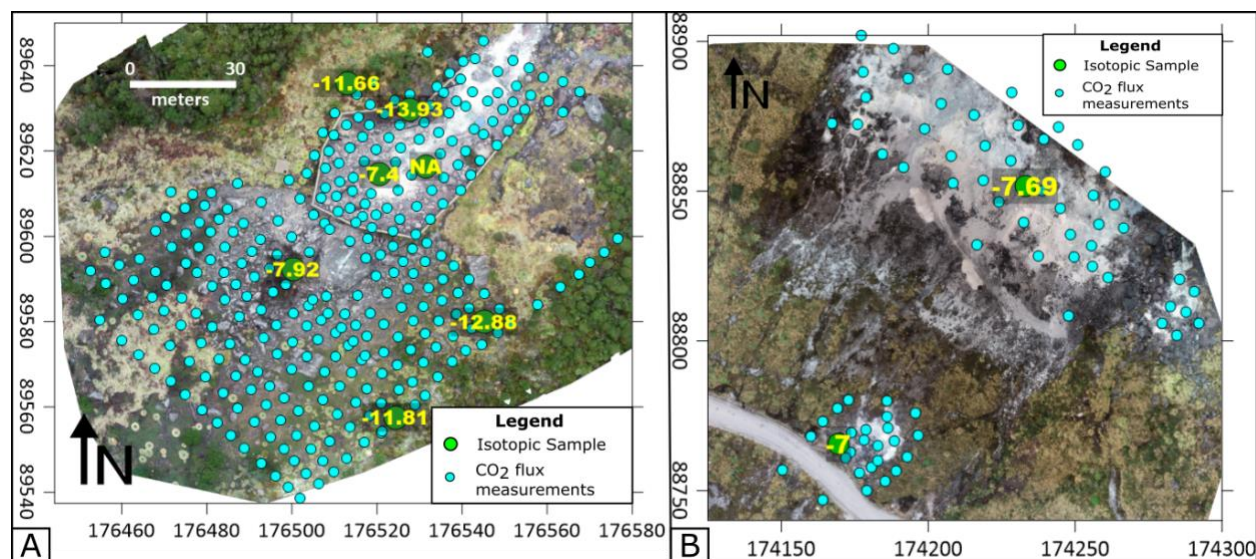


Figure 35. Location of the CO_2 flux measurements and isotopic samples labeled with the isotopic results. A: Aguas Hediondas map. B: Lagunas Verde map. The map coordinates are in meters, UTM – WGS84 18N.

4.3 Soil Temperature

4.3.1 Aguas Hediondas

In Aguas Hediondas, we took 286 soil temperature measurements at the same points where the CO₂ flux measurements were taken. The temperature values range from 1.70 to 28.60 °C. The average of the values is 10.38 °C, as is shown in Table 5.

Figure 36 shows the distribution of soil temperature measurements. We can appreciate that the highest values are located in the restricted area. The highest value is located on the border of the hydrothermal spring channel, at the edge of the restricted area walls. In contrast, the measurements of the rest of the area are mainly medium values and some low values without a great variability. We can find the lowest value in the northern part, outside the restricted area.

Table 5. Statistical parameters of the measured Soil temperature at Aguas Hediondas and Lagunas Verdes during December 2020.

Area	No. of measurements	Min. Soil Temperature (°C)	Max. Soil Temperature (°C)	Average Soil Temperature (°C)
Aguas Hediondas	286	1.70	28.60	10.38
Lagunas Verdes	74	5.90	13.20	9.26

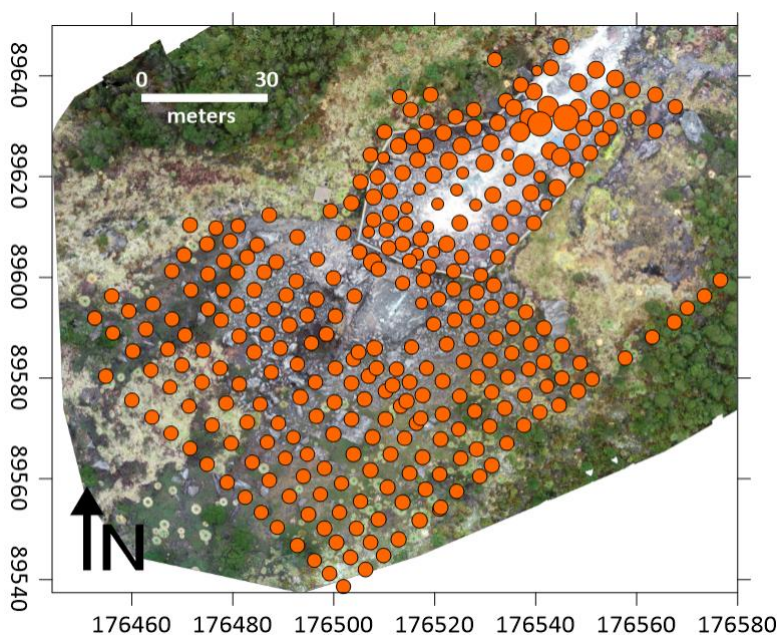


Figure 36. Map of the soil temperatures measurements (°C) from Aguas Hediondas. The dot sizes are proportional to the soil temperature, higher temperatures correspond to bigger dots. The map coordinates are in meters, UTM – WGS84 18N.

We have followed the same statistical process as for the CO₂ flux to model the soil temperature distribution. Therefore, our first step was creating the histogram of the data (Figure 37A), and, as it did not follow a normal distribution, we transformed it into a normal score distribution (Figure 37B).

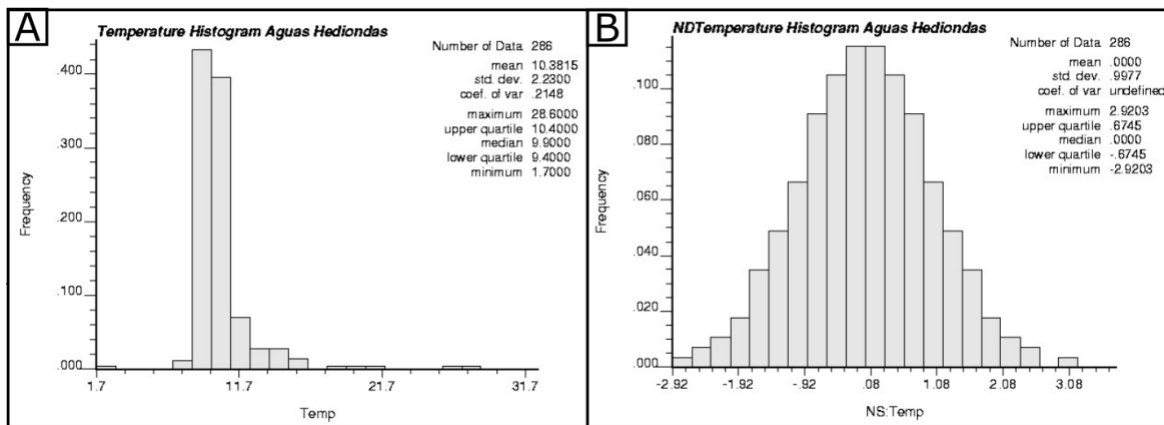


Figure 37. Histograms from the soil temperature (°C) collected in Aguas Hediondas. A: Histogram of the collected data of soil temperature (°C) in Aguas Hediondas. B: Histogram of the normal score transformed soil temperature (°C) in Aguas Hediondas.

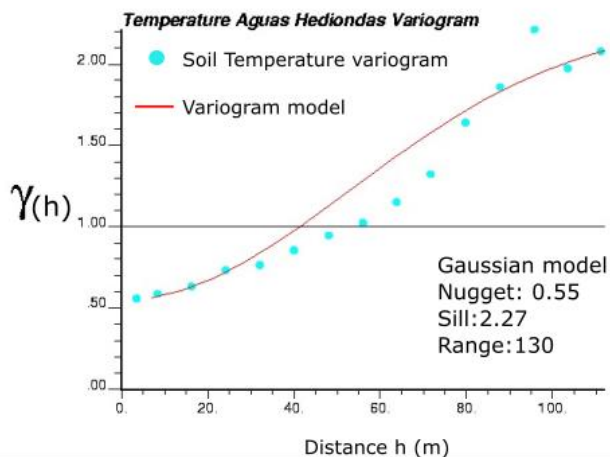


Figure 38. Experimental variogram and variogram model. The light blue dots show the variogram for the normal score transformed Aguas Hediondas Soil Temperature. The red line represents the ideal variogram model that better fits the data.

The next step was to create the best variogram to have the best fit curve of the normalized soil temperature data. A Gaussian variogram model was used, with a sill of 2.27, a range of 130 meters and a nugget of 0.55.

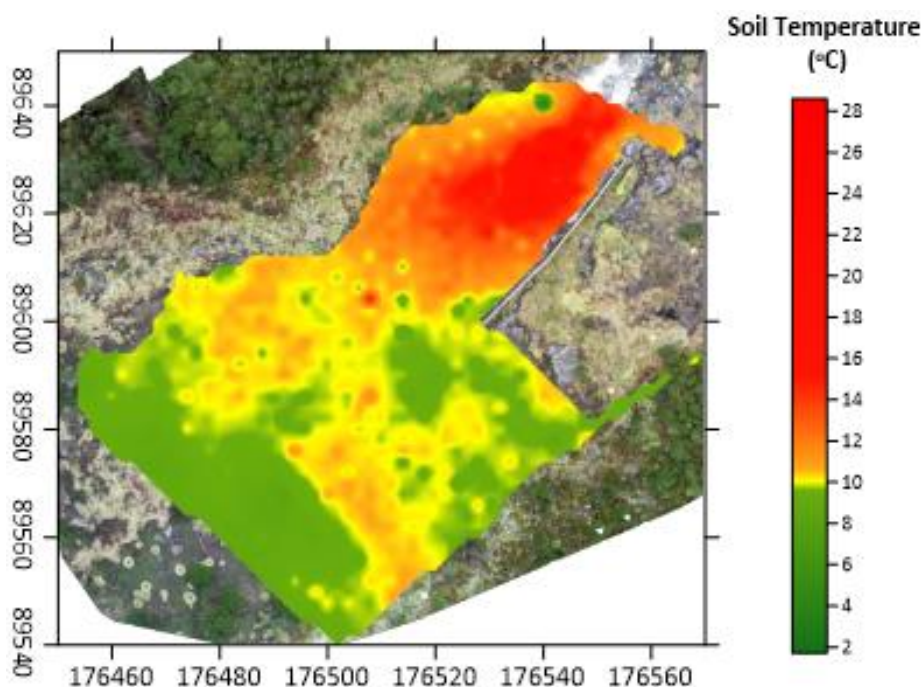


Figure 39. Map of the Soil Temperature distribution in Aguas Hediondas. E-type map of the Spatial distribution of the average of the 100 sequential Gaussian simulations. The map coordinates are in meters, UTM – WGS84 18N.

The result from the E-type map of the soil temperature distribution in Aguas Hediondas is shown in Figure 39. The average of 100 simulations of the soil temperature shows a similar tendency as Figure 36. The highest values are concentrated mainly in the restricted area, at the northeastern edge. The highest values (red color) follow the hydrothermal spring channel. On the other hand, we can see the minimum value in the northern part, outside the restricted area. The rest of the area has medium values predominance, with some areas in greenish that represent low values.

4.3.2 Lagunas Verdes

The soil temperature measurements in Lagunas Verdes are 74, where the minimum and maximum values are 5.90 and 13.20 °C, respectively. The average of the values is 9.26 °C. These statistical values are summarized in Table 5.

Figure 40 shows the location of the measured soil temperature in Lagunas Verdes. We observe that the highest values (bigger dots) are located predominantly in the upper part of the survey area. The lower part is mainly constituted by lower values (smaller dots). High values do not show a clear tendency in the distribution, they are dispersed along the upper area.

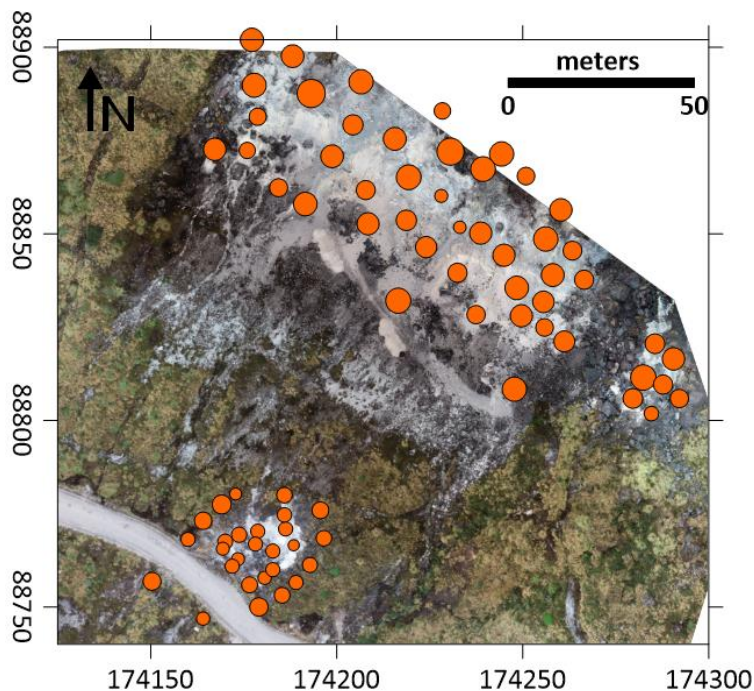


Figure 40. Map of the Soil temperatures measurements ($^{\circ}\text{C}$) from Lagunas Verdes. The dot sizes are proportional to the Soil temperature, higher temperatures correspond to bigger dots. The map coordinates are in meters, UTM – WGS84 18N.

The histogram for soil temperatures at Lagunas Verdes shows more variability in the values than in the case of Aguas Hediondas. Nevertheless, the data is not normally-distributed and requires a normal score transformation (Figure 41) before performing the sGs.

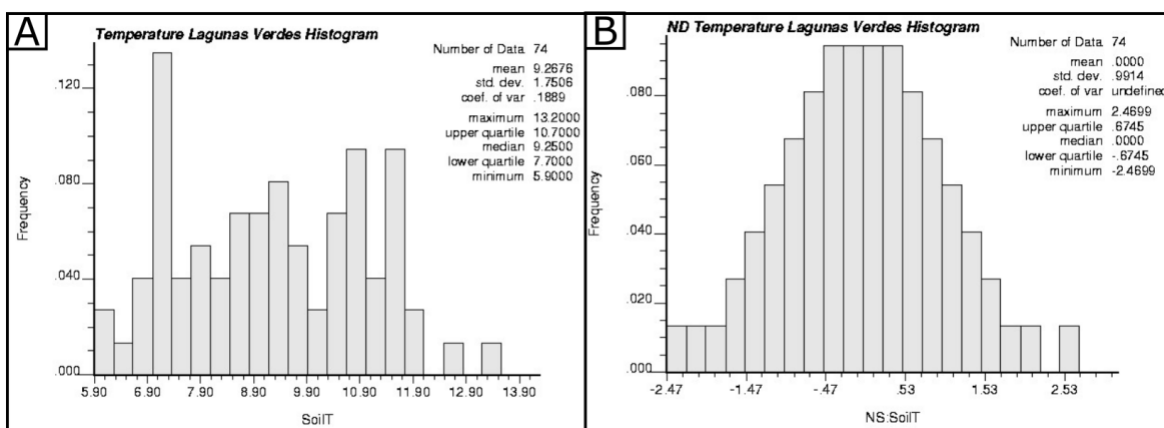


Figure 41. Histograms from the Soil Temperature ($^{\circ}\text{C}$) collected in Lagunas Verdes. A: Histogram of the collected data of Soil Temperature ($^{\circ}\text{C}$) in Lagunas Verdes. B: Histogram of the normal score transformed Soil Temperature in Lagunas Verdes.

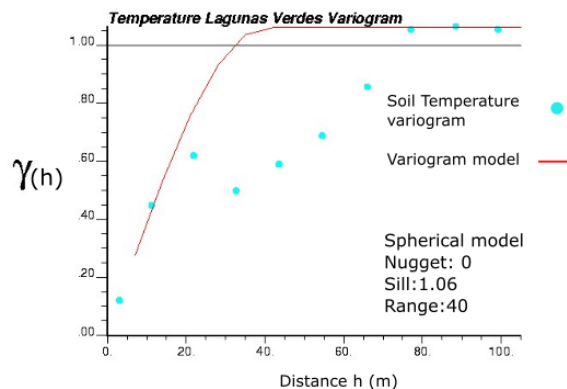


Figure 42. Experimental variogram and variogram model. The light blue dots show the variogram for the normal score transformed Lagunas Verdes Soil Temperature. The red line represents the ideal variogram model that better fits the data.

In this case, the experimental variogram was modelled with a sill at 1.06 in a range of 40 meters and nugget of 0 (Figure 42). In this case, we applied a spherical model, which was the type that best fitted the data. The E-type map of the soil Temperature distribution for the Lagunas Verdes area is presented in Figure 43. The 100 simulation average shows similarities with the distribution of the values in Figure 40. The highest values are located in the upper part, where the predominant color is yellow-reddish, representing the highest values of the data. However, we can note that there are some parts with lower values (greenish areas). The green color covers the lower part of the area, representing the lower soil temperature values.

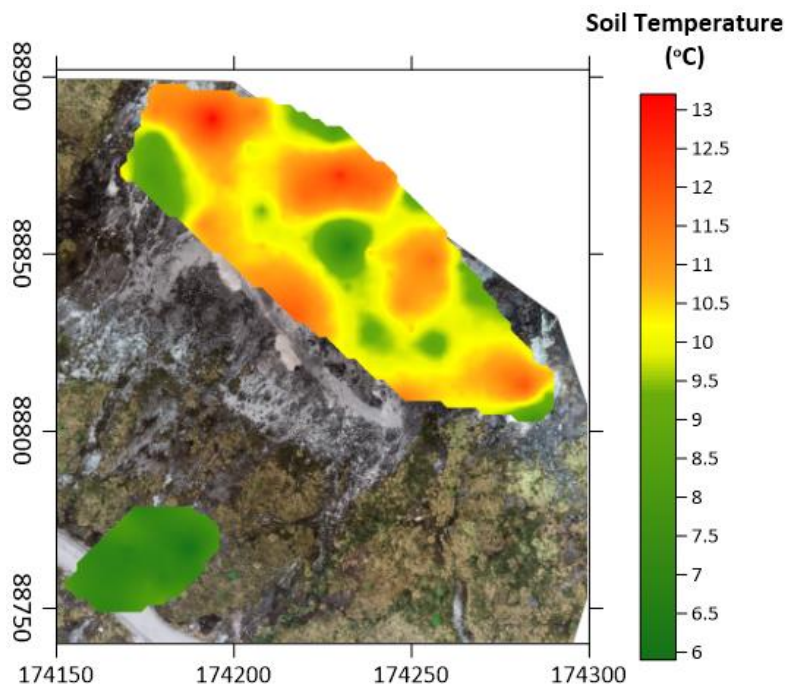


Figure 43. Map of the Soil Temperature distribution in Lagunas Verdes. E-type map of the Spatial distribution of the average of the 100 sequential Gaussian simulations. The map coordinates are in meters, UTM – WGS84 18N.

CHAPTER 5: DISCUSSION

5.1 Control points

Despite CO₂ soil emission appearing to be only influenced by biogenic and hydrothermal sources, several studies have shown that environmental factors can significantly influence CO₂ flux. Meteorological changes like air temperature, soil moisture, soil temperature, barometric pressure, and wind speed, in some instances, can be responsible for more than 50% of the flux variations (Granieri et al., 2003, 2010; Viveiros et al., 2009, 2015; Oliveira et al., 2018).

In Aguas Hediondas, we took control points in two locations in the area to recognize the flux variation and the different parameters that influence it. The first point, 'Wall Control Point,' is located on the east side of the restricted area wall near to the hydrothermal spring area. The second point is located in the southern part of the area, near the paramo forest (Figure 22). Table 6 summarizes the different measurements taken at both control points. The control points were taken at the beginning of the fieldwork (morning) and the end of the fieldwork (afternoon) each day. However, in some cases, just one measurement was taken.

Table 6. Control point measurements. Different parameters measured in the control points taken in Aguas Hediondas on different days. Detail explains if the sample point was measured during the morning (around 7:00 to 8:00 am) or in the afternoon (around 4:00 pm).

Field work day	Date	Detail	CO ₂ Flux (g m ⁻² d ⁻¹)	Air Temp (°C)	Soil Moisture (% VWC)	Soil Temp (°C)	Barometric Pressure (mbar)
Wall Control point							
2	7-Dec-20	Afternoon	4.33	10.1	32.6	10.6	662.2
3	8-Dec-20	Morning	0.00	6.4	35.9	9.6	664.7
	8-Dec-20	Afternoon	1.33	11.2	34.7	11.7	663.7
5	10-Dec-20	Morning	0.00	6.8	45.3	7.4	663.5
	10-Dec-20	Afternoon	6.50	8.6	40.8	15.4	662.2
6	11-Dec-20	Morning	0.00	8.3	44	10.6	662.9
Paramo Control point							
3	8-Dec-20	Morning	14.33	6.52	47.5	8.5	664.7
	8-Dec-20	Afternoon	12.90	11.2	38.4	9.4	662.6
5	10-Dec-20	Morning	0.00	7.12	44.9	8.3	662.8
	10-Dec-20	Afternoon	7.08	8.6	17.8	8.7	661
6	11-Dec-20	Morning	5.88	8.3	33	7.9	660.3

5.1.1 The role of barometric pressure

According to Viveiros et al. (2009), barometric pressure is one of the meteorological factors that most influences CO₂ fluxes. Table 6 and Figure 44 show the variation between the barometric pressure and the CO₂ flux. In 'Wall Control point,' we can appreciate the association between the highest CO₂ flux measurement and the lowest barometric pressure in the afternoon measurement field workday 5. The highest barometric pressures are, in turn, associated with low or null CO₂ fluxes. This inverse correlation has been observed in other studies in long time series of CO₂ flux data (Chiodini et al., 1998; Evans et al., 2001; Granieri et al., 2003; Viveiros et al., 2009). The barometric pumping effect can explain the negative relationship between barometric pressure and CO₂ flux. The pressure gradient drives this effect. In the degassing system, the pore pressure at depth is usually larger than at the surface. When the atmospheric pressure decreases, the gradient across the surface increases, allowing more CO₂ degassing from depth. On the opposite, the high atmospheric pressure forces it back into the ground (Viveiros et al., 2009; Rinaldi et al., 2012).

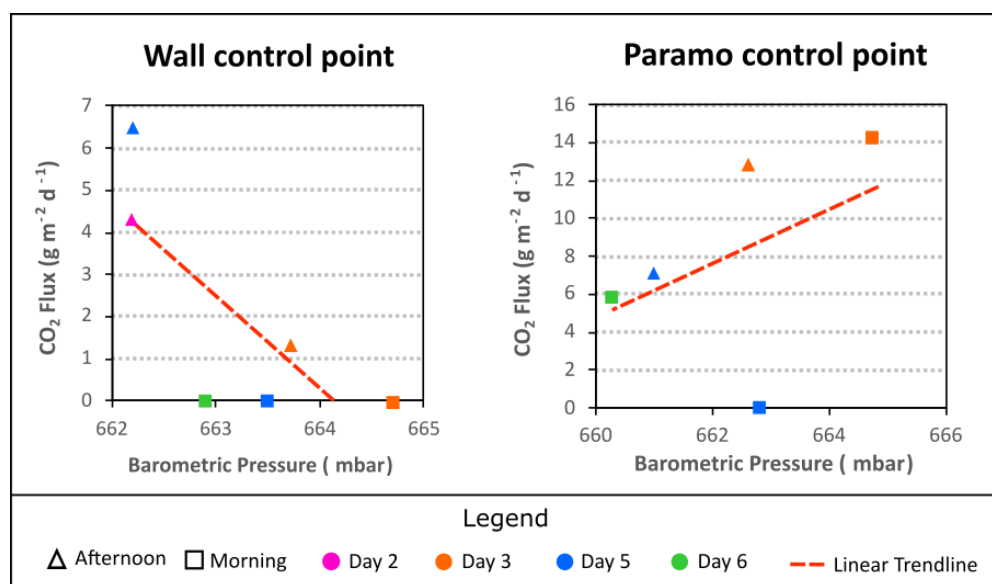


Figure 44. Atmospheric pressure (mbar) vs. CO₂ flux (g m⁻² d⁻¹) of the control points measurements.

In 'Paramo control point,' this tendency is not straightforward. The highest barometric pressure value is associated with the highest CO₂ flux, and the lowest barometric pressure is associated with the second-lowest CO₂ flux value. This could imply that another variable is more influencing in the degasification than the barometric pressure. Besides, the barometric pressure can be directly proportional to the CO₂ flux degassing if we consider that an increase in the barometric pressure can increase the contribution due to density (Rinaldi et al., 2012).

5.1.2 The role of soil moisture

Another measurement taken in the control points was soil moisture which could be related with rainfall. In Table 6 and Figure 45, we can observe that there are changes between the morning and afternoon measurements taken on the same day. In the majority of the cases, we can recognize that in the afternoon, we have greater CO₂ flux. At the same time, the soil moisture decreases in comparison with the morning measurement. Based on this, we can consider a negative relation between the soil moisture and the CO₂ flux, i.e., the CO₂ soil degassing decreases with increasing soil moisture. This effect can be explained by the water effect on the soil porosity. Water infiltration can fill the porosity of soils and create an impermeable barrier and obstruct the release of the gas to the surface dispersing it to a dry area (Granieri et al., 2003; Viveiros et al., 2015). However, this correlation can be highly influenced by other factors such as the topography, the drainage system, and the porosity of the soil (Viveiros et al., 2009).

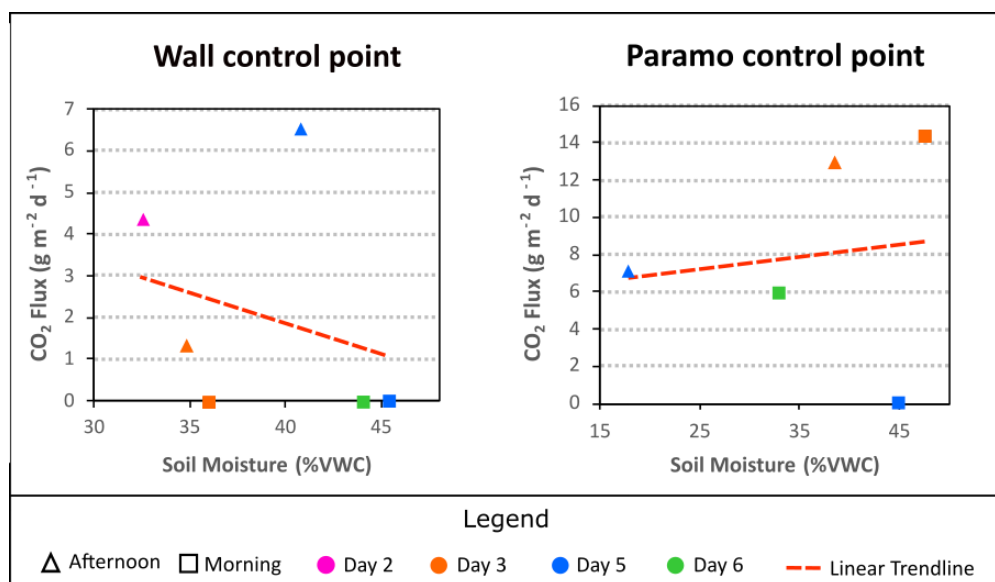


Figure 45. Soil moisture (%VWC) vs. CO₂ flux (g m⁻² d⁻¹) of the control points measurements.

5.1.3 The roll of air temperature

Air temperature is another meteorological variable measured in the control points. Our results show a positive relationship between this variable and the CO₂ fluxes in most of the measurements taken on the same day (Figure 46). Some studies have got as result an inverse correlation between these two variables (Rinaldi et al., 2012; Viveiros et al., 2014). The fluid properties could explain this relation. The air temperature changes the gas fluid mobility relating lower temperature with lower viscosity and higher CO₂ density. Thanks to buoyancy properties, higher density drives the gas upward motion, resulting in higher CO₂ fluxes (Rinaldi et al., 2012). On the other hand, in the study performed by Oliveira et al. (2018)

they observed a positive correlation between the air temperature and the CO₂ flux. They attribute this kind of relationship to a superposition of more influence environmental variables and the influence of the thermal anomalies where the control points were located. Therefore, in our study case, we cannot determine if the air temperature significantly influences by itself the CO₂ flux emission in both areas.

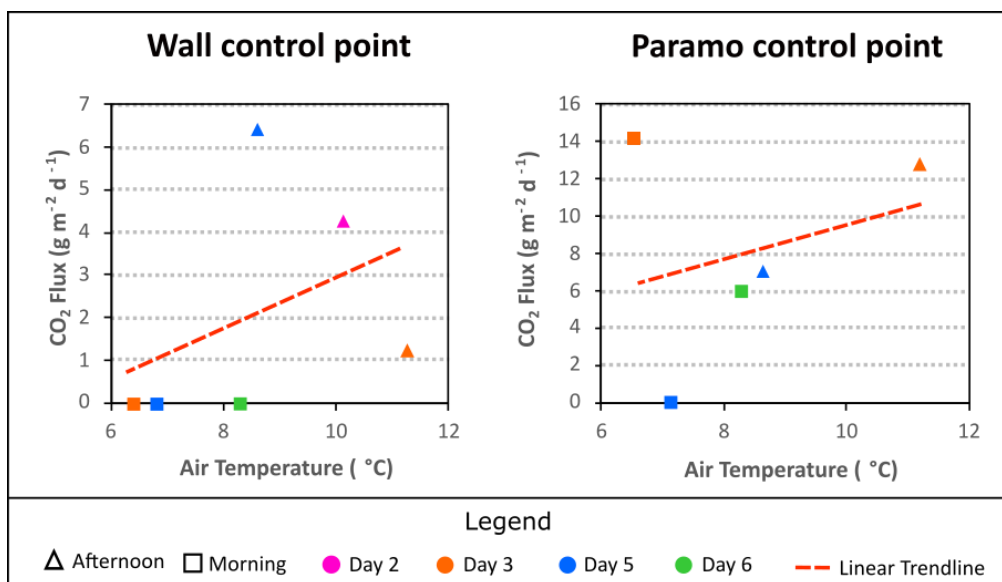


Figure 46. Air temperature (°C) vs. CO₂ flux (g m⁻² d⁻¹) of the control points measurements.

5.1.4 The roll of soil temperature

Soil temperature is the last variable measured in the control points. We can notice a variation in this variable between both control points (Figure 47). In the case of 'Wall Control Point,' in general, we got higher soil temperature values (Table 6) than in 'Paramo Control point.' Now analyzing each control point, we can appreciate that in the case of 'Wall Control Point,' the highest fluxes are associated with the highest soil temperature. On the other hand, the lowest fluxes are associated with the lowest CO₂ fluxes. In the case of the Paramo control point, the tendency is not so evident. The location of each control point plays a crucial role. The location of the hydrothermal spring near the 'Wall control point' has an influence on the soil temperature in that area. This we do not see in the 'Paramo control point' where the predominant feature of the area is the vegetation that covers the area. However, we can still see higher CO₂ fluxes associated with higher soil temperatures. The positive relation between both variables in the case of 'Wall Control Point' could be explained by the hydrothermal hot spring located in the area. The lack of vegetation in the 'Wall control point' area could also influence the afternoon/morning soil temperature variation. The direct heating from the sun could easily reach the 'Wall control point, which is directly exposed. The case for 'The Paramo control point is different, where we have a vegetation layer

that covers the control point, avoiding the soil's exposure to the sun's rays. Therefore, in the case of the 'Paramo control point, the morning/afternoon soil temperature variation is not too big compared to the 'Wall control point.' On the other hand, in Paramo Control Point, the soil temperature can be influenced more by biological oxidation because of its location. This control point is located on a paramo forest where the oxidation of vegetation can release heat, increasing the soil temperature and increasing the CO₂ flux emission (Viveiros et al., 2015).

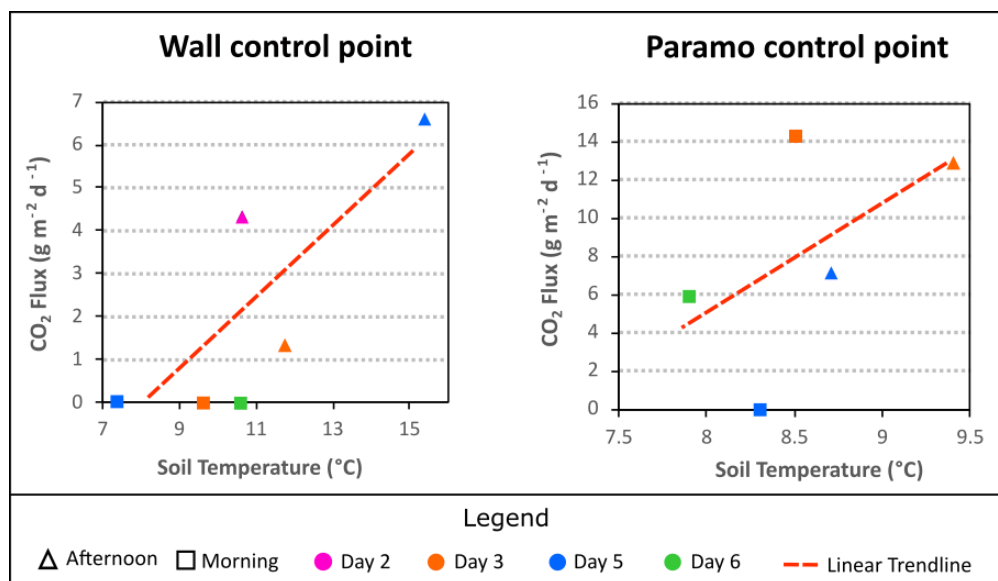


Figure 47. Soil Temperature (°C) vs. CO₂ flux (g m⁻² d⁻¹) of the control points measurements.

5.2 Soil Temperature Distribution

Soil temperature measurements were taken in both survey areas to recognize thermal anomalies and a relationship pattern between soil temperature and soil CO₂ degassing. In previous studies, a positive correlation between these two variables has been found (Fischer & Chiodini, 2015; Giammanco et al., 2016; Roulleau et al., 2017; Taussi et al., 2021). This positive correlation is explained by the ascent of deeper hot hydrothermal fluids. Hot hydrothermal fluids release steam, which condenses near the surface and heats surrounding soil thanks to the thermal energy released. The CO₂, instead, is not a condensable gas; therefore, it is released by diffuse degassing through the soil (Stix, 2015).

Aguas Hediondas is the survey area with more data density. Figure 30 and Figure 39 are the soil CO₂ flux emission map and the soil temperature distribution, respectively. If we compare both maps, we can see some similar patterns. The most remarkable pattern is located inside the walls, 'the restricted area' on the north-east side of the area. As we mentioned in the results, in this area, we got the highest CO₂ flux

emissions in the area. In the same region, we can observe the predominance of red color, which implies that the highest soil temperature follows the hot spring channel. The hydrothermal spring in the area can be the primary driver for this positive correlation for the same reasons as the influence of soil temperature on CO₂ fluxes. Therefore, this area is dominated by the diffusive – advective fluxes, where the hydrothermal hot springs play the role of the pressure-driven viscous flow that transports the hydrothermal gases to the surface and heats the soil at the same time (Taussi et al., 2021). Furthermore, the $\delta^{13}\text{C}$ ‰ values from the samples taken in this area are high, implying a more significant influence of the deep hydrothermal CO₂ source than other sources such as the biogenic CO₂.

The rest of the area follows the same pattern in both maps, with low CO₂ fluxes areas associated with low soil temperature. The areas with medium Soil CO₂ fluxes are associated with medium soil temperature. The deep hydrothermal CO₂ source can drive this relation between the CO₂ flux emission and soil temperature, as was explained before. However, in this case, it is necessary to consider another source of CO₂ and heat which is the biogenic influence. In this area, there is the presence of vegetation which was not the case in the ‘restricted area’ where the vegetation was absent. As explained before, the vegetation can contribute to CO₂ emissions through the respiration process and, besides, heating the soil thanks to the oxidation of organic matter (Viveiros et al., 2015). However, the heat source from the vegetation is cooler compared with the hydrothermal origin source. The contribution of biogenic sources in this area agrees with our isotopic data. In this area, we obtained the lowest $\delta^{13}\text{C}$ ‰ values. Low $\delta^{13}\text{C}$ ‰ values are not associated with deep CO₂ hydrothermal, but with a biogenic CO₂ contribution.

Lagunas Verdes area follows a different pattern between soil CO₂ diffuse degassing and soil temperature. Firstly, we can notice that the maximum soil temperature is lower than the maximum soil temperature in Aguas Hediondas. When we compare Figure 34 and Figure 43, the map of soil CO₂ diffuse degassing map and soil temperature map, we can see some tendencies. The upper area has a positive relationship with the CO₂ emissions. In the majority of the areas where we have high fluxes, we have high soil temperatures. One exception to this tendency is in the location of the higher soil temperature (northwestern corner of the area), which is associated with low CO₂ fluxes. Contrastingly, the soil temperature was the minimum in the lower part, where we measured the highest CO₂ fluxes. This effect suggests a negative correlation between the soil temperature and the soil CO₂ flux in this area.

This relationship can be explained by cold degassing. This effect implies removing the steam component that heats the soil in thermal areas and just having a source of CO₂ flux high enough to create a high CO₂ diffuse degassing at the surface (Rahilly & Fischer, 2021). One process to remove the steam component

could be the mix of deep hydrothermal water and meteoric water. The deep hydrothermal water contributes with hydrothermal gases such as CO₂. The meteoric water cools enough the hydrothermal water to avoid the creation of hot water vapor at depth (Bergfeld et al., 2012).

Last but not least is essential to mention that the vegetation in the area is very little, being much less than in Aguas Hediondas. Besides, considering that the two $\delta^{13}\text{C}$ ‰ values from the CO₂ gas samples in this area are high, it implies a more significant contribution from deep hydrothermal CO₂ compared to its biogenic counterpart. Therefore, we can expect less biogenic influence in both measurements, CO₂ flux, and soil temperature.

5.3 Volcanic CO₂ contribution to the Diffuse Degassing

5.3.1 Mixing model with isotopes

Discriminating between the different sources of CO₂ is one of the main objectives of this study. We decided to use the isotopic composition of the CO₂ gas samples ($\delta^{13}\text{C}_{\text{CO}_2}$) to differentiate between biogenic and hydrothermal CO₂ contributions. The results that we obtained for the isotopic analysis in both sites (Table 4) have shown mainly that in areas without vegetation, the samples have higher isotopic values (-7 to -8 ‰). The values are lower in areas with vegetation (-11 to -14 ‰) (Figure 35). Here we can remember the isotopic signature; we can see that the highest values of $\delta^{13}\text{C}_{\text{CO}_2}$ usually correspond to volcanic hydrothermal emissions and the lowest to biogenic CO₂ emissions. Therefore, we realized that variations of $\delta^{13}\text{C}_{\text{CO}_2}$ values could suggest the presence of three different populations: deep hydrothermal CO₂, biogenic CO₂, and a mixture of the two.

We can estimate the isotopic ¹³C signature of hydrothermal and biogenic CO₂ from the literature. There is no fumarolic data for Chiles, but data from Cumbal (less than 10 km away) and Galeras (70 km away), two close-by volcanoes (Figure 5A), indicate a deep CO₂ source with $\delta^{13}\text{C}_{\text{CO}_2}$ values of around -7 ‰ (Fischer et al., 1997; Sano et al., 1997; Lewicki et al., 2000). For the biogenic, plants have varying values according to the plant type, but a study of paramo soils in Ecuador, in a similar environment, gave a value of -24 ‰ (Chapela et al., 2001). We applied a mixing model (Figure 48) to determine the biogenic flux, i.e., how much CO₂ is produced from biogenic processes only. It was modeled using an isotopic ¹³C composition for the hydrothermal source of -7 ‰ and for the biogenic source of -24 ‰, the values between these two would represent a mixture of both sources. The mixing curve lines for the biogenic flux were modeled based on this. A biogenic flux of 7 g m⁻² d⁻¹ does not explain some of the values measured, with two sample points outside the curve. With a flux of 50 g m⁻² d⁻¹, the mixing curve is too far from the sample points. A

flux of $15 \text{ g m}^{-2} \text{ d}^{-1}$ best fits the data. As a result, we estimate that the biogenic flux has a maximum value of $15 \text{ g m}^{-2} \text{ d}^{-1}$.

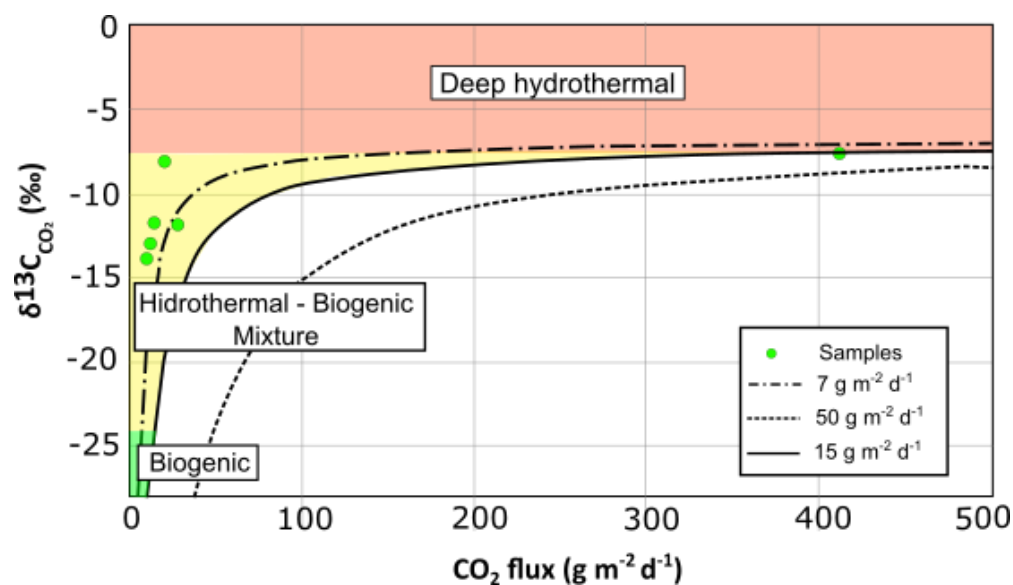


Figure 48. Diagram plotting $\delta^{13}\text{C}_{\text{CO}_2}$ ‰ isotopic composition vs. CO_2 flux ($\text{g m}^{-2} \text{ d}^{-1}$) of each gas sample taken in the field. The different lines represent theoretical flux rates based on a mixing model. The plot represents the corresponding ranges from the different CO_2 sources: Biogenic, deep hydrothermal, and a mixture.

5.3.2 Probability maps for soil CO_2 flux

Probability maps are excellent for estimating the deep hydrothermal CO_2 contribution to an area soil CO_2 diffuse degassing. Besides, they are helpful to identify DDS (Viveiros et al., 2010). The probability map requires a cut-off value to estimate the probability that, at a certain point, the CO_2 flux exceeds this threshold. We used as a cut-off value $30 \text{ g m}^{-2} \text{ d}^{-1}$, twice the maximum biogenic flux estimated before ($15 \text{ g m}^{-2} \text{ d}^{-1}$). Viveiros et al. (2010) recommend using two times higher the estimated maximum biogenic flux to decrease the uncertainty caused by the variability of the biogenic CO_2 fluxes. As a result, probability maps highlight areas where the soil CO_2 diffuse degassing is strongly influenced by deep hydrothermal CO_2 . Thus, we can estimate the CO_2 from a volcanic origin emitted in an area.

Figure 49 shows the resulting probability maps for Aguas Hediondas (A) and Lagunas Verdes (B). In Aguas Hediondas, we can observe 16 locations in the vicinity of the hot spring with a probability of 1 to present a deep CO_2 hydrothermal contribution. This result agrees with the distribution of the CO_2 flux emission, which highest values were located in the same area. The rest of the area presents a low probability of being fed by volcanic origin CO_2 solely. Therefore, we can conclude that in this part of the area, the

biogenic CO₂ source predominates. The conclusion agrees with the fact that the area is covered by more vegetation than in the hot spring area, and it has low CO₂ flux values associated.

Lagunas Verdes in general shows more influence of deep hydrothermal CO₂ than Aguas Hediondas (Figure 49B). The presence of an active fumarole could determine the predominance of direct degassing in the area of Aguas Hediondas. In the case of Lagunas Verdes, the area corresponds to an old fumarolic field; however, there is no evidence of some direct degassing structure in the area. This characteristic implies a predominance of soil CO₂ diffuse degassing in the area, having several points with a probability of 1 of having a contribution of volcanic CO₂ origin. In the lower part of the area, the high probabilistic values are concentrated in one closed circular area, which could represent a DDS. We have less high probabilistic values in the upper area than in the lower part. Nevertheless, some areas have a probability of more than the 50%. The high contribution of deep hydrothermal CO₂ in Lagunas Verdes agrees with our isotopic data obtained there and with the fact that the vegetation is very little in the zone where what prevails is the hydrothermal alteration. Due to the nature of the zone, a good explanation of the high volcanic CO₂ degassing in this area is the presence of a hidden tectonic structure in the area and a significant influence of a deep hydrothermal source that cutcrosses the area beneath the surface.

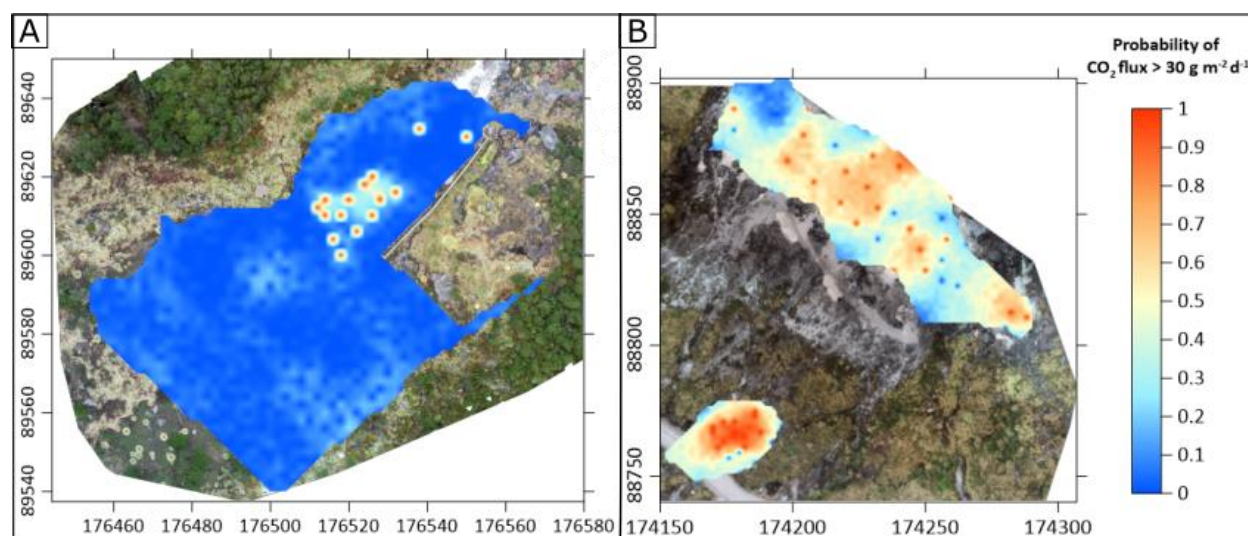


Figure 49. Probability maps for soil CO₂ diffuse degassing at A: Aguas Hediondas and B: Lagunas Verdes. The color scale shows the probability of soil CO₂ flux exceeding the cut-off value (30 g m⁻² d⁻¹). The maps coordinates are in meters, UTM – WGS84 18N.

5.3.3 CO₂ total emission

Finally, following the assumption that the contribution of deep hydrothermal CO₂ source starts with fluxes higher than 30 g m⁻² d⁻¹ we can estimate the total volcanic CO₂ origin emitted per day (Table 7). As we expected, in Lagunas Verdes, the contribution of deep hydrothermal CO₂ emission is more than 80% of

the total CO₂ diffuse degasification of the area (Table 7, column 7). At Aguas Hediondas, instead, it seems to be divided in half between the volcanic CO₂ origin and another source of CO₂ that, in this case, could be a biological source. These total emission values can be helpful as baseline values for further studies in the area, to see variations in the degasification and as a tool for the Chiles volcano activity monitoring.

Table 7. Total CO₂ diffuse degassing output at Aguas Hediondas and Lagunas Verdes. Estimation based on the realization of the 100 Sequential Gaussian Simulation (sGs).

Site	Area (km ²)	Number of points	Total CO ₂ diffuse degassing (t d ⁻¹)	Total CO ₂ emission per area (t d ⁻¹ km ⁻²)	Total deep hydrothermal CO ₂ diffuse degassing	
					(t d ⁻¹)	(%)
Aguas Hediondas	0.006	339	0.11 ± 0.01	18.33 ± 2	0.06±0.02	54.55
Lagunas Verdes	0.005	76	1.66 ± 0.08	332 ± 16	1.49±0.08	89.76

5.3.4 CO₂ diffuse degassing around the world

Soil CO₂ diffuse degassing has been researched worldwide in different degassing areas. Table 8 summarizes some places where the total diffuse degassing was estimated. Comparing this data with our results, we realize that the total CO₂ diffuse degassing estimated in our area is low. However, it is essential to take into account some variables that influence total emissions. The first factor is the survey area extension. In most cases, the survey area covers several kilometers. In our case study, we covered a few meters. Besides, geological factors that also influence the geological framework of the area, tectonic setting, the last volcano eruption, or the current volcano activity state. Besides, environmental factors could influence too, as it was discussed previously in the control points section.

For the purpose of making a good comparison, the CO₂ flux emissions were standardized to obtain the CO₂ emission per unit of area (t d⁻¹ km⁻²). As we can observe in Table 8 in column 5, the emissions are similar to or lower than the resulting CO₂ flux emission per unit of area in Chiles volcano obtained in this research (Table 7, column 5). In Lagunas Verdes, we got an emission of 332 t d⁻¹ km⁻², which result be much higher than the other places in Ecuador, like Cuicocha, and Pululahua calderas. Besides, the value is pretty significant, comparable with places with great volcanic activity, such as Furnas volcano in the Azores

archipelago. This implies tremendous importance in the CO₂ emission in this area, not only on a regional level but on a world scale.

According to Ritchie et al. (2020), the total CO₂ emission in Ecuador correspond to 30.93 million tons just in 2020. This value implies the emission per day is 84 744.55 tons of CO₂. The primary anthropogenic sectors that emit CO₂ in the country are land-use change and forestry, transport, agriculture, waste, and electricity and heat. Comparing this value with the deep hydrothermal CO₂ emission found in this research related to the Chiles volcano, the CO₂ hydrothermal-related input corresponds to 0.002% of the total CO₂ emission in the country. Besides, compared with a significant anthropogenic source such as the transport CO₂ emission, it represents 0.004%. The percentage could appear to be insignificant. However, it is essential to consider that these values just represent the emission of a small area near just one volcano out of the many volcanoes in the country. If we had more data about the CO₂ diffuse emission coming from all active/dormant volcanoes in the country, the percentage would be higher.

Table 8. CO₂ diffuse degassing emitted by degassing areas in different countries.

Study Area	CO ₂ Flux (t d ⁻¹)	Area (km ²)	Number of Points	Total CO ₂ emission per area (t d ⁻¹ km ⁻²)	Reference
Cuicocha Caldera, Ecuador	106	13.30	172	7.97	Padrón et al., 2008
Pululahua caldera, Ecuador	270	27.60	217	9.78	Padrón et al., 2008
Complejo Volcánico Copahue – Caviahue, Argentina	208.5	9	2380	23.16	Lamberti et al., 2020
Peteroa volcano, Argentina	6.5	0.07	125	92.80	Lamberti et al., 2020
Solfatarra volcano, Italy	1500	1	333	1500	Chiodini et al., 2001
Vulcano island, Italy	75	1.90	423	39.47	Chiodini et al., 1996
Furnas volcano, Azores archipelago	968	4.8	2605	201.16	Viveiros et al., 2010
Furnas do Enxofre, Azores archipelago	2.54	0.02	281	127	Viveiros et al., 2020

5.3.5 Diffuse Degassing Structures

Using probabilistic maps, we can recognize diffuse degassing structures (DDS). The locations that show a probability greater than 50% of emitting a CO₂ flux higher than the threshold could be considered a DDS (Viveiros et al., 2010). Following this, we can recognize DDS in Aguas Hediondas and Lagunas Verdes. In Aguas Hediondas, the DDS is located inside the walls in the ‘restricted area.’ They are highly connected with the presence of the hydrothermal spring. On the other hand, in Lagunas Verdes there is the presence of more DDS in different parts of the area. One is located in the lower part of the area, where we got the highest fluxes. Another DDS in the upper part is distributed along the area without following a linear pattern.

Usually, DDS are connected with tectonic structures such as lineaments, fractures and faults. In order to visualize some relationship between tectonic structures and DDS, we map the faults and lineaments in Chiles volcano Area (Figure 50A). In Figure 50A, we can observe that the two surveyed areas are located in areas near faults and lineaments. Lagunas Verdes is near two faults, but not precisely on them; therefore, a relationship between the DDS and one of these faults could be dismissed. However, a hidden tectonic structure could be the main driver for the degassing in this zone. Therefore, it is necessary a deeper understanding of the tectonic setting of the area to understand the degassing pattern found in the area.

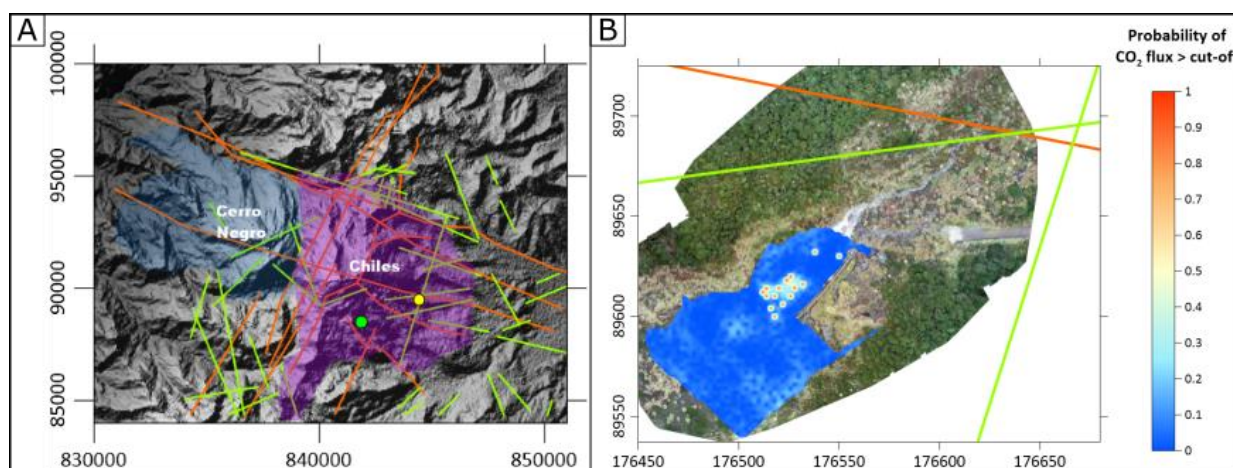


Figure 50. Lineaments (green) and Faults (Orange) that are located in Chiles volcano. A: Chiles volcano general view with the faults and lineaments and the location of the two surveyed areas, Aguas Hediondas (Yellow) and Lagunas Verdes (Green). B: Aguas Hediondas probability map with the lineaments and faults near the area. The maps coordinates are in meters, UTM – WGS84 18N.

Now in the case of Aguas Hediondas, it is located near one fault and two lineaments (Figure 50B). However, it is not located precisely above them. Therefore, we can conclude that the DDS is more related

to the presence of the hydrothermal spring than to a tectonic structure in the area. Besides, these tectonic structures near the area could influence the minor deep hydrothermal CO₂ contribution that we found in the rest of the Aguas Hediondas area. As faults and lineaments represent weak zones, they are good paths for rising CO₂ to the surface. Therefore, further studies near these tectonic structures are crucial to better understand the diffuse degassing of the area.

CHAPTER 6: CONCLUSIONS AND FUTURE WORK

The main conclusions of this research are:

1. Chiles volcano is an area with a geothermal potential that shows superficial expression of the internal heat. It does this not only through hydrothermal springs and active fumaroles but, also by diffuse degassing in the surrounding areas.
2. We can recognize soil CO₂ degasification and thermal anomalies in two areas: Aguas Hediondas and Lagunas Verdes.
3. The isotopic data reveals three populations: deep hydrothermal CO₂, biogenic CO₂ and a mixture of the two. The mixed population is a mix between a deep source with isotopic values of ¹³C ~ -7 ‰, and a biogenic source with isotopic values of ~ -24 ‰ and a flux of 15 g m⁻² d⁻¹.
4. In Aguas Hediondas in general, it seems that most gases are degassing through direct degassing, while diffuse degassing is restricted. It is an area where the soil CO₂ diffuse degassing is dominated by the hydrothermal spring located in the area. The total diffuse degassing in an area of 6 000 m² approx. was about 0.11 t d⁻¹ of which 0.6 t d⁻¹ are contributed by a deep hydrothermal CO₂ source. Moreover, in this area we can appreciate the influence of biogenic CO₂ source due to the presence of abundant vegetation.
5. Lagunas Verdes shows a higher CO₂ flux. It is an area where the deep hydrothermal CO₂ source is predominant along the area. In an area of 5 000 m² covered, the total CO₂ flux degasification corresponds to 1.66 t d⁻¹, of which more than the 80% shows the contribution of a volcanic CO₂ source, 1.49 t d⁻¹. The lack of abundant vegetation in this area just proves the predominance of the volcanic CO₂ source. The DDS in this area could be associated more with a hidden tectonic structure and a deep hydrothermal reservoir which contributes to the area with the hydrothermal gases.
6. The total diffuse CO₂ emissions in the surveyed areas apparently seem lower than in the other studied areas in Ecuador and worldwide. However, comparing the CO₂ emission per day per unit of the area, we can notice a tremendous CO₂ emission rate compared with other diffuse degassing active areas, predominantly what regards Lagunas Verdes. This fact only reinforces the evidence of the geothermal potential of the Chiles volcano.
7. The CO₂ flux emitted in the surveyed areas in Chiles volcano represents 0.002% of the total CO₂ emission in Ecuador in 2020. Besides, it represents 0.004% of a significant anthropogenic source such as the vehicle CO₂ emission. This information can help to refine the global carbon budget where the natural CO₂ inputs need to be better estimated.

For future work a more rigorous survey at Lagunas Verdes could be implemented. Lagunas Verdes is where we got the highest CO₂ fluxes and the more volcanic-related CO₂ δ¹³C ‰ values. Therefore, performing a survey with a regular measurement grid covering a larger area and collecting more isotopic samples for analysis could help us better understand and estimate the CO₂ diffuse degassing capacity in the area.

Besides, a regular CO₂ diffuse degassing in both areas could help understand the Chiles volcano's internal activity. Using the results obtained in this research as a baseline, we can notice variations in the CO₂ diffuse degassing over long periods of time. The results got in this research denote a significant diffuse degassing in the area predominantly regards Lagunas Verdes, which is worthy of regular monitoring.

Extending the survey area would be a good idea, knowing that there is evidence of places such as Lagunas Verdes with high CO₂ diffuse degassing. Performing the same methodology in other hydrothermal areas or other locations around the Chiles volcano can help us better estimate the total CO₂ emission related to the volcano.

The faults and lineaments in the area play a crucial role in diffuse degassing. Therefore, performing a new field mapping campaign to improve the map faults and widen the knowledge about the tectonic structures of the area would help with the understanding and interpretation of the CO₂ diffuse degassing of the area.

Finally, as Chiles volcano is very known for its geothermal potential, research to estimate the thermal energy release and quantify the area's geothermal potential would benefit future geothermal projects. The thermal energy released can be estimated using H₂O/ CO₂ ratio. Therefore, the estimation of CO₂ diffuse degassing of the area is fundamental for this study. As a result, we could see the thermal energy released by the geothermal area in megawatts (MW), which is crucial for implementing geothermal power plants.

REFERENCES

- Agehara, S., & Warncke, D. (2005). Soil alternate wetting and drying pure and temperature effects on nitrogen release from organic nitrogen sources. *Soil Sci Soc Am J*, *69*, 1844–1855.
- Allard, P. (1992). Diffuse degassing of carbon dioxide through volcanic systems.; Observed facts and implications. *Chishitsu Chosajo Hokoku (Report, Geological Survey of Japan);(Japan)*, *279*.
- Angermann, D., Klotz, J., & Reigber, C. (1999). Space-geodetic estimation of the Nazca-South America Euler vector. *Earth and Planetary Science Letters*, *171*(3), 329–334.
- Aspden, J. A., McCourt, W. J., & Brook, M. (1987). Geometrical control of subduction-related magmatism: the Mesozoic and Cenozoic plutonic history of Western Colombia. *Journal of the Geological Society*, *144*(6), 893–905. <https://doi.org/10.1144/GSJGS.144.6.0893>
- Bergfeld, D., Evans, W. C., Lowenstern, J. B., & Hurwitz, S. (2012). Carbon dioxide and hydrogen sulfide degassing and cryptic thermal input to Brimstone Basin, Yellowstone National Park, Wyoming. *Chemical Geology*, *330*, 233–243.
- Bernard, B., & Andrade, D. (2011). Mapa de volcanes cuaternarios del Ecuador continental. *Quito, Ecuador. IGEPN/IRD Poster Informativo*.
- Berner, R., & Lasaga, A. (1989). Modeling the Geochemical Carbon Cycle. *Scientific American*, *222*, 74–82. <https://doi.org/10.1038/scientificamerican0389-74>
- Bezyk, Y., Sówka, I., & Górká, M. (2021). Assessment of urban CO2 budget: Anthropogenic and biogenic inputs. *Urban Climate*, *39*, 100949.
- Blong RJ. (1984). *Volcanic hazards. A sourcebook on the effects of eruptions*. Academic Press.
- Bocanegra, L. C., & Sánchez, J. J. (2017). Mapa de fallas de los volcanes Chiles-Cerro Negro (Nariño) a partir de minería de datos y confirmación de campo. *Boletín de Geología*, *39*(3). <https://doi.org/10.18273/revbol.v39n3-2017005>
- Branney, M., & Acocella, V. (2015). Calderas. In *The encyclopedia of volcanoes* (pp. 299–315). Elsevier.
- Bunt, J. S., & Rovira, A. D. (1954). Oxygen uptake and carbon dioxide evolution of heat-sterilized soil [16]. *Nature*, *173*(4417), 1242. <https://doi.org/10.1038/1731242a0>
- Cardellini, C., Chiodini, G., & Frondini, F. (2003). Application of stochastic simulation to CO2 flux from soil: Mapping and quantification of gas release. *Journal of Geophysical Research: Solid Earth*, *108*(B9). <https://doi.org/10.1029/2002JB002165>
- CELEC, & ISAGEN. (2015). *Informe Geológico Parcial del Proyecto Geotérmico Binacional Tufiño-Chiles-Cerro Negro*. [https://www2.sgc.gov.co/Noticias/boletinesDocumentos/INFORME ESPECIAL CHILES-CERRO NEGRO - 2019 - N1.pdf](https://www2.sgc.gov.co/Noticias/boletinesDocumentos/INFORME%20ESPECIAL%20CHILES-CERRO%20NEGRO%20-2019%20-20N1.pdf)
- Chapela, I. H., Osher, L. J., Horton, T. R., & Henn, M. R. (2001). Ectomycorrhizal fungi introduced with exotic pine plantations induce soil carbon depletion. *Soil Biology and Biochemistry*, *33*(12), 1733–1740. [https://doi.org/https://doi.org/10.1016/S0038-0717\(01\)00098-0](https://doi.org/https://doi.org/10.1016/S0038-0717(01)00098-0)
- Chimbolema, S., Suárez, D., Peñafiel, M., Acurio, C., & Paredes, T. (2013). Guía de plantas de la Reserva ecológica el Angel. *Quito: DCG IMPRESORES*.

- Chiodini, G., Caliro, S., Cardellini, C., Avino, R., Granieri, D., & Schmidt, A. (2008). Carbon isotopic composition of soil CO₂ efflux, a powerful method to discriminate different sources feeding soil CO₂ degassing in volcanic-hydrothermal areas. *Earth and Planetary Science Letters*, 274(3–4). <https://doi.org/10.1016/j.epsl.2008.07.051>
- Chiodini, G., Cioni, R., Guidi, M., Raco, B., & Marini, L. (1998). Soil CO₂ flux measurements in volcanic and geothermal areas. *Applied Geochemistry*, 13(5), 543–552. [https://doi.org/10.1016/S0883-2927\(97\)00076-0](https://doi.org/10.1016/S0883-2927(97)00076-0)
- Chiodini, G., Frondini, F., Cardellini, C., Granieri, D., Marini, L., & Ventura, G. (2001). CO₂ degassing and energy release at Solfatara volcano, Campi Flegrei, Italy. *Journal of Geophysical Research: Solid Earth*, 106(B8), 16213–16221. <https://doi.org/https://doi.org/10.1029/2001JB000246>
- Chiodini, G., Frondini, F., & Raco, B. (1996). Diffuse emission of CO₂ from the Fossa crater, Vulcano Island (Italy). *Bulletin of Volcanology*, 58(1), 41–50. <https://doi.org/10.1007/S004450050124>
- Coplen, T. B. (1996). New guidelines for reporting stable hydrogen, carbon, and oxygen isotope-ratio data. *Geochimica et Cosmochimica Acta*, 60(17), 3359–3360.
- Cortés, G., & Calvache, M. (1997). Informe sobre la evaluación de la amenaza volcánica del Chiles y Cerro Negro. *IGEOMINAS*.
- Delmelle, P., & Stix, J. (2000). *Encyclopedia of volcanoes*. Academic Press: San Diego.
- Deutsch, C., & Journel, A. (1998). *GSLIB Geostatistical Software Library and user's guide*. <http://www.sidalc.net/cgi-bin/wxis.exe/?IsisScript=orton.xis&method=post&formato=2&cantidad=1&expresion=mfn=072548>
- Ebmeier, S. K., Elliott, J. R., Nocquet, J.-M., Biggs, J., Mothes, P., Jarrín, P., Yépez, M., Aguaiza, S., Lundgren, P., & Samsonov, S. V. (2016). Shallow earthquake inhibits unrest near Chiles–Cerro Negro volcanoes, Ecuador–Colombian border. *Earth and Planetary Science Letters*, 450, 283–291.
- Edwards, N. T. (1975). Effects of Temperature and Moisture on Carbon Dioxide Evolution in a Mixed Deciduous Forest Floor. *Soil Science Society of America Journal*, 39(2), 361–365. <https://doi.org/10.2136/sssaj1975.03615995003900020034x>
- Evans, W. C., Sorey, M. L., Kennedy, B. M., Stonestrom, D. A., Rogie, J. D., & Shuster, D. L. (2001). High CO₂ emissions through porous media: transport mechanisms and implications for flux measurement and fractionation. *Chemical Geology*, 177(1–2), 15–29. [https://doi.org/10.1016/S0009-2541\(00\)00379-X](https://doi.org/10.1016/S0009-2541(00)00379-X)
- Fischer, T. P., & Chiodini, G. (2015). Volcanic, magmatic and hydrothermal gases. In *The encyclopedia of volcanoes* (pp. 779–797). Elsevier.
- Fischer, T. P., Sturchio, N. C., Stix, J., Arehart, G. B., Counce, D., & Williams, S. N. (1997). The chemical and isotopic composition of fumarolic gases and spring discharges from Galeras Volcano, Colombia. *Journal of Volcanology and Geothermal Research*, 77(1–4), 229–253.
- Franck, S., Kossacki, K., & Bounama, C. (1999). Modelling the global carbon cycle for the past and future evolution of the earth system. *Chemical Geology*, 159(1–4), 305–317.
- Frondini, F., Chiodini, G., Caliro, S., ... C. C.-B. of, & 2004, undefined. (2004). Diffuse CO₂ degassing at Vesuvio, Italy. *Springer*, 66(7), 642–651. <https://doi.org/10.1007/s00445-004-0346-x>

- Gansser, A. (1973). Facts and theories on the Andes: twenty-sixth William Smith Lecture. *Journal of the Geological Society*, 129(2), 93–131.
- Giammanco, S., Melián, G., Neri, M., Hernández, P. A., Sortino, F., Barrancos, J., Lopez, M., Pecoraino, G., & Perez, N. M. (2016). Active tectonic features and structural dynamics of the summit area of Mt. Etna (Italy) revealed by soil CO₂ and soil temperature surveying. *Journal of Volcanology and Geothermal Research*, 311, 79–98.
- Goossens, P. J., Le, D., & Superieur, C. (1970). The geology of Ecuador Explanatory note for the geological map of the Republic of Ecuador (1:500.000). <https://Popups.Ullege.Be/0037-9395>, 255–263.
- Goovaerts, P. (1999). Geostatistics in soil science: state-of-the-art and perspectives. *Geoderma*, 89(1–2), 1–45. [https://doi.org/10.1016/S0016-7061\(98\)00078-0](https://doi.org/10.1016/S0016-7061(98)00078-0)
- Granieri, D., Avino, R., & Chiodini, G. (2010). Carbon dioxide diffuse emission from the soil: ten years of observations at Vesuvio and Campi Flegrei (Pozzuoli), and linkages with volcanic activity. *Bulletin of Volcanology*, 72(1), 103–118.
- Granieri, D., Chiodini, G., Marzocchi, W., & Avino, R. (2003). Continuous monitoring of CO₂ soil diffuse degassing at Phlegraean Fields (Italy): influence of environmental and volcanic parameters. *Earth and Planetary Science Letters*, 212(1–2), 167–179.
- Guillier, B., Chatelain, J.-L., Jaillard, E., Yepes, H., Poupinet, G., & Fels, J.-F. (2001). Seismological evidence on the geometry of the orogenic system in central-northern Ecuador (South America). *Wiley Online Library*, 28(19), 3749–3752. <https://doi.org/10.1029/2001GL013257>
- Hall, M. L., & Beate, B. (1991). El volcanismo plio-cuaternario en los Andes del Ecuador. *Estudios Geograficos*, 4, 5–38.
- Hoefs, J. (1980). *Stable Isotope Geochemistry*. Springer Berlin Heidelberg. <https://doi.org/10.1007/978-3-662-09998-8>
- Hoefs, J. (2004). Isotope fractionation mechanisms of selected elements. In *Stable isotope geochemistry* (pp. 31–76). Springer.
- IG-EPN. (2015). *Triptych Chiles Cerro Negro Volcanic Complex*. <https://www.igepn.edu.ec/publicaciones-para-la-comunidad/comunidad-eng/19269-triptych-chiles-cerro-negro-volcanic-complex/file>
- IG-EPN. (2020). *Reporte de los trabajos efectuados en el Complejo Volcánico Chiles - Cerro Negro (MultiGAS, Parámetros físico - químicos)*. <https://webcam.igepn.edu.ec/servicios/noticias/1781-reporte-de-los-trabajos-efectuados-en-el-complejo-volcanico-chiles-cerro-negro-multigas-parametros-fisico-quimicos>
- IG - EPN. (2014). *Informe del volcán Chiles - Cerro Negro No.23 -20 Octubre 2014*. <https://www.igepn.edu.ec/servicios/noticias/916-informe-del-volcan-chiles-cerro-negro-n-23-20-octubre-2014>
- IG - EPN, & SGC - OSVP. (2019). *Informe volcánico Chiles - Cerro Negro Negro – 2019 - N° 1 “Actualización del estado de actividad.”* <https://duckduckgo.com/?q=informe+volcanico+CHiles++Cerro+Negro&t=brave&ia=web>
- INAMHI. (1994). *Anuario Meteorológico 1994*.

- https://www.inamhi.gob.ec/docum_institucion/anuarios/meteorologicos/Am_1994.pdf
- Instituto Geofísico - EPN. (2014, June 7). *CHILES - CERRO NEGRO*. <https://igepn.edu.ec/chiles-cerro-negro>
- Isaaks, E. H., Isaaks, D. A. E. S. E. H., Srivastava, R. M., & (Firm), K. (1989). *Applied Geostatistics*. Oxford University Press. <https://books.google.com.ec/books?id=vC2dcXFLI3YC>
- Jaillard, E., Hérail, G., Monfret, T., Díaz-Martínez, E., Baby, P., Lavenu, A., & Dumont, J. F. (2000). Tectonic evolution of the Andes of Ecuador, Peru, Bolivia and northernmost Chile. *Tectonic Evolution of South America*, 31, 481–559.
- James, D. E. (1971). Plate tectonic model for the evolution of the Central Andes. *Geological Society of America Bulletin*, 82(12), 3325–3346.
- Javoy, M., Pineau, F., & Delorme, H. (1986). Carbon and nitrogen isotopes in the mantle. *Chemical Geology*, 57(1), 41–62. [https://doi.org/https://doi.org/10.1016/0009-2541\(86\)90093-8](https://doi.org/https://doi.org/10.1016/0009-2541(86)90093-8)
- Johansson, L., Zahirovic, S., & Müller, R. D. (2018). The interplay between the eruption and weathering of large igneous provinces and the deep-time carbon cycle. *Geophysical Research Letters*, 45(11), 5380–5389.
- Jong, E. de, Schappert, H. J. V., & MacDonald, K. B. (1974). Carbon dioxide evolution from virgin and cultivated soil as affected by management practices and climate. *Canadian Journal of Soil Science*, 54(3), 299–307. <https://doi.org/10.4141/cjss74-039>
- Kerrick, D. M. (2001). Present and past nonanthropogenic CO₂ degassing from the solid earth. In *Wiley Online Library* (Vol. 39, Issue 4). Blackwell Publishing Ltd. <https://doi.org/10.1029/2001RG000105>
- Lamberti, M., Llano, J., Massenzio, A., Yiries, J., Nogues, V., & Agosto, M. (2020). *Emisiones Difusas De Dióxido De Carbono Como Herramienta Para El Cálculo De La Potencia Térmica De Un Sistema Geotermal*.
- Larson, K. M., Freymueller, J. T., & Philipson, S. (1997). Global plate velocities from the Global Positioning System. *Journal of Geophysical Research: Solid Earth*, 102(B5), 9961–9981.
- Lee, J., Six, J., King, A. P., van Kessel, C., & Rolston, D. E. (2006). Tillage and field scale controls on greenhouse gas emissions. *Journal of Environmental Quality*, 35(3), 714–725. <https://doi.org/10.2134/jeq2005.0337>
- Lewicki, J. L., Fischer, T., & Williams, S. N. (2000). Chemical and isotopic compositions of fluids at Cumbal Volcano, Colombia: evidence for magmatic contribution. *Bulletin of Volcanology*, 62(4), 347–361.
- Marty, B., & Tolstikhin, I. N. (1998). CO₂ fluxes from mid-ocean ridges, arcs and plumes. *Chemical Geology*, 145(3), 233–248. [https://doi.org/https://doi.org/10.1016/S0009-2541\(97\)00145-9](https://doi.org/https://doi.org/10.1016/S0009-2541(97)00145-9)
- Mégard, F. (1987). Cordilleran Andes and Marginal Andes: a Review of Andean Geology North of the Arica Elbow (18 S). *Circum-Pacific Orogenic Belts and Evolution of the Pacific Ocean Basin*, 18, 71–95.
- NIOSH/OSHA. (1981). Occupational Health Guidelines for Chemical Hazards, DHHS (NIOSH). *U.S. Government Printing Office*.
- Norabuena, E., Leffler-Griffin, L., Mao, A., Dixon, T., Stein, S., Sacks, I. S., Ocola, L., & Ellis, M. (1998).

- Space geodetic observations of Nazca-South America convergence across the central Andes. *Science*, 279(5349), 358–362.
- O’Leary, M. H. (1988). Carbon Isotopes in Photosynthesis: Fractionation techniques may reveal new aspects of carbon dynamics in plants. *BioScience*, 38(5), 328–336.
<https://doi.org/10.2307/1310735>
- Oliveira, S., Viveiros, F., Silva, C., & Pacheco, J. E. (2018). Automatic filtering of soil CO₂ flux data: different statistical approaches applied to long time series. *Frontiers in Earth Science*, 208.
- Padrón, E., Hernández, P. A., Toulkeridis, T., Pérez, N. M., Marrero, R., Melián, G., Virgili, G., & Notsu, K. (2008). Diffuse CO₂ emission rate from Pululahua and the lake-filled Cuicocha calderas, Ecuador. *Journal of Volcanology and Geothermal Research*, 176(1).
<https://doi.org/10.1016/j.jvolgeores.2007.11.023>
- Parkinson, K. J. (1981). An Improved Method for Measuring Soil Respiration in the Field. *The Journal of Applied Ecology*, 18(1), 221. <https://doi.org/10.2307/2402491>
- Perdomo, G., Ardila, R., & Meneses, L. (1986). Estudio geológico para prospección de azufre en el área de Cumbal-Chiles-Mayasquer (Nariño). *Trabajo de Grado, Universidad Nacional de Colombia, Bogotá, Colombia*. 145p.
- Pineau, F., & Javoy, M. (1983). Carbon isotopes and concentrations in mid-oceanic ridge basalts. *Earth and Planetary Science Letters*, 62(2), 239–257. [https://doi.org/10.1016/0012-821X\(83\)90087-0](https://doi.org/10.1016/0012-821X(83)90087-0)
- Rahilly, K. E., & Fischer, T. P. (2021). Total diffuse CO₂ flux from Yellowstone caldera incorporating high CO₂ emissions from cold degassing sites. *Journal of Volcanology and Geothermal Research*, 419, 107383.
- Rahman, M. M. (2013). Carbon Dioxide Emission from Soil. *Agricultural Research*, 2(2), 132–139.
<https://doi.org/10.1007/s40003-013-0061-y>
- Ramsay, P. (2001). *The ecology of Volcán Chiles: high-altitude ecosystems on the Ecuador-Colombia border* (1st ed.). Pebble & Shell.
- Rastogi, M., Singh, S., & Pathak, H. (2002). Emission of carbon dioxide from soil. *Current Science*, 82(5).
<https://doi.org/http://www.jstor.org/stable/24105957>
- Rinaldi, A. P., Vandemeulebrouck, J., Todesco, M., & Viveiros, F. (2012). Effects of atmospheric conditions on surface diffuse degassing. *Journal of Geophysical Research: Solid Earth*, 117(B11).
- Rogie, J. D., Kerrick, D. M., Sorey, M. L., Chiodini, G., & Galloway, D. L. (2001). Dynamics of carbon dioxide emission at Mammoth Mountain, California. *Earth and Planetary Science Letters*, 188(3), 535–541. [https://doi.org/https://doi.org/10.1016/S0012-821X\(01\)00344-2](https://doi.org/https://doi.org/10.1016/S0012-821X(01)00344-2)
- Rosman, K. J. R., & Taylor, P. D. P. (1998). Isotopic compositions of the elements 1997 (Technical Report). *Pure and Applied Chemistry*, 70(1), 217–235.
- Rouilleau, E., Bravo, F., Pinti, D. L., Barde-Cabusson, S., Pizarro, M., Tardani, D., Muñoz, C., Sanchez, J., Sano, Y., & Takahata, N. (2017). Structural controls on fluid circulation at the Cavihue-Copahue Volcanic Complex (CCVC) geothermal area (Chile-Argentina), revealed by soil CO₂ and temperature, self-potential, and helium isotopes. *Journal of Volcanology and Geothermal Research*, 341, 104–118.

- Sano, Y., Gamo, T., & Williams, S. N. (1997). Secular variations of helium and carbon isotopes at Galeras volcano, Colombia. *Journal of Volcanology and Geothermal Research*, 77(1–4), 255–265.
- Schidlowski, M., & Aharon, P. (1992). *Carbon Cycle and Carbon Isotope Record: Geochemical Impact of Life over 3.8 Ga of Earth History BT - Early Organic Evolution: Implications for Mineral and Energy Resources* (M. Schidlowski, S. Golubic, M. M. Kimberley, D. M. McKirdy, & P. A. Trudinger (eds.); pp. 147–175). Springer Berlin Heidelberg. https://doi.org/10.1007/978-3-642-76884-2_11
- SGC. (2021). *Redes de monitoreo Volcán Cerro Negro*. <https://www2.sgc.gov.co/sgc/volcanes/VolcanCerroNegro/Paginas/redes-monitoreo-Cerro-Negro.aspx>
- Smith, B. N., & Epstein, S. (1971). Two Categories of $^{13}\text{C}/^{12}\text{C}$ Ratios for Higher Plants. *Physiology*, 47(3), 380–384.
- Smith, Rochette, P., Monreal, C., Desjardins, R., Pattey, E., & Jaques, A. (1997). The rate of carbon change in agricultural soils in Canada at the landscape level. *Canadian Journal of Soil Science*, 77, 219–229.
- Still, C. J., Berry, J. A., Ribas-Carbo, M., & Helliker, B. R. (2003). The contribution of C_3 and C_4 plants to the carbon cycle of a tallgrass prairie: an isotopic approach. *Oecologia*, 136(3), 347–359. <https://doi.org/10.1007/s00442-003-1274-8>
- Stix, J. (2015). Part VI Volcanic Interactions. In H. Sigurdsson (Ed.), *The Encyclopedia of Volcanoes (Second Edition)* (Second Edi, pp. 777–778). Academic Press. <https://doi.org/https://doi.org/10.1016/B978-0-12-385938-9.02008-3>
- Taussi, M., Nisi, B., Vaselli, O., Maza, S., Morata, D., & Renzulli, A. (2021). Soil CO_2 flux and temperature from a new geothermal area in the Cordón de Inacaliri Volcanic Complex (northern Chile). *Geothermics*, 89, 101961.
- Telenchana, E. (2017). *Estudio Geovulcanológico del volcán Chiles - Provincia del Carchi*. Escuela Politécnica Nacional.
- U.S. DOE. (2012). *Hydrothermal Resources Factsheet*. <http://pubs.usgs.gov/fs/2008/3082/>.
- Van Geldern, R., Nowak, M. E., Zimmer, M., Szzybalski, A., Myrtilinen, A., Barth, J. A. C., & Jost, H. J. (2014). Field-Based Stable Isotope Analysis of Carbon Dioxide by Mid-Infrared Laser Spectroscopy for Carbon Capture and Storage Monitoring. *Analytical Chemistry*, 86(24), 12191–12198. <https://doi.org/10.1021/AC5031732>
- Viveiros, F., Cardellini, C., Ferreira, T., Caliro, S., Chiodini, G., & Silva, C. (2010). Soil CO_2 emissions at Furnas volcano, São Miguel Island, Azores archipelago: Volcano monitoring perspectives, geomorphologic studies, and land use planning application. *Journal of Geophysical Research: Solid Earth*, 115(12). <https://doi.org/10.1029/2010JB007555>
- Viveiros, F., Chiodini, G., Cardellini, C., Caliro, S., Zanon, V., Silva, C., Rizzo, A. L., Hipólito, A., & Moreno, L. (2020). Deep CO_2 emitted at Furnas do Enxofre geothermal area (Terceira Island, Azores archipelago). An approach for determining CO_2 sources and total emissions using carbon isotopic data. *Journal of Volcanology and Geothermal Research*, 401. <https://doi.org/10.1016/j.jvolgeores.2020.106968>
- Viveiros, F., Ferreira, T., Silva, C., & Gaspar, J. L. (2009). Meteorological factors controlling soil gases and

- indoor CO₂ concentration: a permanent risk in degassing areas. *The Science of the Total Environment*, 407(4), 1362–1372. <https://doi.org/10.1016/j.scitotenv.2008.10.009>
- Viveiros, F., Ferreira, T., Silva, C., Vieira, J. C., Gaspar, J. L., Virgili, G., & Amaral, P. (2015). Permanent monitoring of soil CO₂ degassing at Furnas and Fogo volcanoes (São Miguel Island, Azores). *Geological Society, London, Memoirs*, 44(1), 271–288.
- Viveiros, F., Vandemeulebrouck, J., Rinaldi, A. P., Ferreira, T., Silva, C., & Cruz, J. V. (2014). Periodic behavior of soil CO₂ emissions in diffuse degassing areas of the Azores archipelago: Application to seismovolcanic monitoring. *Journal of Geophysical Research: Solid Earth*, 119(10), 7578–7597.
- Wagner, T., Magill, C. R., & Herrle, J. O. (2018). Carbon Isotopes. In W. M. White (Ed.), *Encyclopedia of Geochemistry: A Comprehensive Reference Source on the Chemistry of the Earth* (pp. 194–204). Springer International Publishing. https://doi.org/10.1007/978-3-319-39312-4_176
- Wefer, G., & Berger, W. H. (1991). Isotope paleontology: growth and composition of extant calcareous species. *Marine Geology*, 100(1), 207–248. [https://doi.org/https://doi.org/10.1016/0025-3227\(91\)90234-U](https://doi.org/https://doi.org/10.1016/0025-3227(91)90234-U)
- Werner, C., & Cardellini, C. (2006). Comparison of carbon dioxide emissions with fluid upflow, chemistry, and geologic structures at the Rotorua geothermal system, New Zealand. *Geothermics*, 35(3), 221–238. <https://doi.org/https://doi.org/10.1016/j.geothermics.2006.02.006>

SECRETARÍA GENERAL
ESCUELA DE CIENCIAS DE LA TIERRA, ENERGÍA Y AMBIENTE
CARRERA DE GEOLOGÍA
ACTA DE DEFENSA No. UITEY-GEO-2022-00011-AD

En la ciudad de San Miguel de Urucuquí, Provincia de Imbabura, a los 13 días del mes de septiembre de 2022, a las 11:00 horas, en el Aula S_CAN de la Universidad de Investigación de Tecnología Experimental Yachay y ante el Tribunal Calificador, integrado por los docentes:

Presidente Tribunal de Defensa	Mgs. RODRIGUEZ CALVOPÍÑA, MARIELA FERNANDA
Miembro No Tutor	Dr. TORO ALAVA, JORGE EDUARDO , Ph.D.
Tutor	Dr. WELLER DEREK JAMES , Ph.D.

Se presenta el(la) señor(ita) estudiante **VILLARROEL BARRENO, ZULAY MICAELA**, con cédula de identidad No. **1805347950**, de la **ESCUELA DE CIENCIAS DE LA TIERRA, ENERGÍA Y AMBIENTE**, de la Carrera de **GEOLOGÍA**, aprobada por el Consejo de Educación Superior (CES), mediante Resolución **RPC-SE-10-No.031-2016**, con el objeto de rendir la sustentación de su trabajo de titulación denominado: **Soil CO2 emissions at Chiles volcano, Ecuador: Survey from Aguas Hediondas and Lagunas Verdes** , previa a la obtención del título de **GEÓLOGO/A**.

El citado trabajo de titulación, fue debidamente aprobado por el(los) docente(s):

Tutor	Dr. WELLER DEREK JAMES , Ph.D.
--------------	--------------------------------

Y recibió las observaciones de los otros miembros del Tribunal Calificador, las mismas que han sido incorporadas por el(la) estudiante.

Previamente cumplidos los requisitos legales y reglamentarios, el trabajo de titulación fue sustentado por el(la) estudiante y examinado por los miembros del Tribunal Calificador. Escuchada la sustentación del trabajo de titulación, que integró la exposición de el(la) estudiante sobre el contenido de la misma y las preguntas formuladas por los miembros del Tribunal, se califica la sustentación del trabajo de titulación con las siguientes calificaciones:

Tipo	Docente	Calificación
Tutor	Dr. WELLER DEREK JAMES , Ph.D.	9,2
Presidente Tribunal De Defensa	Mgs. RODRIGUEZ CALVOPÍÑA, MARIELA FERNANDA	9,5
Miembro Tribunal De Defensa	Dr. TORO ALAVA, JORGE EDUARDO , Ph.D.	9,3

Lo que da un promedio de: **9.3 (Nueve punto Tres)**, sobre 10 (diez), equivalente a: **APROBADO**

Para constancia de lo actuado, firman los miembros del Tribunal Calificador, el/la estudiante y el/la secretario ad-hoc.

VILLARROEL BARRENO, ZULAY MICAELA
Estudiante

Mgs. RODRIGUEZ CALVOPÍÑA, MARIELA FERNANDA
Presidente Tribunal de Defensa



Firmado electrónicamente por:
MARIELA FERNANDA
RODRIGUEZ
CALVOPÍÑA

Dr. WELLER DEREK JAMES , Ph.D.
Tutor

Dr. TORO ALAVA, JORGE EDUARDO , Ph.D.
Miembro No Tutor

TERÁN ROSALES, ANDREA YOLANDA
Secretario Ad-hoc



Firmado electrónicamente por:
ANDREA YOLANDA
TERAN ROSALES



**UNIVERSIDAD DE INVESTIGACIÓN DE TECNOLOGÍA
EXPERIMENTAL YACHAY**

Escuela de Ciencias de la Tierra, Energía y Ambiente

**TÍTULO: SOIL CO₂ EMISSIONS AT CHILES VOLCANO, ECUADOR:
SURVEY FROM AGUAS HEDIONDAS AND LAGUNAS VERDES**

Trabajo de titulación presentado como requisito para la
obtención de título de Geóloga

Autor:

Villarroel Barreno Zulay Micaela

Tutor:

PhD. Weller Dereck

Co-tutor:

PhD. Mandon Celine

PhD. Viveiros Fátima

Urcuquí, Noviembre 2022

AUTORÍA

Yo, **Zulay Micaela Villarroel Barreno**, con cédula de identidad 1805347950, declaro que las ideas, juicios, valoraciones, interpretaciones, consultas bibliográficas, definiciones y conceptualizaciones expuestas en el presente trabajo; así como, los procedimientos y herramientas utilizadas en la investigación, son de absoluta responsabilidad de el/la autora (a) del trabajo de integración curricular. Así mismo, me acojo a los reglamentos internos de la Universidad de Investigación de Tecnología Experimental Yachay.

Urcuquí, Noviembre 2022

Zulay Micaela Villarroel Barreno

CI: 1805347950

AUTORIZACIÓN DE PUBLICACIÓN

Yo, **Zulay Micaela Villarroel Barreno**, con cédula de identidad 1805347950, cedo a la Universidad de Investigación de Tecnología Experimental Yachay, los derechos de publicación de la presente obra, sin que deba haber un reconocimiento económico por este concepto. Declaro además que el texto del presente trabajo de titulación no podrá ser cedido a ninguna empresa editorial para su publicación u otros fines, sin contar previamente con la autorización escrita de la Universidad.

Asimismo, autorizo a la Universidad que realice la digitalización y publicación de este trabajo de integración curricular en el repositorio virtual, de conformidad a lo dispuesto en el Art. 144 de la Ley Orgánica de Educación Superior.

Urququí, Noviembre del 2022.

Zulay Micaela Villarroel Barreno

CI: 1805347950

DEDICATION

To my mom, she told me once, 'don't worry, you will make it.' And guess what, mom, I did it.
Thanks for always believing in me, your unconditional support, and the infinite love you give me.

With all my love, this is for you.

Zulay Micaela Villarroel Barreno

ACKNOWLEDGMENTS

First of all, I would like to start by giving a huge thank you to Ph.D. Celine Mandon, Ph.D. Elisa Piispa, M.Sc. Domenica Guillén, and M.Sc. Katie Nelson. Without any of them, this thesis project would not have been possible. I am eternally grateful to have had the incredible experience we shared during this project fieldwork. I am really thankful to them for their unconditional help and mentorship throughout this learning journey. This thesis is thanks to you. Also, thank Ph.D. Fatima Viveiros, who was a fundamental pillar of this work. Fatima had the patience to teach us and explain all the necessary concepts for this investigation. Indeed, each of these incredible women represents an inspiration for what I would like to become one day.

Thanks again to Ph.D. Celine Mandon for having me as her thesis student. Her passion for volcanology is an inspiration to me. Thank you for sharing with me as a teacher and as a friend. For all the advice, support, and encouragement she gave me throughout this arduous process of writing the thesis. I am truly grateful to live for having had the opportunity to coincide with her in this life.

A special thanks to Prefectura del Carchi, who gave us permission to perform the survey on the area of Aguas Hediondas. Thanks to Edwin Fraga, who helped us by giving us access to the Tourist complex every day of the survey.

Thank you to all the teachers from whom I had the privilege of learning. I am eternally grateful to have had unconditional teachers from whom, more than learning academic things, I realized what vocation is and how to make things with love. Thanks to Yaniel, Germán, Rafael, Anna, Jorge, Luis, Luis Felipe, Alejandra, Celine, and Elissa, for sharing their infinite passion for science and geology with me and, above all, for always giving more than what we expected as students. All my training as a Geologist, person, and friend is thanks to you. I promise to follow in your footsteps and spread the passion for science.

I want to thank my family, my mother Elena, my father Tito, my sister Gabriela, my brothers Justin, Tito, and my niece Mabel. They play a fundamental role in my life, they have been my support since I was born, and this would not be possible without their efforts.

A sincere thanks to Nicolas, one of the most beautiful people I have ever met. Literally, this work would not have seen the light without him since he lent me the computer on which this thesis was done. Thank you for the constant support and motivation he has given me since I met him.

Thanks to 'my girls' Jhuliana, Paola, and Sahori, for being my partners on this trip to called university. Thanks to them for teaching me about true unbelievable friendship and for all the beautiful experiences I have thanks to them. Thanks to 'los geoamigos,' the best career companions you may have had. I have kept with great affection all those incredible experiences, shared beers, and endless talks that we had on field trips. Thank you for being a representation of what camaraderie is.

Thanks to my alma mater, Yachay Tech University, which gave me the best experience of my life, coincided with the best people I have ever met, and made me who I am. Last but not least, thanks to me. For forcing me to get out of bed despite the intense anxiety that gripped my body. For the strength, I have gained and for allowing me to cry but not give up. You are powerful.

Zulay Micaela Villarroel Barreno

RESUMEN

La desgasificación difusa de CO₂ en volcanes inactivos es un proceso bien conocido, pero se desconocen las emisiones de CO₂ en muchos volcanes. Este estudio presenta los resultados de la desgasificación difusa de CO₂ del volcán Chiles. El Complejo Volcánico Chiles-Cerro Negro está ubicado en la frontera entre Colombia y Ecuador. A pesar de su potencial geotérmico, el volcán de Chile ha sido muy poco estudiado debido a su ubicación geográfica y discrepancias políticas. Las termas son un atractivo turístico a ambos lados de la frontera, con notorias emisiones de gases. Sin embargo, este último nunca ha sido cuantificado. Presentamos los resultados de un estudio de emisiones de CO₂ en suelo en dos lugares estratégicos del entorno del volcán Chiles: Aguas Hediondas y Lagunas Verdes. En Aguas Hediondas, medimos en 303 puntos de flujo de CO₂ en una grilla de 5 metros cubriendo un área de 6 000 m², junto con 14 muestras para análisis de $\delta^{13}\text{C}_{\text{CO}_2}$. Tomamos otras 76 mediciones de flujo de CO₂ y cuatro muestras para $\delta^{13}\text{C}_{\text{CO}_2}$ en el área más pequeña de Lagunas Verdes, cubriendo un área de 5 000 m².

Presentamos mapas de desgasificación difusa para las dos áreas de estudio, donde ubicamos áreas de flujo de anomalías de CO₂ e interpretamos su distribución espacial con estructuras tectónicas del complejo volcánico. Además, para comprender mejor el comportamiento hidrotermal del área, realizamos mapas de distribución de la temperatura del suelo para identificar las anomalías de calor relacionadas con las estructuras de desgasificación difusa. Utilizando un enfoque estadístico y datos isotópicos, estimamos los flujos de CO₂ derivados de las profundidades. Gracias al análisis de $\delta^{13}\text{C}_{\text{CO}_2}$, discriminamos entre dos fuentes de CO₂: CO₂ biogénico y CO₂ hidrotermal profundo. En resumen, en Aguas Hediondas obtuvimos una desgasificación difusa de CO₂ total de 0,11 t d⁻¹ de las cuales 0,06 t d⁻¹ presentan aporte hidrotermal profundo de CO₂. En el caso de Lagunas Verdes, la emisión total es más significativa, siendo de 1,66 t d⁻¹, de las cuales más del 80% (1,49 t d⁻¹) presenta aporte de CO₂ de fuente volcánica.

La estimación de las emisiones totales contribuirá a nuestra comprensión de la contribución natural de CO₂ de los volcanes a la atmósfera durante la desgasificación difusa. Por lo tanto, este estudio es significativo, llenando los vacíos de conocimiento sobre el volcán Chiles a pesar de su alto potencial geotérmico. Además, aporta conocimientos esenciales sobre el peligro que suponen las elevadas emisiones de CO₂ en una zona turística.

Palabras clave: desgasificación de CO₂ del suelo, flujo de CO₂, dióxido de carbono, isótopos de carbono, sistema hidrotermal, temperatura del suelo, volcán Chiles.

ABSTRACT

Diffuse CO₂ degassing at dormant volcanoes is a well-known process, yet CO₂ emissions are unknown at many volcanoes. This study presents results of CO₂ diffuse degassing from Chiles volcano. Chiles-Cerro Negro Volcanic Complex is located on the border between Colombia and Ecuador. Despite its geothermal potential, Chiles volcano has been very seldom studied due to its geographical location and political discrepancies. Hot springs are a tourist attraction on both sides of the border, with well-known gas emissions. Yet, the latter has never been quantified. We present results from a CO₂ soil emission survey in two strategic places in the surroundings of Chiles volcano: Aguas Hediondas and Lagunas Verdes. In Aguas Hediondas, we measured in 303 CO₂ flux points in a 5-meter grid covering an area of 6 000 m², along with 14 samples for δ¹³C_{CO2} analysis. We took another 76 CO₂ flux measurements and four samples for δ¹³C_{CO2} in the smaller area of Lagunas Verdes, covering an area of 5 000m².

We present diffuse degassing maps for the two survey areas, where we located CO₂-anomalies flux areas and interpreted their spatial distribution with tectonic structures of the volcanic complex. Moreover, to understand better the hydrothermal behavior of the area, we performed maps of the soil temperature distribution to identify the heat anomalies related to diffuse degassing structures. Using a statistical approach and isotopic data, we estimated the deep-derived CO₂ fluxes. Thanks to the δ¹³C_{CO2} analysis, we discriminate between two CO₂ sources: biogenic CO₂ and deep hydrothermal CO₂. In summary, in Aguas Hediondas, we obtained a total CO₂ diffuse degassing of 0.11 t d⁻¹ of which 0.06 t d⁻¹ presents a deep CO₂ hydrothermal contribution. In the case of Lagunas Verdes, the total emission is more significant, being 1.66 t d⁻¹, of which more than the 80% (1.49 t d⁻¹) presents a volcanic source CO₂ contribution.

Estimation of total emissions will contribute to our understanding of the natural contribution of CO₂ from volcanoes to the atmosphere during diffuse degassing. Therefore, this study is significant, filling the gaps in knowledge on the Chiles volcano despite its high geothermal potential. Moreover, it brings essential knowledge regarding the hazard posed by elevated CO₂ emissions in a touristic area.

Keywords: CO₂ soil degassing, CO₂ flux, carbon dioxide, carbon isotopes, hydrothermal system, soil temperature, Chiles volcano.

TABLE OF CONTENTS

AUTORÍA	I
AUTORIZACIÓN DE PUBLICACIÓN	II
DEDICATION	III
ACKNOWLEDGMENTS	IV
ABSTRACT.....	V
CHAPTER 1: INTRODUCTION	1
1.1 The contribution of volcanic systems to the Carbon cycle.....	1
1.2 Volcanic Hydrothermal Systems	1
1.3 Diffuse Degassing.....	2
1.4 Biogenic carbon dioxide.....	3
1.5 Distinction between CO ₂ sources	4
1.6 Chiles Volcano.....	5
1.7 Statement of the problem	5
1.8 Objectives	6
CHAPTER 2: CHILES VOLCANO	7
2.1 Geological Background	7
2.1.1 The Andes Cordillera.....	7
2.1.2 Chiles Volcano.....	8
2.2 Survey Areas	12
2.2.1 Aguas Hediondas	12
2.2.2 Lagunas Verdes.....	13
2.3 Vegetation of Chiles Volcano.....	14
2.3.1 Types of plants in the area	14
CHAPTER 3: METHODOLOGY	16
3.1 CO ₂ flux measurements	16
3.2 Other measurements.....	19
3.3 Isotopic Samples	20
3.3.1 Sampling strategy and collection.....	20
3.3.2 Isotopic analysis.....	22
3.3.3 Mapping strategy.....	23

3.4	Data processing.....	24
3.4.1	Preparation and correction of the data.....	24
3.4.2	Sequential Gaussian Simulation (sGs)	25
3.4.3	Variograms.....	27
CHAPTER 4:	RESULTS	29
4.1	CO ₂ fluxes.....	29
4.1.1	Aguas Hediondas	29
4.1.2	Lagunas Verdes.....	32
4.2	Isotopic Data	34
4.3	Soil Temperature	36
4.3.1	Aguas Hediondas	36
4.3.2	Lagunas Verdes.....	38
CHAPTER 5:	DISCUSSION.....	41
5.1	Control points	41
5.1.1	The role of barometric pressure	42
5.1.2	The role of soil moisture	43
5.1.3	The roll of air temperature	43
5.1.4	The roll of soil temperature.....	44
5.2	Soil Temperature Distribution	45
5.3	Volcanic CO ₂ contribution to the Diffuse Degassing.....	47
5.3.1	Mixing model with isotopes	47
5.3.2	Probability maps for soil CO ₂ flux	48
5.3.3	CO ₂ total emission	49
5.3.4	CO ₂ diffuse degassing around the world	50
5.3.5	Diffuse Degassing Structures.....	52
CHAPTER 6:	CONCLUSIONS AND FUTURE WORK.....	54
REFERENCES	56

CHAPTER 1: INTRODUCTION

1.1 The contribution of volcanic systems to the Carbon cycle

Nowadays, climate change is one of the biggest challenges for human beings. CO₂ emissions are responsible for 60% of greenhouse gas effects, therefore, understanding the Carbon cycle is one of the main priorities for researchers (Rastogi et al., 2002). The CO₂ input into the atmosphere from non-anthropogenic sources has been detected as a factor that controls the long-term climate of Earth (Marty & Tolstikhin, 1998; Rogie et al., 2001). Non-anthropogenic sources mean sources related to geological processes like geochemical cycles of rocks and igneous/metamorphic activity. Calculating the contribution from igneous and metamorphic processes is one of the biggest challenges for researchers who have been working on models of the global carbon cycle (Bernier & Lasaga, 1989; Franck et al., 1999; Johansson et al., 2018).

Volcanic activity contributes to CO₂ emissions into the atmosphere, during eruptions and quiescent periods. During eruptions, we can have direct and diffuse degassing from active volcanoes. Direct degassing refers to CO₂ discharges directly from the crater, known as a “volcanic plume” (Kerrick, 2001). However, most of the measurements related to CO₂ degassing have been taken during quiescent periods. Quiescent periods refer to degassing during a non-eruptive process of a volcano (Kerrick, 2001).

1.2 Volcanic Hydrothermal Systems

Hydrothermal systems are defined as the sum of a permeable porous layer, an aquifer, and a heat source. In this system each component is fundamental, the permeable soil allows the infiltration of water to the aquifer; the aquifer as the groundwater reserve and the heat source would be the main energy source for the system (U.S. DOE, 2012). The heat source heats up the aquifer, changing the physicochemical water properties' before it comes to the surface such as altering the water composition with the addition of hydrothermal gases. Volcanic hydrothermal system refers to systems in which the heat source is a magmatic body, related with an active or dormant volcano (Delmelle & Stix, 2000). The interaction of groundwater reservoirs and the heat released by an active magma chamber results in hot hydrothermal fluids contaminated with magmatic volatiles (Branney & Acocella, 2015).

Figure 1 illustrates a general view of the dynamic of a volcanic hydrothermal system. The recharge zone is on the volcano's flanks, with meteoric water being the main source. The magma chamber represents

the heat source . Fumaroles, CO₂ diffuse degassing, and hydrothermal springs are the surface expressions of volcanic hydrothermal systems. The hydrothermal springs represent the discharge area where faults and cracks play a fundamental role in this superficial expression of volcanic hydrothermal systems, allowing fluids to seep to the surface.

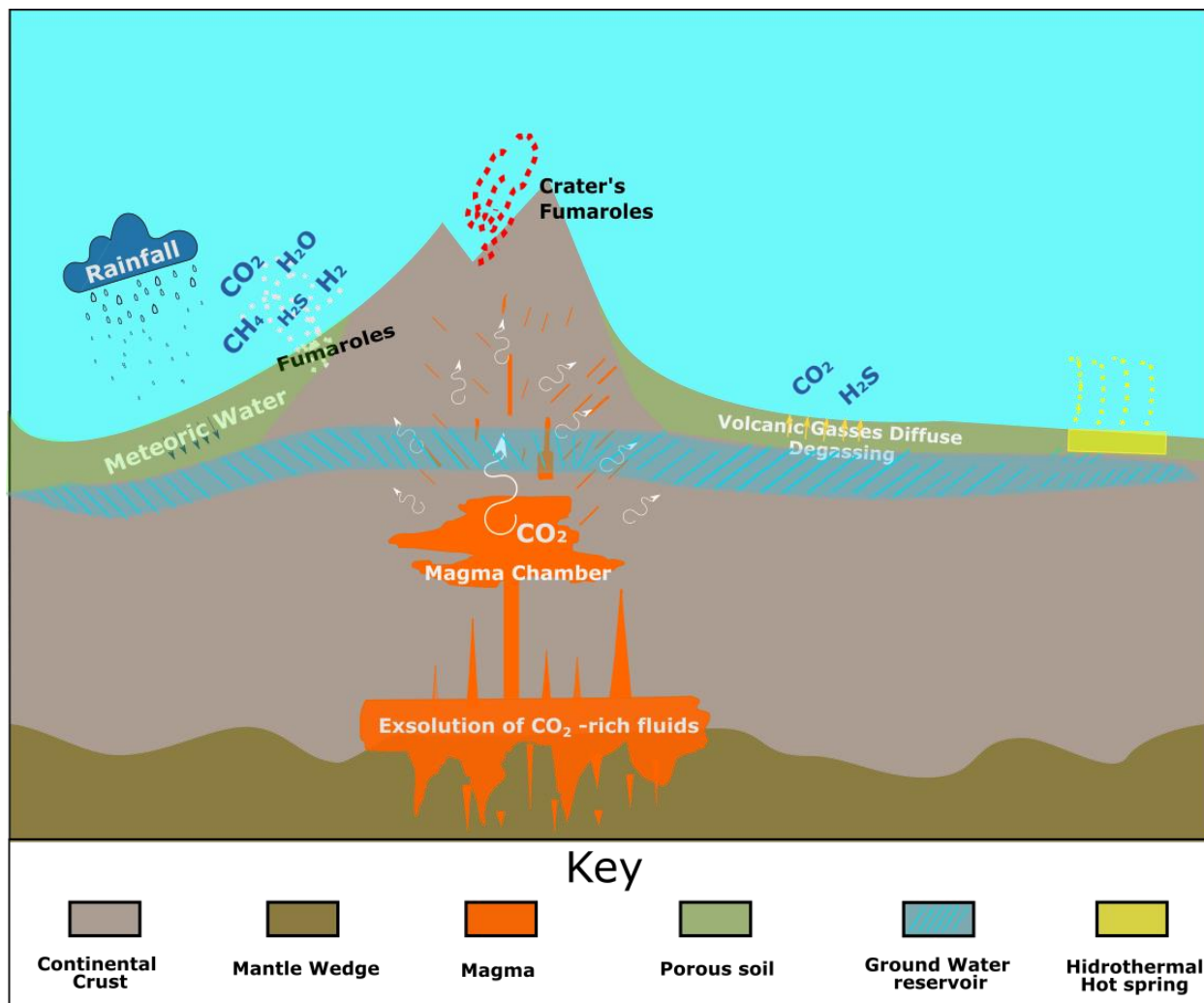


Figure 1. General Sketch of a Volcanic Hydrothermal System.

1.3 Diffuse Degassing

Hydrothermal gases result from the interaction between magmatic gas and a liquid phase (Stix, 2015). Magmatic gases are released by the magma stored at depth in the crust. The main gases released by magma are H₂O and CO₂, with lower amounts of other gases such as SO₂ and halogens. In the case of hydrothermal gases, the other main gases that we can find despite H₂O and CO₂ are H₂S and CH₄. Although

SO₂ is a gas that can be found at high concentrations in magmatic gases, can't be found in hydrothermal gasses. When H₂O comes to the surface, it condenses, releasing thermal energy. On the other hand, CO₂ is less condensable, so it is released through the soil as diffuse degassing along diffuse degassing structures (Fischer & Chiodini, 2015).

As Fischer & Chiodini (2015) describe, diffuse degassing refers to the volatile exsolution to the surface from the magma degassing. Diffuse degassing starts with the magma vesiculation leading to the separation of the gas phase from the melt and, as a result, the gas emission enters into the atmosphere or hydrosphere. The composition of the exsolved gas depends on several physicochemical parameters, such as the magma composition, the volatile solubility, pressure and temperature. Diffuse degassing is a permanent and non-observable process that needs specific instruments to detect the gas emission in volcanically active regions. It is important also to mention that CO₂ is the main gas released in these kinds of areas (Allard, 1992). The most common way in which the gases get to the surface is through diffuse degassing structures (DDS) producing what is better known as soil diffuse degassing.

The most common diffuse degassing structures are small vents, tectonic structures (faults), and steaming ground (Stix, 2015). Several authors have concluded that the degassing patterns could correlate with hidden tectonic structures such as faults and fractures (Chiodini et al., 2001; Werner & Cardellini, 2006; Viveiros et al., 2010). Faults and fractures can represent a weak zone creating an easy path for deep gases to the surface (Viveiros et al., 2010). Therefore, identifying tectonic structures is essential in soil degassing studies.

Soil CO₂ fluxes (the rate of CO₂ flowing per area unit) are measured using the accumulation chamber method (Chiodini et al., 1998). The accumulation chamber method uses an inverted circular chamber to catch the CO₂ gas that comes up from the soil. Maintaining an isolated system between the chamber and the soil is essential. Inside the accumulation chamber, the gas is mixed with a fan. Finally, the gas is analyzed, read, computed, and recorded in the field (Chiodini et al., 2008).

1.4 Biogenic carbon dioxide

Aside from hydrothermal and magmatic sources, CO₂ can be from a biogenic origin. The biogenic source refers to the CO₂ emitted by a living organism's activity. The most usual way of biogenic CO₂ release is through soil respiration, representing 20% of total CO₂ emissions to the atmosphere (Smith et al., 1997) and could represent more than the 16% of the total urban carbon emissions of a city over the course of one year (Bezyk et al., 2021). Soil respiration comprises three biological processes: root respiration, faunal

respiration and microbial respiration (Jong et al., 1974; Edwards, 1975). Soil microflora decomposition is another source of CO₂ soil respiration (Bunt & Rovira, 1954) which depends on the soil conditions, such as temperature, water content and alternate wetting (Agehara & Warncke, 2005; Lee et al., 2006; Rahman, 2013).

1.5 Distinction between CO₂ sources

Carbon comprises two stable isotopes: ¹²C (abundance of 98.93%) and ¹³C (abundance of 1.07%) (Rosman & Taylor, 1998). Analyzing the carbon isotopic composition of CO₂ can be a more precise way to study the gas origin and discriminate between different CO₂ sources found in nature (Chiodini et al., 2008). This technique has been used successfully in recent studies (Chiodini et al., 2008; Viveiros et al., 2010; Lamberti et al., 2020). The most commonly used geochemical terminology for isotopic composition is in terms of delta (δ) values. Delta represents the difference between a standard value and a mean value (Hoefs, 2004). In the case of carbon isotopes, the most frequent standard used is the Vienna Pee Dee Belemnite (VPDB) which is an international isotopic reference material (Coplen, 1996). Following these terminologies, which was applied in the isotopic data along this study, the isotopic composition is defined by Equation [1]:

$$\delta^{13}C = \left[\frac{\left(\frac{^{13}C}{^{12}C}\right)_{muestra}}{\left(\frac{^{13}C}{^{12}C}\right)_{VPDB}} - 1 \right] \times 1000 \quad [1]$$

In general, δ¹³C_{CO₂} value differs depending on how CO₂ was formed, through exsolution from the magma at depth or by biological processes in the soil. The typical value of δ¹³C_{CO₂} for volcanic-hydrothermal CO₂ is between -10‰ to -3‰ vs. VPDB (Pineau & Javoy, 1983; Javoy et al., 1986) (Figure 2). The δ¹³C_{CO₂} composition for biogenic CO₂ ranges from -34‰ to -12‰ vs. VPDB (Hoefs, 1980; O'Leary, 1988). Plants can be classified based on each plant's process of photosynthesis. C³ and C⁴ plants are examples of this classification. Both types of plants differ in their δ¹³C_{CO₂} composition. Studies such as the one performed by Smith & Epstein (1971) have demonstrated that each type of plant has its own isotopic signature range value (Figure 2). Flux values and isotopic compositions are therefore useful to distinguish CO₂ soil diffuse degassing origin, which is crucial to understand the degassing behavior of the area, the tectonic structures, and the volcanic-hydrothermal system.

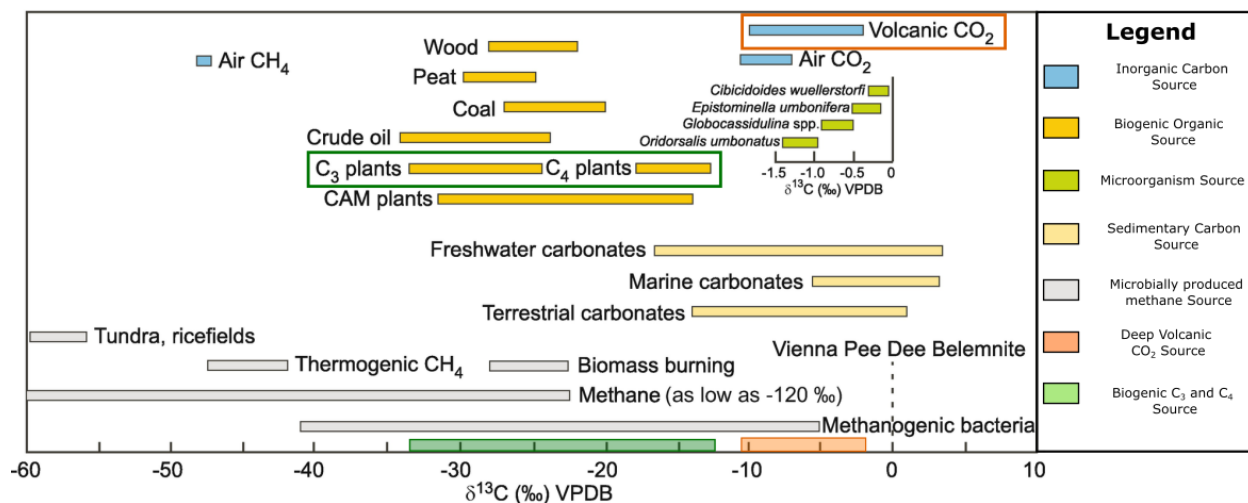


Figure 2. Summarized data of carbon 13 isotope signatures for different sources. It is remarked with orange and green rectangles the sources of interest for this study, Volcanic and Biogenic (C₃ and C₄ plants) sources, respectively. (Source: Wefer & Berger, 1991; Schidlowski & Aharon, 1992; Wagner et al., 2018).

1.6 Chiles Volcano

The volcanic-hydrothermal system of interest in this study is the one related to Chiles volcano. Chiles is a stratovolcano located on the border between Colombia and Ecuador, belonging to the Chiles-Cerro Negro Volcanic Complex. In Ecuador, it is located in the Northern part of the Western Cordillera in the Andes Cordillera. The nearest town to the volcano in Ecuador is Tufiño, in the Carchi province, 9 km to the west of the summit. Chiles is the nearest town in Colombia, located 10 km west of the volcano. Chiles volcano is known due to its geothermal potential. A binational project called 'Tufiño-Chiles-Cerro Negro' was carried out (CELEC & ISAGEN, 2015). The presence of hot springs, gas emissions, and some old fumarolic fields in the area make it an ideal location for a diffuse degassing study.

1.7 Statement of the problem

Despite the fact that Chiles volcano has a high geothermal potential, there are few studies carried out in the area. There is very little information about gas emissions, and there is no previous work related to CO₂ diffuse degassing. Approximately 2300 people live nearby the volcano and many tourists visit this rare high-altitude landscape and its hot springs. CO₂ is an odorless and colorless gas, and if concentrated (>15 vol%) can cause asphyxia (NIOSH/OSHA, 1981; Blong RJ, 1984). Hazardous conditions can be produced when the gas flux increases due to changes in meteorological variables such as pressure and rainfall (Viveiros et al., 2009) or if CO₂ accumulates in a depression. Better knowledge on CO₂ diffuse degassing is therefore critical to better understand the risk associated with the Chiles volcano, as well as to help in

the global quantification of volcanic CO₂ emissions and increase our knowledge on the Chiles magmatic-hydrothermal system.

1.8 Objectives

The main objective of this study is to provide the first CO₂ diffuse degassing quantification of the Chiles volcano and to contribute to the challenge of understanding the carbon input of non-anthropogenic CO₂ into the atmosphere. This study's specific objectives are as follows:

- Realize a CO₂ soil emission survey at Aguas Hediondas and Lagunas Verdes and collect samples for carbon isotope analysis to differentiate between biogenic and volcanic-hydrothermal CO₂ sources.
- Estimate the total flux of deep volcanic CO₂ using a statistical approach combined with isotopic composition of the gases.
- Create a map of the soil degassing flux in relation to tectonic structures using statistical analysis to interpolate the data.
- Compare CO₂ degassing with degassing at other volcanoes to have a better context of the CO₂ input from volcanoes to the atmosphere.

CHAPTER 2: CHILES VOLCANO

2.1 Geological Background

2.1.1 The Andes Cordillera

Chiles volcano is located in Ecuador, on the Northern end of the Andes Cordillera. The Andes Cordillera represents the most outstanding geological feature in South America. The Andean volcanic belt was formed due to the subduction of the Nazca plate beneath the South American Plate. The beginning of this plate tectonic convergence has been dated during the late Triassic - Early Jurassic (James, 1971; Aspden et al., 1987). Nowadays, the convergence rate between the two plates has been estimated around 8 cm/y (Larson et al., 1997; Norabuena et al., 1998; Angermann et al., 1999). Researchers have defined that the Nazca plate has a subduction angle of 25-35° plunging until a depth around 200 km (Guillier et al., 2001). The Cordillera extends along the western border of Chile to Venezuela, getting an extension of 8000 km (Jaillard et al., 2000). Due to the different orientations and structural characteristics, this mountain chain has been divided into three segments. Gansser (1973) defines these subdivisions as the Southern or Patagonian Andes, The Central Andes, and the Northern Andes (Figure 3). The Southern Andes extends from the continent southern tip in the Chilean and Argentine territory to the Gulf of Penas, Chile. The Central Andes extends from the Gulf of Penas, Chile, to the Peruvian – Ecuadorian border. Finally, the Northern Andes starts from southern Ecuador until the northern part of Venezuela.

Two parallel mountain ranges compose the Andes in the Ecuadorian territory. The westernmost range is called 'Cordillera Occidental' and the easternmost mountain range called 'Cordillera Real'. The two cordilleras are divided by a well-defined topographic depression called 'Inter-Andean Valley' (Goossens et al., 1970) (Figure 4). Both cordilleras harbor several dormant and active volcanoes. The volcanoes in Ecuador present an extensive variability in their geochemical composition, morphology, and eruptive styles (Hall & Beate, 1991). Bernard & Andrade (2011) defined 84 Quaternary volcanoes in continental Ecuador, classified according to their last eruption. For dormant volcanoes, the last eruption was older than 10 000 years. Potentially active volcanoes had their last eruption in the last 1 000 years, while active volcanoes had an eruption in the last 500 years.

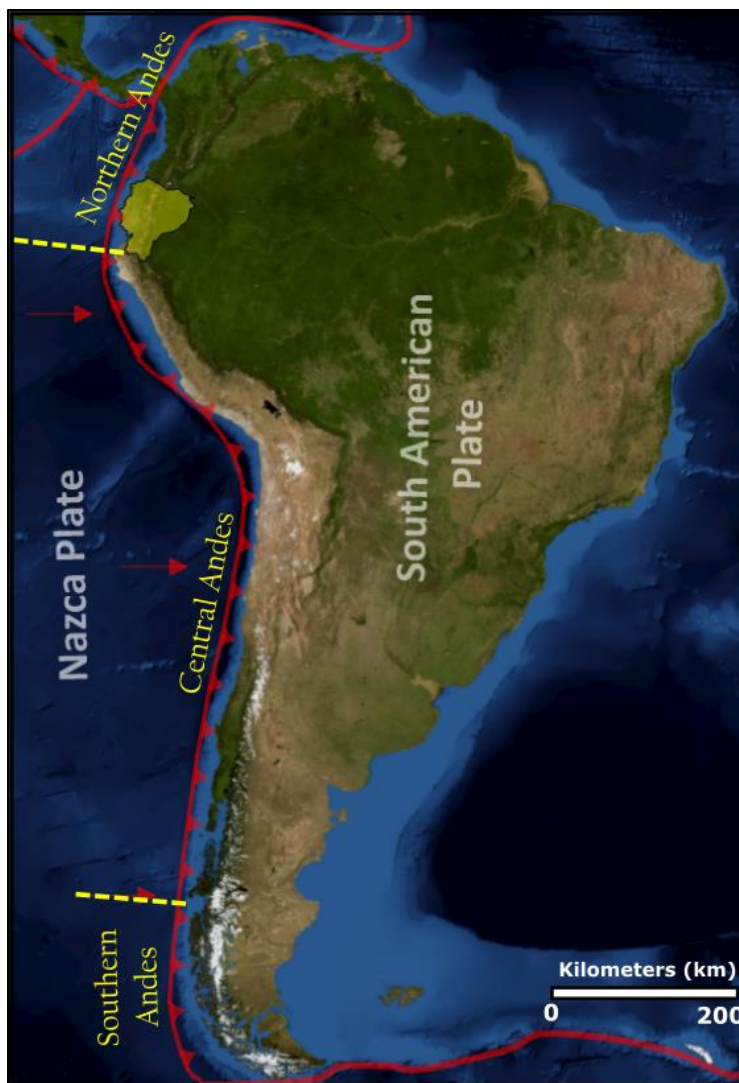


Figure 3. The Andes Cordillera. Map showing the subduction of the Nazca plate underneath the South American plate. In yellow are drawn the cordillera subdivisions proposed by Gansser (1973). Ecuador is shaded in yellow.

2.1.2 Chiles Volcano

The Chiles volcano ($0^{\circ} 49' 0''$ N, $77^{\circ} 56' 05''$ W) is located on the border between Ecuador and Colombia (Figure 5A). The Chiles volcano forms part of the Chiles - Cerro Negro Volcanic Complex. It is located in the Carchi province, 24 km from Tulcán, and 130 km north of the Ecuadorian capital, Quito. Chiles is part of the Western Cordillera (Figure 4). It covers an area of 36.44 km^2 and its summit lies at 4748 meters above sea level (masl). Chiles is a stratovolcano formed mainly by lava flows distributed radially around the crater. After the lava flow deposition, they were eroded by glaciation periods creating glacial deposits more commonly known as moraines (Telenchana, 2017). Besides, the volcano exhibits a 1 km diameter collapse scar on the northern flank (Figure 5B) (Cortés & Calvache, 1997).

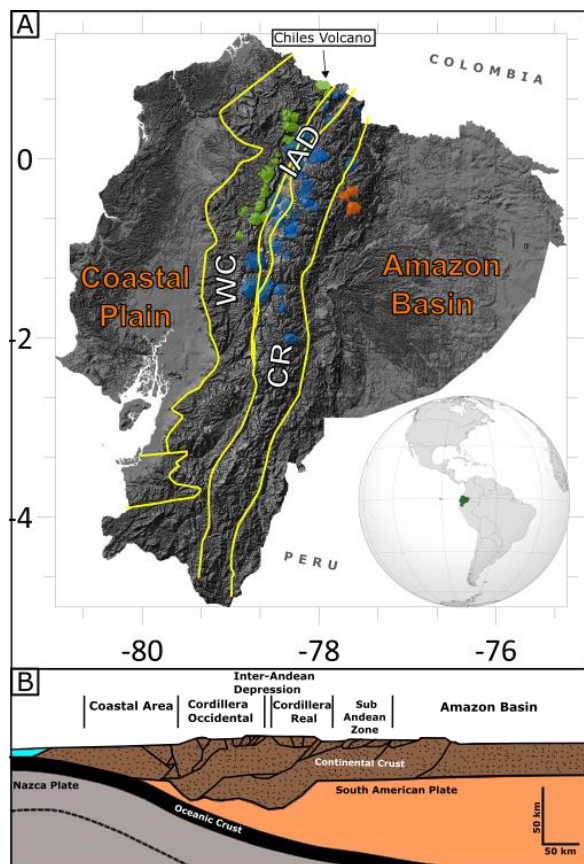


Figure 4. Tectonic setting of Ecuador. A: Digital Elevation Model (DEM from SIGTIERRAS) showing the structural subdivisions of the Andes Cordillera in Ecuador: Western Cordillera (WC), Intern Andean Depression (IAD), Cordillera Real (CR), Coastal Plain and Amazon Basin. Quaternary volcanoes are shown in green for the volcanic front, blue for the main arc and orange for the back arc. B: Structural W-E sketch of the subduction of the Nazca plate beneath the South American plate and the main orogenic structures in Ecuador (After Mégard, 1987).

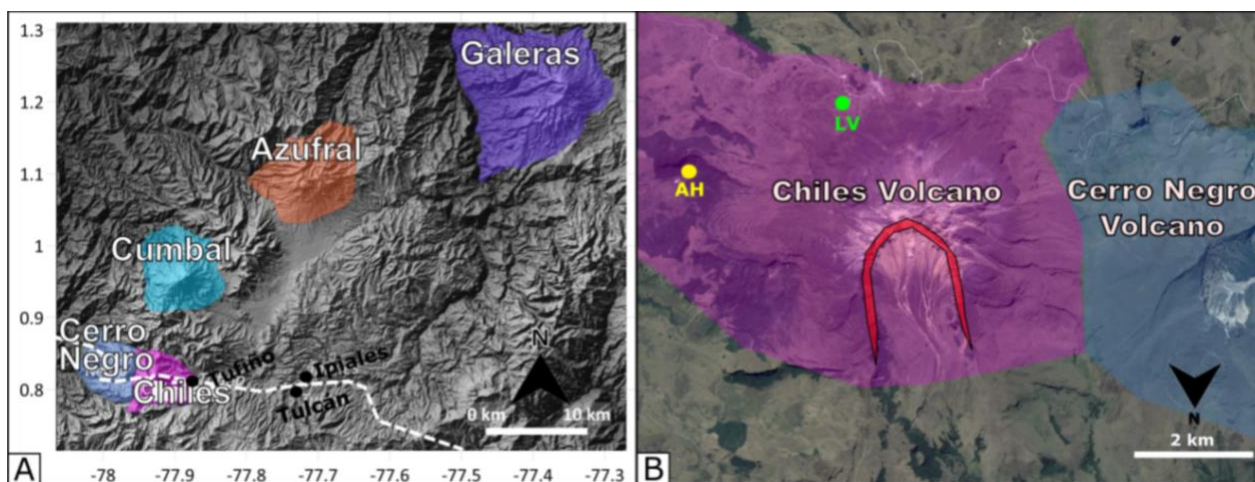


Figure 5. Geographical Location of Chiles Volcano. A: Location of Chiles volcano and the nearest volcanoes. The dashed white line represents the borderline between Ecuador and Colombia. The map coordinates are in decimal degrees. B: Collapse scar on the northern flank of Chiles Volcano (red) and location of the two surveyed areas: Aguas Hediondas (AH) and Lagunas Verdes (LV). Image taken from Google Earth.

Chiles volcano was classified by Instituto Geofísico - EPN (2014) as a potentially active volcano based on the assumption that its last eruption happened in the course of the last 10 000 years. There is however no record of its last eruption. The oldest lava flow is dated at around 572 ka BP while the youngest is dated around 42 ka BP (Telenchana, 2017). The lava flows vary between basaltic-andesite and rhyodacite compositions ($\text{SiO}_2 = 55\text{-}70$ wt%) (Cortés & Calvache, 1997). Telenchana (2017) has defined two units that form the structure of Chiles volcano: CHILES I and CHILES II. Both units are similar in their geochemical rock composition, calc-alkaline, a typical rock composition at subduction-related volcanoes.

Structural and tectonic features have been described around Chiles. It is located on a chevron fold in the West direction. The main fault system has a preferred direction of N20E (Bocanegra & Sánchez, 2017). Perdomo et al. (1986) defined the main structural faults in the area. The most outstanding faults are Chiles – Cumbal, Chiles-Norte, Chiles – Cerro Negro, Cerro Negro – Nasate, Tufiño, and Nasate (Figure 6).

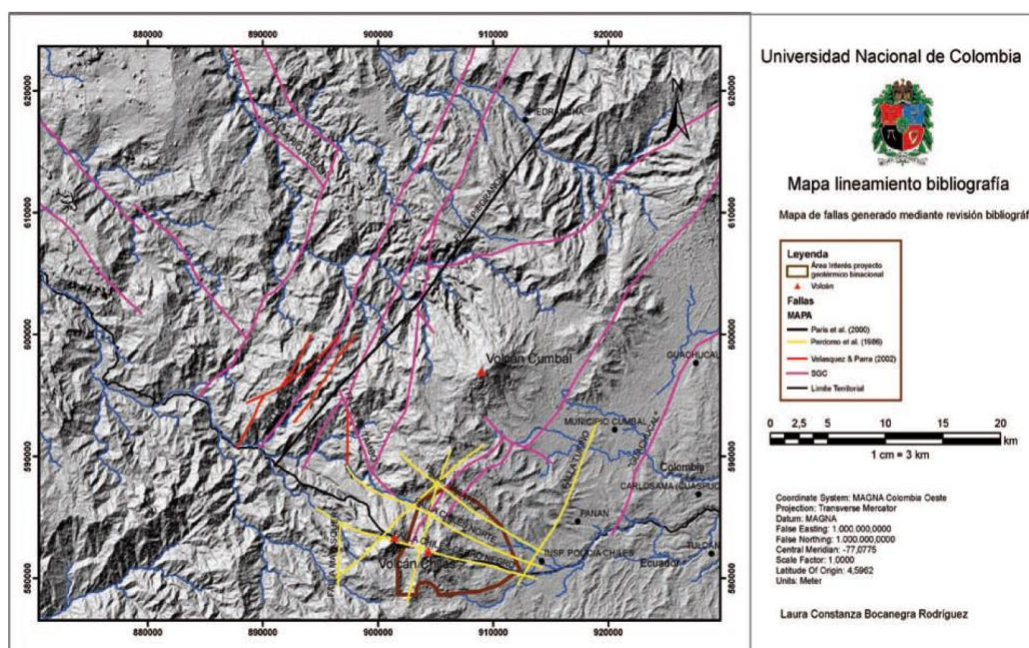


Figure 6. Fault Map in Chiles volcano area. It is a bibliographic compilation of different sources showing the main faults identified in the area. Source: Bocanegra and Sánchez (2017).

As a result of its location and structural setting, the surrounding area of Chiles volcano is susceptible to suffer a high seismic activity. The internal activity of the volcano could also lead to seismic swarms in the area, more commonly known as Volcano Tectonic Seismicity. Volcano Tectonic Seismicity can be an effect of hydrothermal fluids and magma movement (Ebmeier et al., 2016). Chiles volcano did not have a historical seismic activity until 2013. In October 2013, seismic activity started around 2-6 km south of the

volcano with a seismic swarm with more than 1000 recorded events per day. A couple of months later, in February-May and September-December 2014, two more swarm events occurred in the area with an incidence of events per day varying between 10 to 100. The largest registered earthquake had a magnitude of 5.6 M_{LV} (local magnitude calculated with the vertical component of the whole seismic record of the area) and happened at 13 km of depth. It occurred on the 20th of October 2014 at 19:33 UTC. It was felt in Tulcán and Tufiño in Ecuador and, consequently, several damages in the surrounding towns to Chiles Volcano were registered (IG - EPN, 2014). The last seismic episode was during September 2018 and July 2019, where more than 147 000 events were registered. The earthquake magnitude, in general, is less than 3.6 M_{LV} . The most significant earthquake during this period was of M_{LV} 4.0 at 4 km depth that happened on the 25th of July 2019 (IG - EPN & SGC - OSVP, 2019).

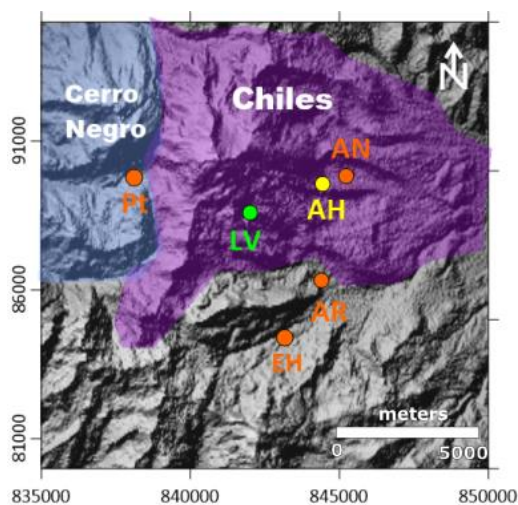


Figure 7. Location of the Hydrothermal hot springs and fumarolic fields monitored by IG-EPN. The hot springs and fumarolic fields are: Potrerillos (Pt), El Hondón (EH), Artezón (AR), Aguas Negras (AN). This study's surveyed areas are green and yellow, corresponding to Lagunas Verdes (LV) and Aguas Hedionds (AH), respectively. The map coordinates are in meters, UTM – WGS84, 18N.

IG-EPN and SGC-OSVP (Servicio Geológico de Colombia- observatorio Sismológico y Volcanológico de Pasto) are the two institutions in charge of monitoring Chiles volcano. IG-EPN monitors the volcano in the Ecuadorian territory and SGC in the Colombian territory. The monitoring network is based on seismicity, deformation, geochemistry and temperature of hydrothermal hot springs (Instituto Geofísico - EPN, 2014; SGC, 2021). The seismicity is monitored thanks to two broadband seismic stations, and in 2014 new stations were installed due to the increases in the Chiles's volcano seismic activity (IG-EPN, 2015). The deformation is mainly tracked with inclinometers and GNSS (Global Navigation Satellite System). The geochemistry and temperature of hydrothermal hot springs monitoring are performed in 6 sites of interest in the Ecuadorian territory: Potrerillos, Lagunas Verdes, Artezón, Aguas Negras, El Hondón and

Aguas Hediondas (Figure 7). where the main physico-chemical parameters measured are temperature, pH and conductivity. Besides, gases are measured in the hydrothermal areas using a multi-GAS instrument. Moreover, samples of the water are taken for major element analysis (IG-EPN, 2020).

2.2 Survey Areas

2.2.1 Aguas Hediondas

Aguas Hediondas ($0^{\circ}48'35''$ N, $77^{\circ}54'22''$ W) is a hot spring located on the eastern flank of Chiles (Figure 7). A tourism complex with pools was built few meters to the South East of the hot spring, preventing people to access the spring area where gas emanations have caused casualties in the past. It is located 4 km East of Chiles summit. The hot spring is in a restricted area due to the known gas emissions of CO_2 and H_2S (IG - EPN, 2020) (Figure 8B). During the last measurements made by IG-EPN (2020), the water temperature ranged from 57 to 59 $^{\circ}\text{C}$, as is shown in Table 1. The emission of H_2S provides to the area a characteristic smell of rotten eggs, which gave its name to the place 'Aguas Hediondas' meaning 'stinking waters'. In the area, there is evidence of hydrothermal alteration (Figure 8D). The survey area around the hot spring is covered mainly by paramo vegetation in the upper part, and all around is an extensive paramo forest. However, inside the restricted area, there is no vegetation; the soil is predominantly loose soil and rocks. A landslide occurred in the beginning of the 20th century, covering the location of the hot spring which re-emerged lower down.



Figure 8. Photos of Aguas Hediondas survey area A: Entrance to the tourist complex 'Aguas Hediondas'. B: The entrance to the restricted hot spring area marked with warning signals. Photo Credits: Celine Mandon. C: Photo showing the hot spring and survey area, as well as the pools built lower down in the tourist complex. Photo Credits: Celine Mandon. D: An active fumarole surrounded by hydrothermally altered rock. It is located right next to the spring.

Table 1. Physico-chemical parameters of water and gas measurement in Aguas Hediondas. Source: IG - EPN, 2020.

Date	Temperature (°C)	pH	H ₂ O/CO ₂	CO ₂ /H ₂ S
Jul-31-2019	58	3.64	21.55	4.85
Oct-23-2019	59.1	3.6	1	4.45
Dec-12-2019	57.8	3.7	0.25	5.89

2.2.2 Lagunas Verdes

Lagunas Verdes (0°48'10" N, 77°55'36" W) is the name given to little lakes on the southern flank of Chiles (Figure 9A), next to which sits an old fumarolic field (Figure 9B). Like Aguas Hediondas, the fumarolic field above Lagunas Verdes presents hydrothermal alteration (Figure 9C) and the characteristic smell of rotten eggs. The survey area is mainly covered by little consolidated rocks and very little vegetation. Lagunas Verdes also is known for the emission of CO₂ and H₂S. Since 2014 IG-EPN has measured the physical and chemical properties of the released gas using mainly a Multi-Gas instrument. Besides, they measure the temperature and pH of the water of the lagoons, as is shown in Table 2.

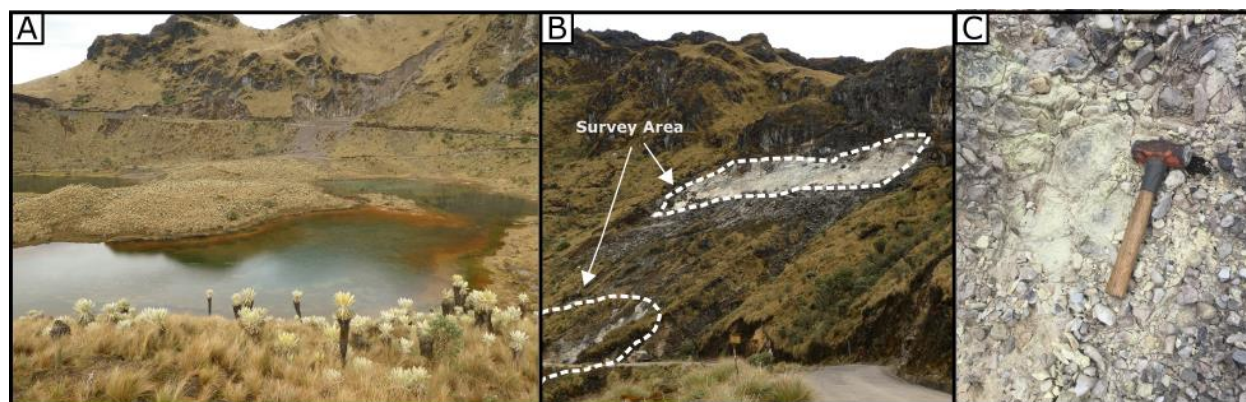


Figure 9. Lagunas Verdes survey area. A: The touristic zone of 'Lagunas Verdes'. B: The two survey areas. C: Hydrothermal alterations in the rocks of the survey area. Photos Credits: Celine Mandon.

Table 2. Physico-chemical parameters of water and gas measurement in Lagunas Verdes. Source: IG - EPN, 2020.

Date	Temperature °C	pH	H ₂ O/CO ₂	CO ₂ /H ₂ S
Jul-31-2019	9.1	5.58	1.2	71.2
Oct-22-2019	9.4	6.42	4.77	66.5

2.3 Vegetation of Chiles Volcano

2.3.1 Types of plants in the area

In Chiles volcano, the climate is the typical climate of the high mountain paramo. According to the Ecuadorian Institute of Meteorology and Hydrology (INAMHI), the climate in Chiles volcano is mainly cold, with mean temperatures ranging between 9 and 11 °C (INAMHI, 1994). However, it can reach 22 °C during the day, and be below zero degree during the night. The precipitation reaches on average 1500 mm per year, but the precipitation varies from day to day. The vegetation in the area is characterized by the protected giant rosette plant whose scientific name is *Espeletia pycnophylla ssp. angelensis*, better known by the community as Frailejón (Figure 10 & Figure 11L). This particular plant grows at altitudes of about 3 200 to 4 200 masl (Ramsay, 2001).



Figure 10. Picture of Chiles volcano with the surrounding vegetation formed mainly by Frailejones.

In general, the vegetation in Chiles volcano area is constituted by paramo vegetation. Paramo vegetation is distinguished by tree-less vegetation. A study recorded 569 plant species of 90 families in Chiles surroundings, where the most considerable families are Asteraceae with 75 species, Poaceae with 45 species, and Orchidaceae with 35 species (Ramsay, 2001).

These plants cover mainly the area of Aguas Hediondas, where the surrounding area is a paramo forest, and some parts of the soil are covered with small shrub vegetation and moss. On the other hand, there is not too much vegetation in the survey area of Aguas Verdes. The soil is mainly formed by rock debris and unconsolidated soil. The most abundant plants in the survey area, following the work of Ramsay (2001) and Chimbolema et al. (2013) are showed in Figure 11.

Different types of plants exist according to the photosynthetic pathway composition (Still et al., 2003), out of which C3 and C4 are the most common. In the case of Chile's volcano vegetation, most of the plants are C3 plants due to the paramo environment, climate, and soil type. According to the study performed by Smith & Epstein (1971) the mean isotopic $\delta^{13}\text{C}_{\text{CO}_2}$ composition in C3 plants is -27‰. This mean value agrees with the isotopic analyses of the study by Chapela et al. (2001). These authors focused on the paramo grasslands of Ecuador and concluded that the isotopic mean value of paramo soil for $\delta^{13}\text{C}_{\text{CO}_2}$ is -24‰.

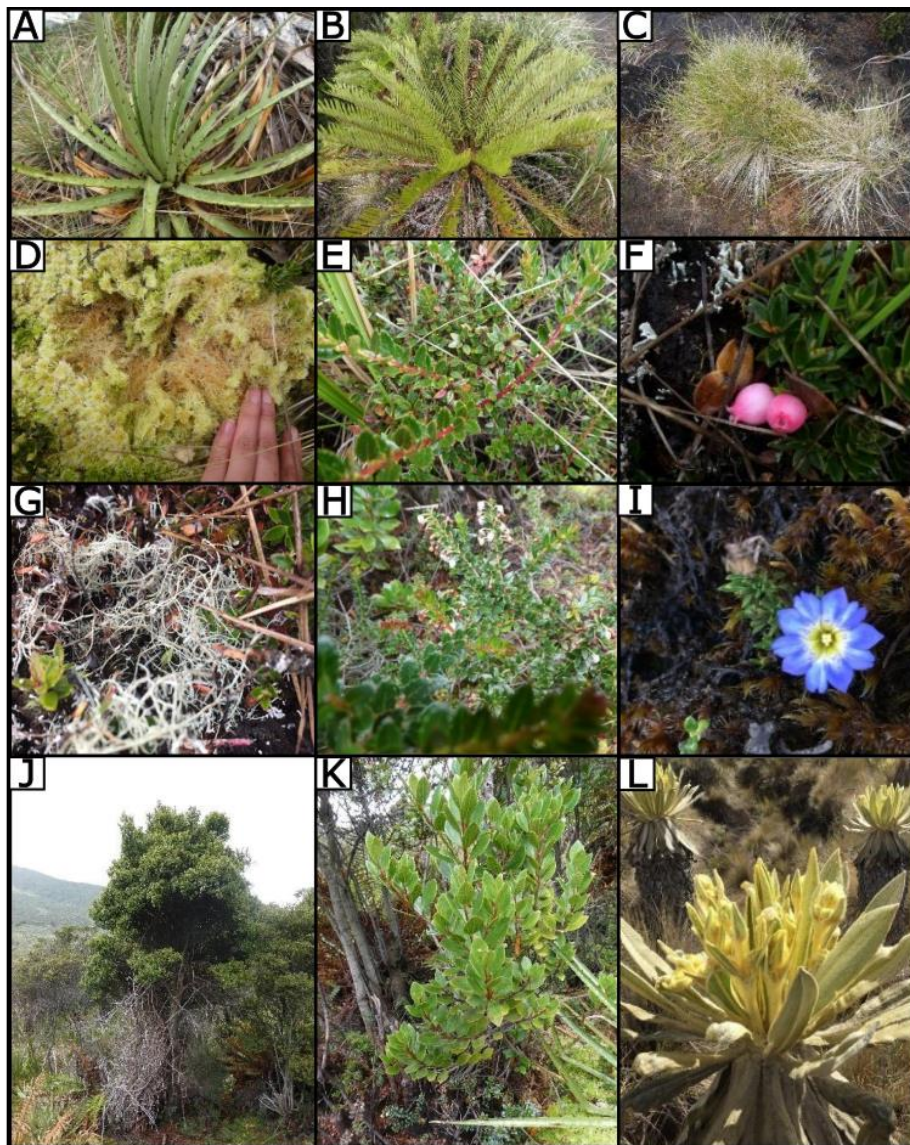


Figure 11. Compilation of the vegetation found in Aguas Hediondas and Lagunas verdes. A: 'Achupalla' *Puya Hamata* L.B. Sm. B: *Blechnum auratum* (Fée) R.M. Tryon & Stolze. C: "Sigse" *Cortaderia nitida* (Kunth) Pilg. D: 'Mosses' *Breutelia*. E: "Flor del andinista" "*chuquiragua*" *jussieui* Hieron. F: "Pasinu chirimote" *Disterigma empetrifolium* (Kunth) Drude. G: *Cladina* (Nyl.) Nyl. H: "Ashpa mortiño" *Pernettya prostrata* (Cav.) Sleumer. I: "Kuyana yuyo" "amor sachá" *Gentiana sedifolia* Kunth. J: *Polylepis incana* KUNTH. K: "Aretes" *Brachyotum lindenii* Cogn. L: "Frailejón" *Espeletia pycnophylla* subsp. *angelensis* Cuatrec

CHAPTER 3: METHODOLOGY

3.1 CO₂ flux measurements

Direct and indirect methods can be used for measuring the CO₂ soil diffuse degassing. The direct method is an in-situ methodology based on directly measuring the flux from the soil and seeing the values in real-time. The indirect methods are based on estimating the CO₂ concentrations at different depths applying a theoretical gas flow in a porous media model (Fick's first law). The latter has some limitations because it is necessary to know the soil porosity properties and transport mechanism. Moreover, it must be applied only in steady-state diffusive fluxes (Chiodini et al., 1998).

The accumulation chamber method is a direct measuring method. This method was initially applied successfully to determine soil respiration in agricultural science (Parkinson, 1981). Then, this method was used in volcanological-geothermal studies in different places around the world (Chiodini et al., 1996; Padrón et al., 2008; Viveiros et al., 2010; Lamberti et al., 2020).

We chose the accumulation chamber method to perform the survey in this study. As the name suggests, this method is based on an inverted chamber that is pressed against the soil to create a closed-system with the atmosphere. A spectrometer measures the CO₂ concentration inside the chamber during a particular time. A constant or decreasing concentration signifies that there is no CO₂ soil degassing, i.e., the concentration in the chamber is that of the atmosphere and does not vary. On the contrary, if the concentration increases, it highlights CO₂ diffuse emission coming from the soil and trapped inside the chamber (Chiodini et al., 1998). The flux value (Φ_{CO_2}) is calculated after the next equation:

$$\Phi_{CO_2} = cf \times \frac{d[CO_2]}{dt} \quad [2]$$

where Φ_{CO_2} is soil CO₂ flux, and *cf* is the proportional factor and dC_{CO_2}/dt is the variation in CO₂ concentration in the chamber as a function of time. The proportional factor was derived from a laboratory test by Chiodini et al. (1998). The equipment was tested emitting Φ_{CO_2} on a 'synthetic soil' made of 10 cm thick dry sand located in a box with an open top. As a result, *cf* was estimated as the dC_{CO_2}/dt and Φ_{CO_2} flux best-fit. It was showed that measuring the increasing concentration for a long enough time makes it reliable to determine the CO₂ flux from the soil with this mathematical relation (Chiodini et al., 1998).

The West System Classic Portable Fluxmeter (Figure 12A) was used for measuring the CO₂ diffuse degassing in this study. This equipment is composed of:

1. A LICOR® LI-840A CO₂/H₂O infrared gas analyzer with a range of 0 – 20000 ppm (parts per million) (Figure 12B)
2. An AD (analogue – digital) converter (Figure 12B)
3. A metallic circular accumulation chamber (West System model B) with an area of approximately 0.0314 m² and with a volume of 0.006231 m³ (Figure 12C)
4. A field computer with FluxManager software allowing for real-time concentration readings (Figure 12D)

The equipment was kindly provided by Michigan Technological University (MTU) and was calibrated in the same institution.



Figure 12. The West System Fluxmeter equipment used for the study. A: The Classic Portable Fluxmeter. B: The AD (analogue – digital) converter and the LICOR® infrared gas analyzer is located inside a box adapted as a backpack to be transported. C: The metallic accumulation chamber (model B). D: The field computer, connected via Bluetooth to the AD converter

The functioning of the Portable Fluxmeter is shown in Figure 13. The accumulation chamber is pressed against the soil, avoiding holes between the ground and the chamber to ensure a closed system with respect to the atmosphere. The diffusing gas that comes from the soil is emitted inside the chamber, where a fan allows for homogenization of the gas phase. The mixed gas is pumped to the infrared sensor. After analysis, the gas is returned to the chamber to not modify the natural gas flux of the soil. The results from the infrared gas analysis are converted by the AD converter and shared via Bluetooth with the computer. The FluxManager program allows seeing a real-time graph of C_{CO₂} vs. time and the

corresponding measuring values for each point (Figure 14). Additionally, this program saves the measured values at each survey point, which can later be revised and corrected if needed.

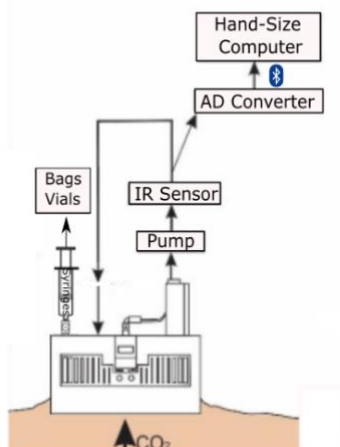


Figure 13. Sketch representing the steps followed by CO_2 gas to be measured using the accumulation chamber method. Modified from: Lamberti et al., 2020.

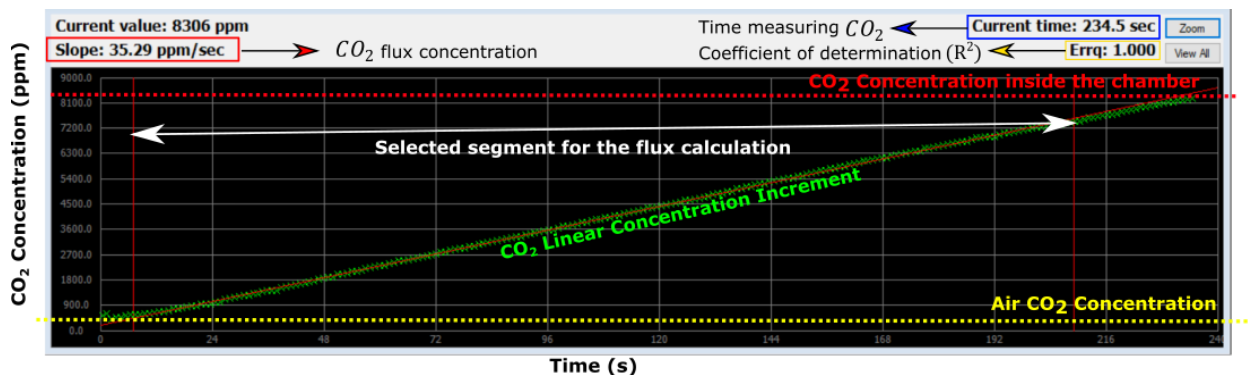


Figure 14. A screenshot of the FluxManager software, where the increase in CO_2 concentration in the accumulation chamber is plotted as a function of time. The initial concentration corresponds to the CO_2 concentration in the chamber at the beginning of the measurement, i.e. the atmospheric CO_2 concentration.

Figure 14 shows an example of CO_2 flux calculation. The CO_2 concentration at the beginning of each measurement is equal to the background value (i.e., the atmospheric CO_2 concentration). As soon as the chamber is pressed against the ground, the concentration increases inside the chamber due to diffuse soil degassing. In order to get the best CO_2 flux estimation, we need to choose the best fit line. The coefficient of determination (R^2) tells us about the quality of the linear relation between both variables, time and CO_2 concentration. R^2 values range from 0 to 1, with best fit being closer to 1. The program allows us to vary the beginning and end of the selected segment to compare the regression coefficients. To obtain the best estimate, we need to adjust the segment until the R^2 value is closest to 1.

3.2 Other measurements

Besides the CO₂ flux measurements, we took other measurements and observations (Figure 15). We measured soil moisture and soil temperature, and we took notes about soil cover, vegetation type, and soil type at each point. Soil moisture was measured with HydroSense II, a handheld Soil Moisture Sensor designed by Campbell Scientific® (Figure 16A). The measurement unit is Volumetric Water Content (VWC). Its water content accuracy is around 3%, and the measurement range is from 0 % to 50% VWC. Soil temperature was measured with a portable thermocouple thermometer patented by HANNA® (Figure 16B). The measurement unit was in Celsius degrees (°C). The resolution of this instrument is 0.1 in the range of -149.9 to 999.9 °C. The accuracy of the equipment is ±0.5°C. These measurements and observations were recorded directly in the ArcGIS collector program, along with the CO₂ flux for each survey point (Figure 17).

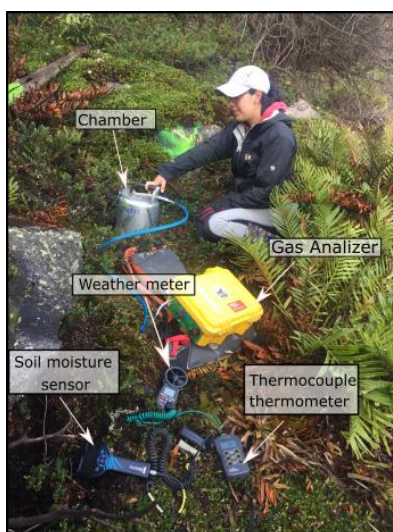


Figure 15. Photograph showing all the instruments used at each survey point to take the measurements during field work.

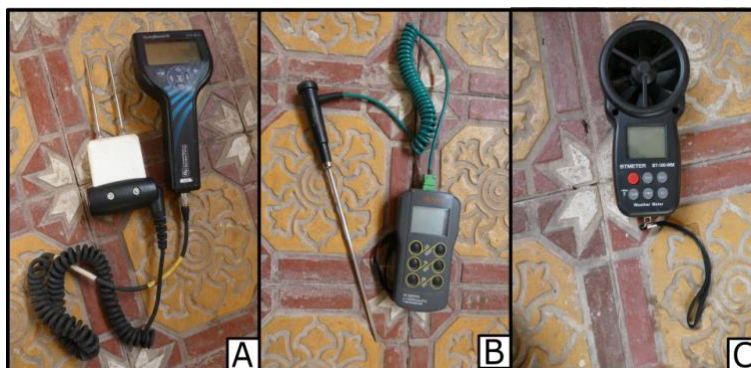


Figure 16. Instruments used in the field to take various measurements. A: handheld Soil Moisture Sensor. B: Portable thermocouple thermometer. C: Anemometer - weather meter.

We took measurements of atmospheric pressure, wind speed, air temperature and humidity during different times throughout the day. These measurements were taken by a BTMETER Anemometer Handheld Digital Barometer Weather Meter (Figure 16C). The atmospheric pressure was recorded in mbar, the wind speed in m/s, and the humidity in $\text{g}\cdot\text{m}^{-3}$. Besides, a sensor is built-in the accumulation chamber which measures the atmospheric pressure in KPa at each point and records it automatically in the FluxManager software.

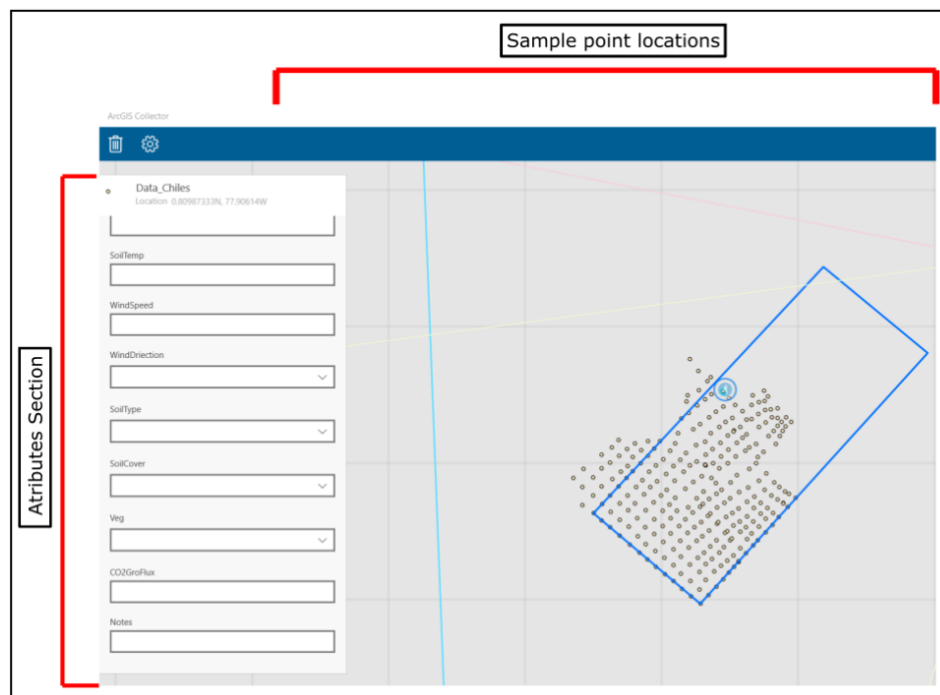


Figure 17. Screenshot from the ArcGIS collector program used to record flux values and observations in the field.

3.3 Isotopic Samples

3.3.1 Sampling strategy and collection

We obtained CO_2 gas samples for isotopic analysis. The gas samples were taken in 12 mL vials (for concentrated samples) and 500 mL bags (for diluted samples) (Figure 18). Gas for isotopic analysis is collected after the gas detector, using a syringe to fill 12 mL vials or directly filling bags from a three-way valve (Figure 19).



Figure 18. Gas sample collection instruments. A: bag used to take gas samples. B: Vials used to take gas samples.

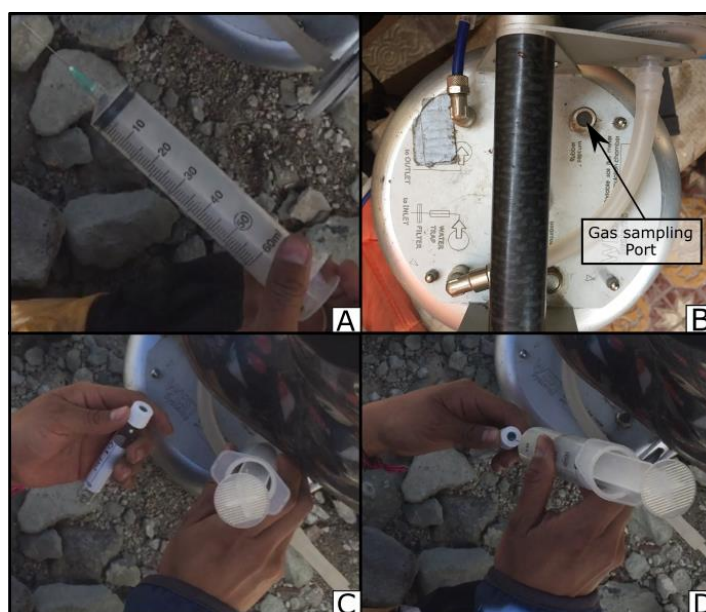


Figure 19. Collection of gas samples for isotope analysis. A: Photograph of the syringe used to take gas sample in the chamber through the gas sampling port. B: Photograph of the chamber showing the location of the gas sampling port. C: Photograph showing the syringe taking the gas sample. D: Photograph while reinjecting the gas sample into the vial.

Isotopic data is used to discriminate between various CO₂ sources. The collection method, developed by Chiodini et al. (2008), consists of collecting two gas samples at each survey point. The first sample (A) is taken at low CO₂ concentration in the chamber after a few seconds of starting the measurement, to allow the mixing of the gas. The second sample (B) is taken later during the flux measurement, when the CO₂ concentration in the chamber is higher. For most of the sites, we collected the second sample (B) when a value of 1000 ppm of CO₂ in the chamber was reached. For two survey points, the concentration was lower than this value due to a very low flux in the first case, and the pump battery dying in the second case. For sites with very high flux, the value of 1000 ppm CO₂ was reached too rapidly, and sample B was

collected at much higher CO₂ concentrations. The final isotopic composition for each survey point is calculated with the following equation:

$$\delta^{13}C_{CO_2} = \frac{\delta^{13}C_{CO_2,B} \times X_{CO_2,B} - \delta^{13}C_{CO_2,A} \times X_{CO_2,A}}{X_{CO_2,B} - X_{CO_2,A}} \quad [3]$$

Where $\delta^{13}C_{CO_2,A}$ and $\delta^{13}C_{CO_2,B}$ correspond to the isotopic composition of the low CO₂ concentration sample A and high CO₂ concentration sample B, respectively, and $X_{CO_2,A}$ and $X_{CO_2,B}$ represent the CO₂ concentrations of samples A and B, respectively, as measured by the accumulation chamber spectrometer.

3.3.2 Isotopic analysis

The gas samples, vials and bags, were sent to Arizona, United States, to be analyzed. The analysis was performed at the Arizona State University a month and a half after the survey using a Thermo Fisher Delta Ray Isotope Ratio Infrared Spectrometer (*Figure 20*). This instrument is based on direct absorption spectroscopy, simultaneously determining $\delta^{13}C$ and $\delta^{18}O$ in CO₂. It consists of a tunable near-infrared diode laser combined with a nonlinear crystal to produce a laser beam. Calibration is performed using a pure CO₂ calibration gas with known $\delta^{13}C$ signature. During analysis, the laser scans the absorption lines of the various CO₂ isotopologues. The isotope composition of the sample is obtained relative to a reference standard (Vienna Pee Dee Belemnite, VPDB) and expressed as delta (δ) per mil (‰) values.

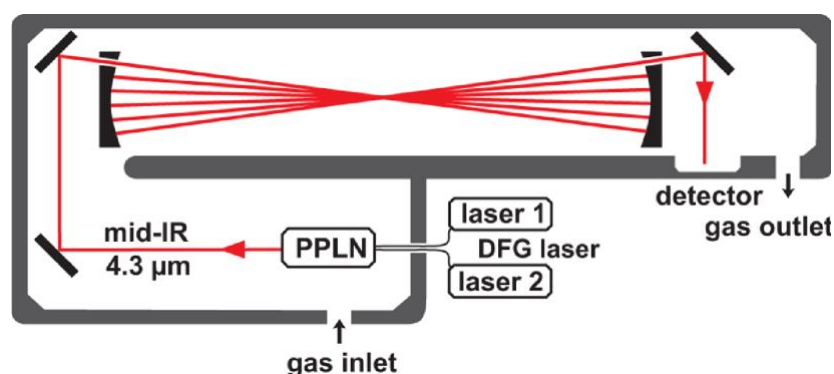


Figure 20. Basic diagram showing how Delta Ray method works for $\delta^{13}C_{CO_2}$ analysis. DFG indicates the difference frequency generation laser and PPLN represents the periodically poled lithium niobate. After: Van Geldern et al. (2014).

3.3.3 Mapping strategy

The survey was carried out from 6th to 12th of December in 2020. We chose two locations on the Chiles volcano flanks to execute the study, at Aguas Hediondas and Lagunas Verdes, both located on the Ecuadorian territory. They are known for their hydrothermal activity and gas emissions. We covered an area of 6 000 m², where we followed a 5-meter grid using a measuring tape as guidelines (Figure 21). We obtained a total of 339 CO₂ flux measurements and 14 samples for isotopic analysis at seven survey points (Figure 22). Furthermore, two locations, one with vegetation and one barren, were chosen as control points, where we repeatedly measured the CO₂ flux at the beginning and end of each workday.



Figure 21. Photographs showing the measuring tape used to perform the 5-meter grid in Aguas Hediondas. A: Measuring tape located in the Western part of the survey area. B: Measuring tape located across the hot spring's channel.

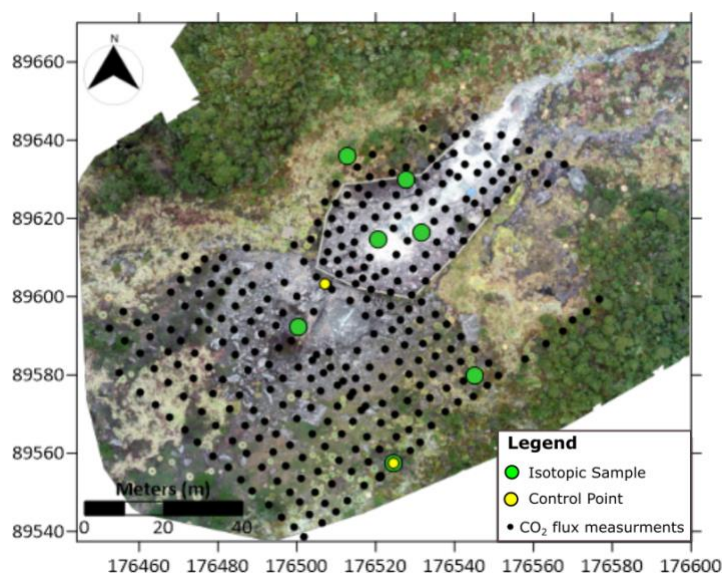


Figure 22. Survey points taken in Aguas Hediondas. Small black points represent the sites where we took CO₂ flux measurements. Green points are locations where we took gas samples for isotopic analysis. Yellow points are the two control points. Orthophoto from December 2020. The map coordinates are in meters UTM – WGS84, 18N.

In Lagunas Verdes, we worked on 6th, 9th, and 12th of December 2020. We covered an area of 5 000 m², where we took 76 CO₂ flux measurements and four samples for isotopic analysis at two survey points (Figure 23). In this case, we followed an irregular grid.

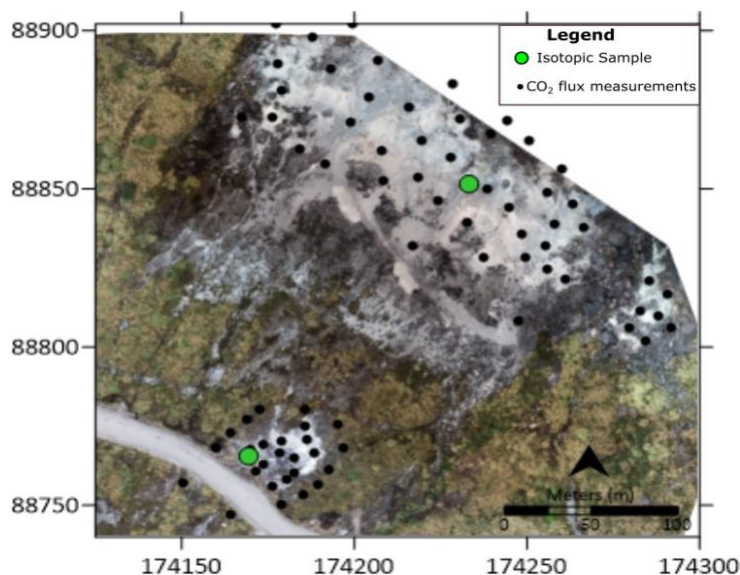


Figure 23. Survey points taken in Lagunas Verdes. Small black points represent the sites where we took CO₂ flux measurements. Green points are locations where we took gas samples for isotopic analysis. Orthophoto from June 2021. The map coordinates are in meters UTM – WGS84, 18N.

The location of the sampling points in both sites was recorded in the ArcGIS collector from a handheld GPS (Figure 17). However, we also used the orthophotos from the area to rectify each survey point location, minimizing the location error associated with the accuracy of the GPS. GPS accuracy was around ± 3 meters in good weather and ± 5 meters in a cloudy sky. Precise location of survey points for the 5-m grid at Aguas Hediondas is critical during spatial interpolation to create CO₂ flux maps.

3.4 Data processing

3.4.1 Preparation and correction of the data

Once the fieldwork is finished with all the data collected, the first step to process the data is to review the flux recorded at each point, to make sure the best CO₂ vs. time slope is chosen. The revision and correction of the data were made using the software developed by West, Flux revision 4.11. This program allows for reprocessing of the CO₂ concentration versus time data. It is mostly important to make sure the window chosen to interpolate the CO₂ flux is correct and representative of the survey point (small variations may happen with time). The CO₂ flux in ppm/s then needs to be converted into more convenient units for

analysis, i.e., grams per square meter per day ($\text{g m}^{-2} \text{d}^{-1}$). We applied the following formulas for the conversion:

$$F_g = F_{ppm} * K * C_{molec} \quad [4]$$

Where:

- F_g is the CO_2 flux in $\text{g m}^{-2} \text{d}^{-1}$.
- F_{ppm} is the CO_2 flux in ppm/s.
- C_{molec} is the molecular weight of CO_2 .

Finally, K needs to be calculated with the following formula:

$$k = \frac{86400 * P}{10^6 * R * T_k} * \frac{V}{A} \quad [5]$$

Where:

- P is the barometric pressure expressed in mbar (HPa).
- R is the gas constant $0.08314510 \text{ bar L K}^{-1} \text{ mol}^{-1}$.
- T_k is the air temperature expressed in Kelvin degrees.
- V is the chamber net volume in cubic meters.
- A is the chamber inlet area in square meters.

The following step is to correct the data using the calibration factor. The calibration was performed at Michigan Technological University. For the calibration tests, the equipment measured CO_2 gas at different concentrations and different flux rates. In this case, the calibration was applied with 99.9% CO_2 , 10% CO_2 , and 1% CO_2 concentrations with various flux rates into the sensor: 10, 8, 7, 5, 4, 2, 1 sccm (standard cubic centimeters) with each gas. The obtained values are converted to the units used in this study ($\text{g m}^{-2} \text{d}^{-1}$). Plotting the real values vs. the measured values create a calibration curve from which a total correction factor is obtained. The CO_2 fluxes measured during our survey are then corrected with this correction factor.

Once the CO_2 fluxes are converted and corrected, we rectified the location of points. We used the orthophotos to georeference the start and end of each grid line in the case of Aguas Hediondas. After this, we just measured the 5-meter distance to locate every sample point in a line. Finally, the coordinates had to be converted from geographic coordinates WGS 1984 to a projected one, WGS84 UTM zone 18N.

3.4.2 Sequential Gaussian Simulation (sGs)

The data obtained during the survey were processed using a geostatistical approach. Geostatistics is a branch of statistics used in geoscience, which basic concept is that there is a relation between the spatial

distribution of the values. It considers that two close points in space are more probable to be similar than two distant points (Isaaks et al., 1989). There are numerous geostatistical methods to create simulations of the variables. The technique used in this study is the Sequential Gaussian Simulation (sGs), defined by Cardellini et al. (2003), as the most appropriate method for diffuse degassing studies. sGs is based on an interpolation technique. The interpolations techniques are used to predict the values in unsampled locations based on the spatial correlation of the sampled data obtained during the fieldwork (Goovaerts, 1999).

The sGs method was applied following the algorithm described by Deutsch & Journel (1998). This algorithm was designed for the Geostatistical Software Library, GSLIB. This algorithm consists of creating a certain number of simulations of the spatial distribution of the variable, which in this case is the CO₂ flux. The algorithm followed is represented in Figure 24, and described below:

- Have the experimental data ready to be processed
- Looking if it is necessary to apply decluster weights or not. Decluster weights are used in the cases where the data is not spread evenly throughout the area, meaning that there is more concentration of data in certain parts than others. When this effect happens, it is necessary to apply a value to equalize the data.
- Transform the data to a normal distribution using a normal score.
- Create experimental variograms of the data normally distributed.
- Modelling the variogram previously created to have the best fit curve of the data.
- Execute sequential Gaussian simulation. In this step, we can apply different parameters according to the goal of each study. The kriging type used in this study was simple kriging.
- Back transform the normally distributed data into the initial data.
- Post-processing data is the final step that allows verifying the spatial distribution, adding the corresponding coordinates to the data, choosing the visualization map type (E-type and probability maps) and estimating the uncertainty.

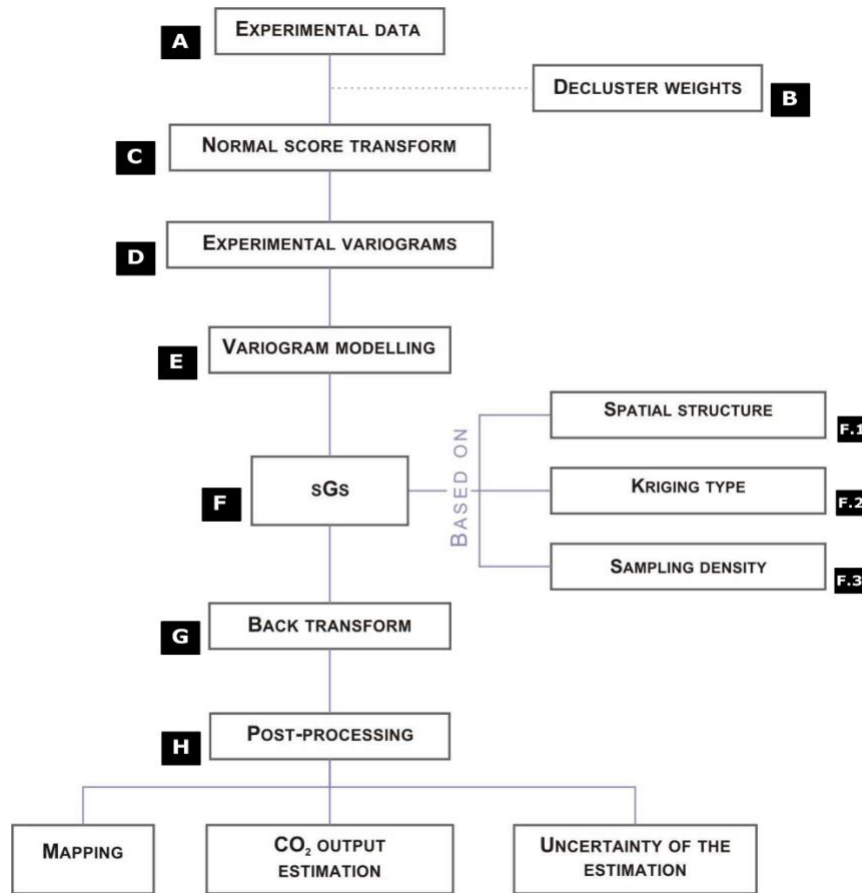


Figure 24. Procedure scheme of the sGs algorithm. Modified from Viveiros et al., (2020) from the original source of Frondini et al., (2004).

Once the sGs is successfully applied, one of the post-processing steps is to choose the map type in which we would like to perform the simulation. In this study, we decided to use two types of maps, E-type and probability maps. The E-type maps display predicted values for each location in the area based on an average of all the data simulations. This type of map is helpful to calculate an estimate of the total diffuse degassing of the area. Instead, the probability maps are beneficial to identify the DDS and estimate deep hydrothermal degassing only. It indicates the probability of the simulated values exceeding a selected threshold value (Cardellini et al., 2003).

3.4.3 Variograms

Step D in the algorithm showed in Figure 24 is about creating an experimental variogram that fits better with the data. Variograms are a statistical tool used to represent the correlation between the spatial data analyzed. It indicates the range within which two data points influence each other. An example of a variogram plot is given in Figure 25. It shows the distance lag vs. semi variance of the data. Sill, range, and

nugget are the values that define the variogram plot. The sill represents the value at which the semi variance reaches the plateau. When this curve attains a plateau, it means that the values are no more correlated. The range is the x-axis value where the sill is reached. The nugget represents the position at which the curve crosses the y-axis. These values are crucial to define the sequential Gaussian simulation for each data set.

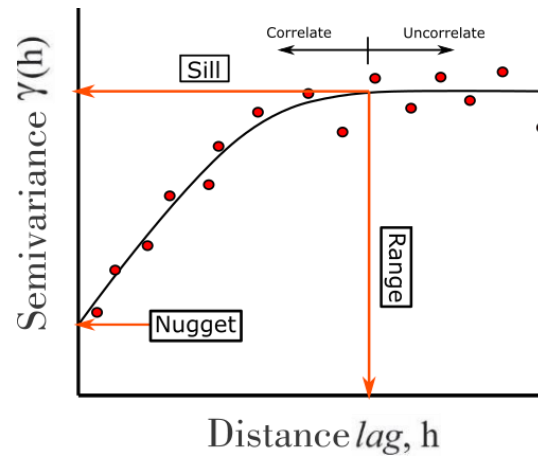


Figure 25. Example of a variogram plot showing its main features. The red circle represents the experimental variogram created from the normally distributed data. The black curve represents the model created to fit the variogram.

Step E is modeling the variogram to get the best fit curve to the experimental variogram. We have different options to model the variograms. The most common models are spherical, exponential, and gaussian (Figure 26).

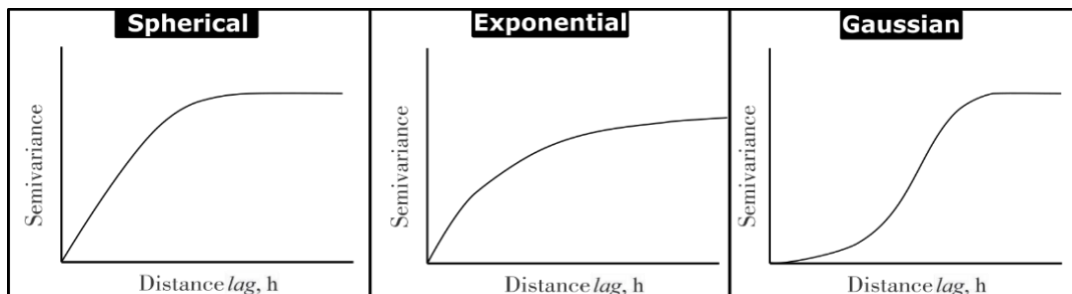


Figure 26. Example of the most used variogram models.

CHAPTER 4: RESULTS

4.1 CO₂ fluxes

4.1.1 Aguas Hediondas

In Aguas Hediondas at the end of the survey we took 303 CO₂ flux measurements, without taking into account the control points. The statistical parameters of the collected data are shown in Table 3. The map in Figure 27 shows the variation in the CO₂ flux measurements. We can observe that the highest values are located inside the restricted area (Figure 8B). We find the two highest values concentrated near the active fumarole and near the hot spring (Figure 8D) and medium values in the surrounding area. Inside the walls, in the restricted area, vegetation is absent. Otherwise, in the external area of the restricted area, the vegetation is more abundant, ranging from small plants and moss to paramo trees that create the surrounding paramo forest. In this part of the surveyed area, we find the lowest values that do not show significant variability.

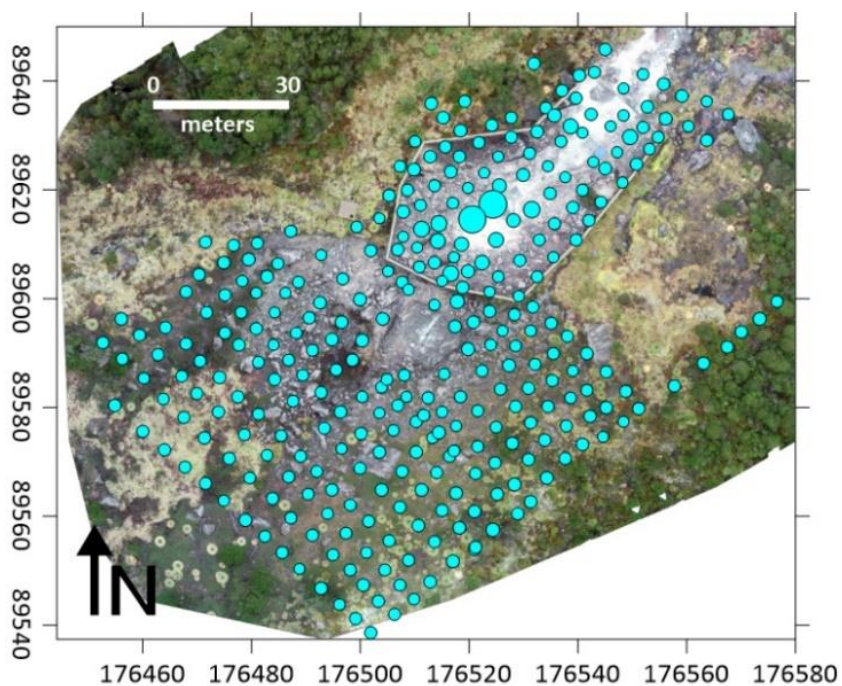


Figure 27. Map of the CO₂ flux measurements ($\text{g m}^{-2} \text{d}^{-1}$) from Aguas Hediondas. The dot sizes are proportional to the CO₂ flux, higher CO₂ fluxes correspond to bigger dots. The map coordinates are in meters, UTM – WGS84 18N.

Table 3. Statistical parameters of the measured CO₂ fluxes at Aguas Hediondas and Lagunas Verdes during December 2020.

Area	No. of measurements	Min.CO ₂ flux (g m ⁻² d ⁻¹)	Max.CO ₂ flux (g m ⁻² d ⁻¹)	Average CO ₂ flux (g m ⁻² d ⁻¹)
Aguas Hediondas	303	0.60	1263.32	17.36
Lagunas Verdes	76	1.59	3614.08	305.92

Following the process to apply the sGs described earlier, we first create the histogram of the collected data (Figure 28A). It is clear that the data does not follow a normal distribution as is usually in Earth sciences data. The histogram is very useful for visualizing the data distribution, which in this case shows the dominance of values around 0 to 100 g m⁻² d⁻¹. On the other hand, we see fewer higher values higher than 1000 g m⁻² d⁻¹. The minimum value besides background value (0 g m⁻² d⁻¹) is 0.60 g m⁻² d⁻¹.

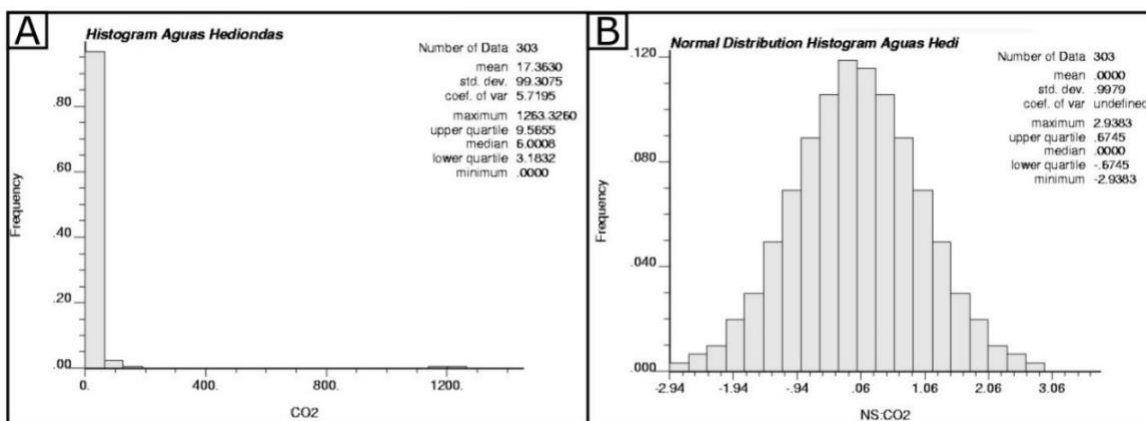


Figure 28. Histograms of the CO₂ flux measurements collected in Aguas Hediondas. A: Histogram of the original collected data of CO₂ flux (g m⁻² d⁻¹) in Aguas Hediondas. B: Histogram of the normal score transformed CO₂ flux data for Aguas Hediondas.

We performed a normal score transformation to convert the data to a normal distribution (Figure 28B). The next step is to create the variogram to be used in the sGs, using the normal score transformed CO₂ fluxes. Once a variogram is obtained, we need to find a model that best fits the variogram. For Aguas Hediondas, the parameters that best fit the data were a spherical model with a sill value of 1.1, a range of 12 meters and a nugget value of 0.7 (Figure 29).

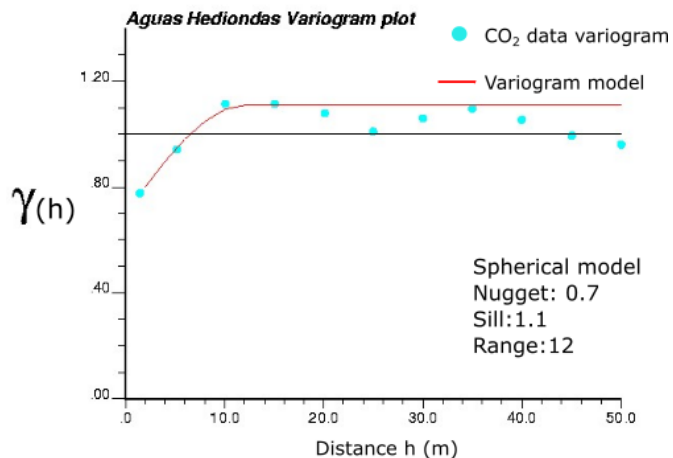


Figure 29. Experimental variogram and variogram model. The light blue dots show the variogram obtained from the normal score transformed Aguas Hediondas CO₂ fluxes. The red line represents the ideal variogram model that best fits the data.

To execute the sequential Gaussian simulation, it is crucial to define the spatial structure of the grid, the kriging type, and the sample density. The kriging type used was simple kriging. The other parameters were defined according to the data properties and the variogram model specifications. Using the results for the simulation, we can visualize the CO₂ flux distribution in the area using the E-type map.

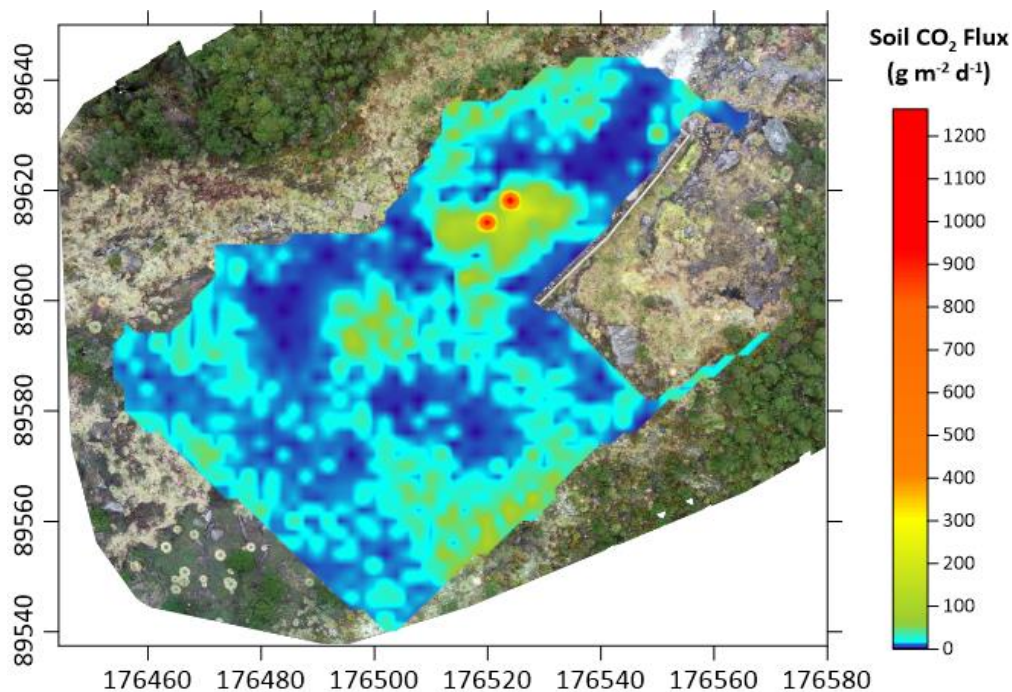


Figure 30. E-type map of the CO₂ diffuse degassing spatial distribution of the average of the 100 sequential Gaussian simulations obtained for Aguas Hediondas survey area. The map coordinates are in meters, UTM – WGS84 18N.

4.1.2 Lagunas Verdes

The total gas measurements in Lagunas Verdes were 76 without the bags/vial samples for isotope analysis. As we see in the statistics summary in Table 3, the maximum value measured in the area is $3614.08 \text{ g m}^{-2} \text{ d}^{-1}$. The average is $305.92 \text{ g m}^{-2} \text{ d}^{-1}$, and the minimum value in spite of the background value is $1.59 \text{ g m}^{-2} \text{ d}^{-1}$.

The map in Figure 31 shows the location of survey points and variation in CO_2 flux. We can observe that high values are located mainly in the lower part of the old fumarolic field. However, we find two high values in the upper part. It is essential to mention that the highest values are located in parts of the survey area where the vegetation was absent. The lowest values are evenly distributed in both parts of the area.

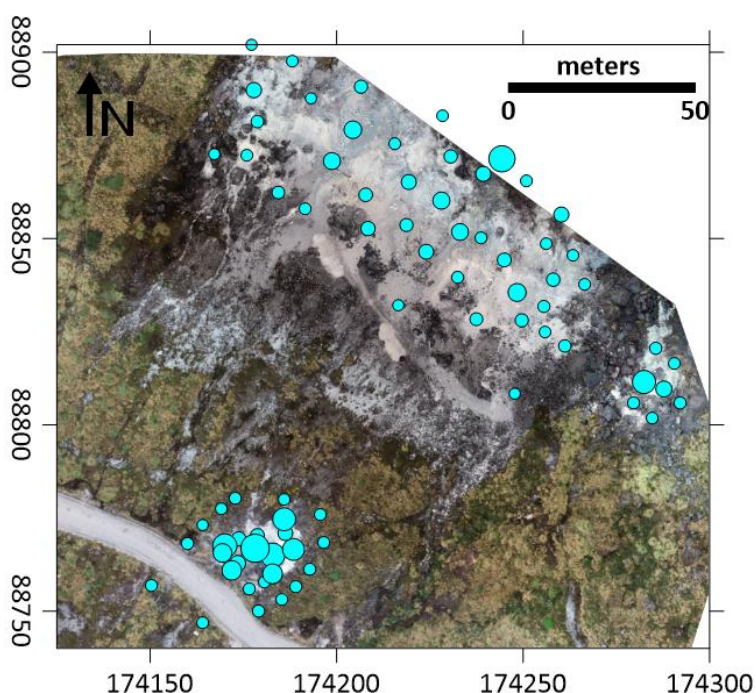


Figure 31. Map of the CO_2 flux measurements ($\text{g m}^{-2} \text{ d}^{-1}$) from Lagunas Verdes. The dot sizes are proportional to the CO_2 flux, higher CO_2 fluxes correspond to bigger dots. The map coordinates are in meters, UTM – WGS84 18N.

Similarly to Aguas Hediondas, the flux data did not follow a normal distribution and we had to apply a normal score transformation (Figure 32). Using the transformed data, we performed the variogram and created the variogram model that best fits the data (Figure 33). The variogram was created using a spherical model with a sill value of 0.97, a range of 22 meters and a nugget value of 0.4.

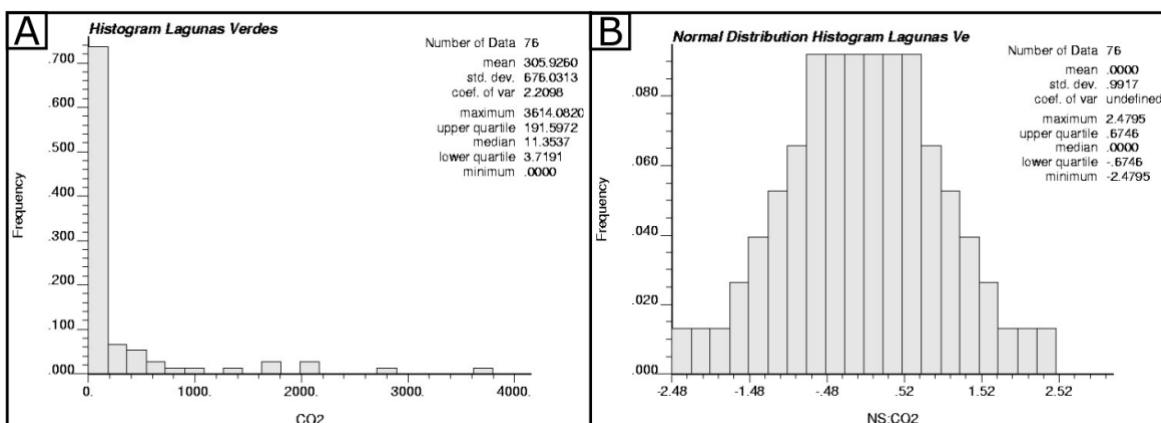


Figure 32. Histograms of the CO_2 flux measurements collected in Lagunas Verdes. A: Histogram of the collected data of CO_2 flux ($g\ m^{-2}\ d^{-1}$) in Lagunas Verdes. B: Histogram of the normal score transformed CO_2 flux data for Lagunas Verdes.

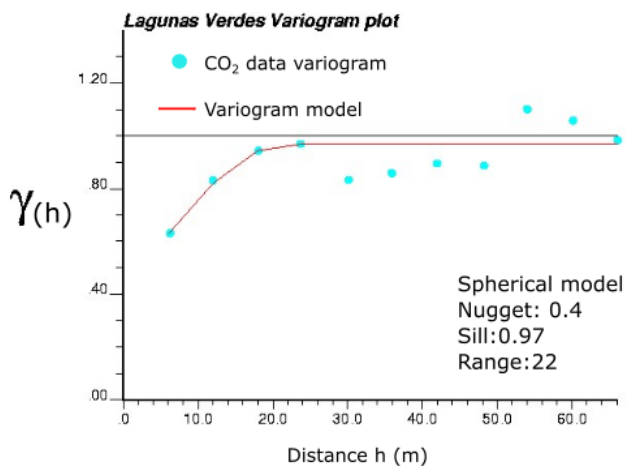


Figure 33. Experimental variogram and variogram model. The light blue dots show the variogram for the normal score transformed Lagunas Verdes CO_2 fluxes. The red line represents the ideal variogram model that better fits the data.

We applied the variogram to the normalized data to perform the 100 simulations. The E-type map resulting from the sGs is shown in Figure 34. As in Figure 31, the data follow the same tendency having high values in the lower part and some in the upper part of the area. Nevertheless, generally, the values in Lagunas Verdes are higher than at Aguas Hediondas.

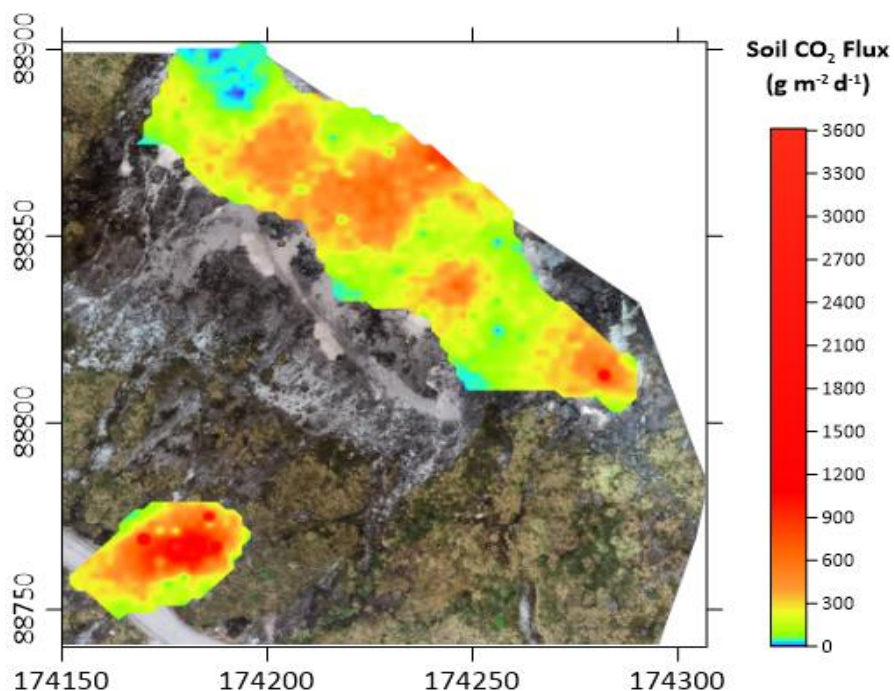


Figure 34. E-type map of the CO_2 diffuse degassing spatial distribution of the average of the 100 sequential Gaussian simulations obtained for Lagunas Verdes survey area. The map coordinates are in meters, UTM – WGS84 18N.

4.2 Isotopic Data

The isotopic analysis results are summarized in Table 4. In Aguas Hediondas, we took 12 samples at seven different survey points. On the other hand, we took four samples in Lagunas Verdes at two survey points. Column 5 in Table 4 contains the isotopic ^{13}C composition measured in the laboratory of each sample. On the other hand, the final $\delta^{13}\text{C}$ ‰ value (Column 8 Table 4) for each survey point was calculated using Equation [3] mentioned in the Methodology chapter, based on the procedure by Chiodini et al. (2008). This procedure is applied mainly to avoid uncertainty in the isotopic composition estimation due to the air pollution from different sources such as anthropogenic CO_2 . This final value was used for the further interpretation of the data.

Table 4. Isotopic $^{13}\text{C}_{\text{CO}_2}$ ($\delta^{13}\text{C}$ ‰) results for both areas, Aguas Hediondas and Lagunas Verdes.

Location	Sample	Sample type	CO_2 flux $\text{g m}^{-2}\text{d}^{-1}$	$\delta^{13}\text{C}$ ‰	\pm	CO_2 ppm (Instrument)	$\delta^{13}\text{C}$ ‰ Final
Aguas Hediondas	CI-2-78L	Bag	25.60	-10.26	0.02	600	-11.81
	CI-2-78H	Bag	18.01	-10.88	0.02	1000	
Aguas Hediondas	CI-3-53L	Bag	19.14	-9.87	0.03	600	-7.92
	CI-3-53H	Bag	12.97	-9.09	0.04	1000	
Aguas Hediondas	CI-5-12L	Bag	11.41	-9.92	0.04	600	-12.88
	CI-5-12H	Bag	8.10	-10.66	0.01	800	
Aguas Hediondas	CI-5-78L	Bag	8.79	-9.87	0.02	550	-13.93
	CI-5-78H	Bag	6.56	-10.08	0.04	580	
Aguas Hediondas	CI-6-9L	Bag	14.20	-10.48	0.01	600	-11.66
	CI-6-9H	Bag	9.91	-10.95	0.03	1000	
Aguas Hediondas	CI-5-49L	Vial	1220.81	-7.155		7000	-7.40
	CI-5-49H	Vial	1165.44	-7.27	0.01	13000	
Lagunas Verdes	CI-7-1L	Vial	412.57	-7.85		4500	-7.69
	CI-7-1H	Vial	408.62	-7.76	0.07	10000	
Lagunas Verdes	CI-7-2L	Vial	731.29	-7.58		5000	-7.00
	CI-7-2H	Vial	706.85	-7.29	0.04	10000	

The location of survey points where samples for isotopic analysis were taken is shown in Figure 35. As we can observe, the values for Aguas Hediondas range from -13.93 to -7.40 ‰, and from -7.69 to -7.00 ‰ in Lagunas Verdes.

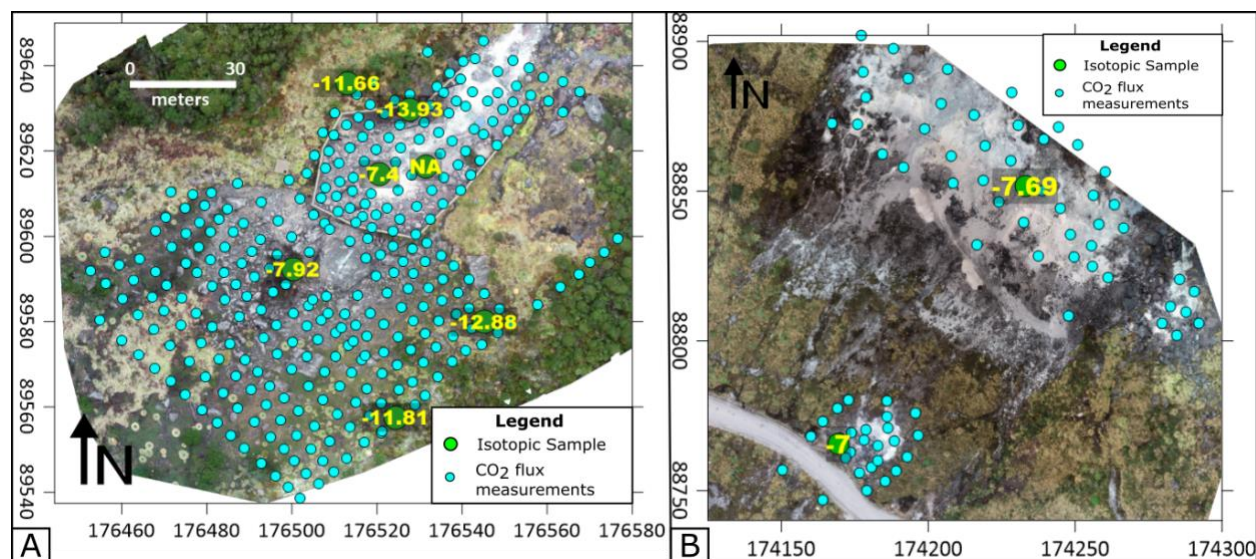


Figure 35. Location of the CO_2 flux measurements and isotopic samples labeled with the isotopic results. A: Aguas Hediondas map. B: Lagunas Verde map. The map coordinates are in meters, UTM – WGS84 18N.

4.3 Soil Temperature

4.3.1 Aguas Hediondas

In Aguas Hediondas, we took 286 soil temperature measurements at the same points where the CO₂ flux measurements were taken. The temperature values range from 1.70 to 28.60 °C. The average of the values is 10.38 °C, as is shown in Table 5.

Figure 36 shows the distribution of soil temperature measurements. We can appreciate that the highest values are located in the restricted area. The highest value is located on the border of the hydrothermal spring channel, at the edge of the restricted area walls. In contrast, the measurements of the rest of the area are mainly medium values and some low values without a great variability. We can find the lowest value in the northern part, outside the restricted area.

Table 5. Statistical parameters of the measured Soil temperature at Aguas Hediondas and Lagunas Verdes during December 2020.

Area	No. of measurements	Min. Soil Temperature (°C)	Max. Soil Temperature (°C)	Average Soil Temperature (°C)
Aguas Hediondas	286	1.70	28.60	10.38
Lagunas Verdes	74	5.90	13.20	9.26

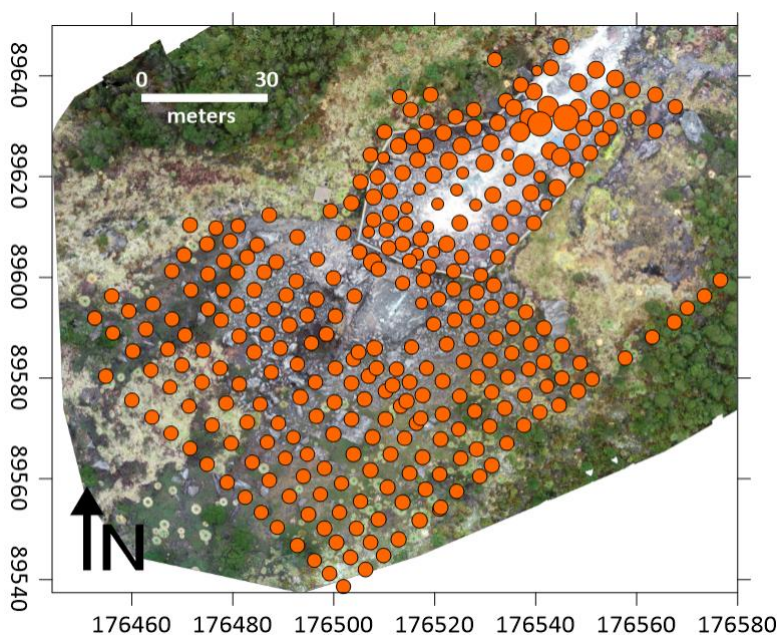


Figure 36. Map of the soil temperatures measurements (°C) from Aguas Hediondas. The dot sizes are proportional to the soil temperature, higher temperatures correspond to bigger dots. The map coordinates are in meters, UTM – WGS84 18N.

We have followed the same statistical process as for the CO₂ flux to model the soil temperature distribution. Therefore, our first step was creating the histogram of the data (Figure 37A), and, as it did not follow a normal distribution, we transformed it into a normal score distribution (Figure 37B).

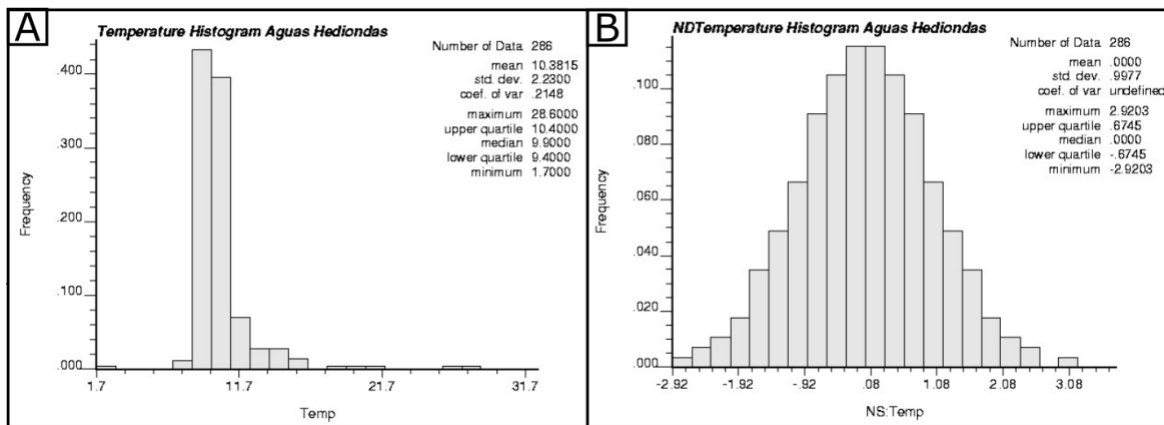


Figure 37. Histograms from the soil temperature (°C) collected in Aguas Hediondas. A: Histogram of the collected data of soil temperature (°C) in Aguas Hediondas. B: Histogram of the normal score transformed soil temperature (°C) in Aguas Hediondas.

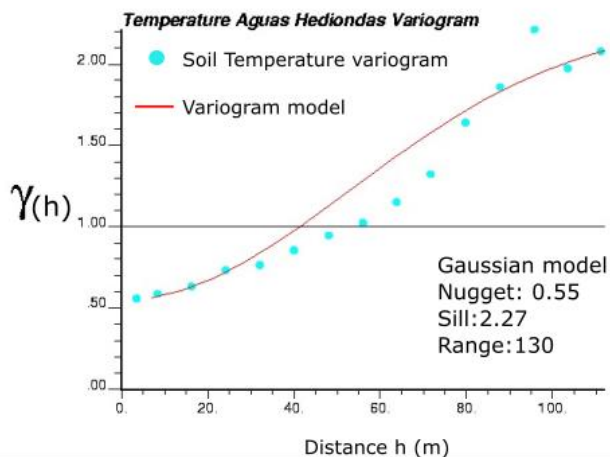


Figure 38. Experimental variogram and variogram model. The light blue dots show the variogram for the normal score transformed Aguas Hediondas Soil Temperature. The red line represents the ideal variogram model that better fits the data.

The next step was to create the best variogram to have the best fit curve of the normalized soil temperature data. A Gaussian variogram model was used, with a sill of 2.27, a range of 130 meters and a nugget of 0.55.

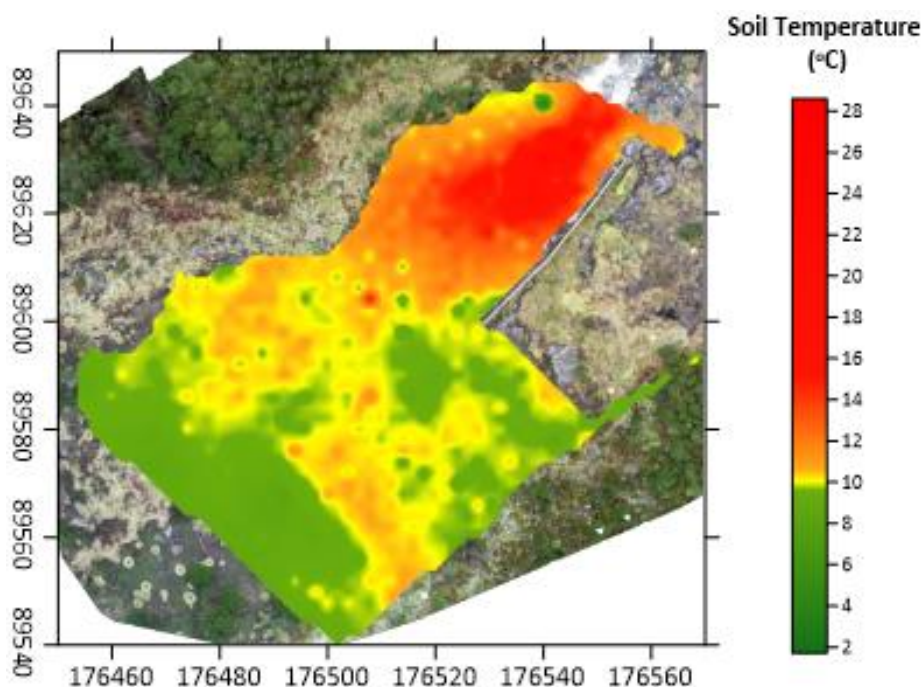


Figure 39. Map of the Soil Temperature distribution in Aguas Hediondas. E-type map of the Spatial distribution of the average of the 100 sequential Gaussian simulations. The map coordinates are in meters, UTM – WGS84 18N.

The result from the E-type map of the soil temperature distribution in Aguas Hediondas is shown in Figure 39. The average of 100 simulations of the soil temperature shows a similar tendency as Figure 36. The highest values are concentrated mainly in the restricted area, at the northeastern edge. The highest values (red color) follow the hydrothermal spring channel. On the other hand, we can see the minimum value in the northern part, outside the restricted area. The rest of the area has medium values predominance, with some areas in greenish that represent low values.

4.3.2 Lagunas Verdes

The soil temperature measurements in Lagunas Verdes are 74, where the minimum and maximum values are 5.90 and 13.20 °C, respectively. The average of the values is 9.26 °C. These statistical values are summarized in Table 5.

Figure 40 shows the location of the measured soil temperature in Lagunas Verdes. We observe that the highest values (bigger dots) are located predominantly in the upper part of the survey area. The lower part is mainly constituted by lower values (smaller dots). High values do not show a clear tendency in the distribution, they are dispersed along the upper area.

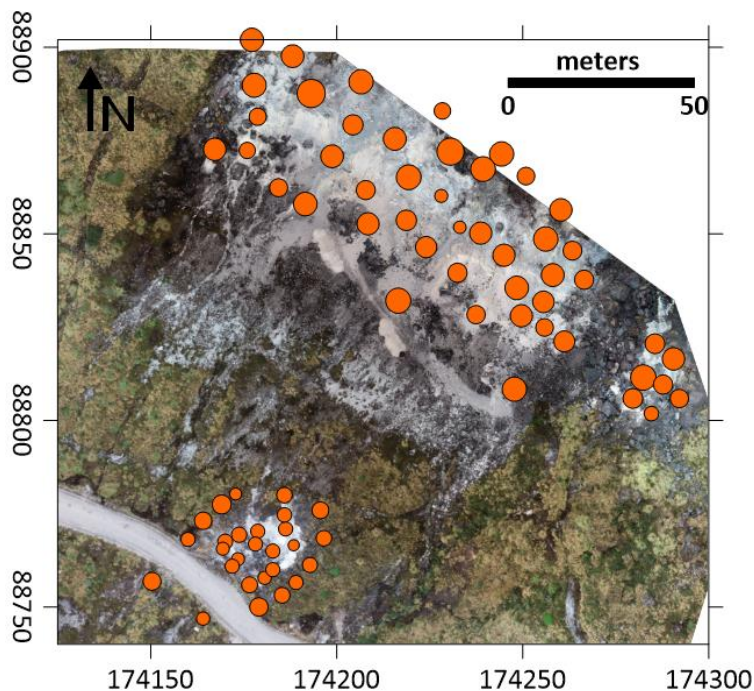


Figure 40. Map of the Soil temperatures measurements ($^{\circ}\text{C}$) from Lagunas Verdes. The dot sizes are proportional to the Soil temperature, higher temperatures correspond to bigger dots. The map coordinates are in meters, UTM – WGS84 18N.

The histogram for soil temperatures at Lagunas Verdes shows more variability in the values than in the case of Aguas Hediondas. Nevertheless, the data is not normally-distributed and requires a normal score transformation (Figure 41) before performing the sGs.

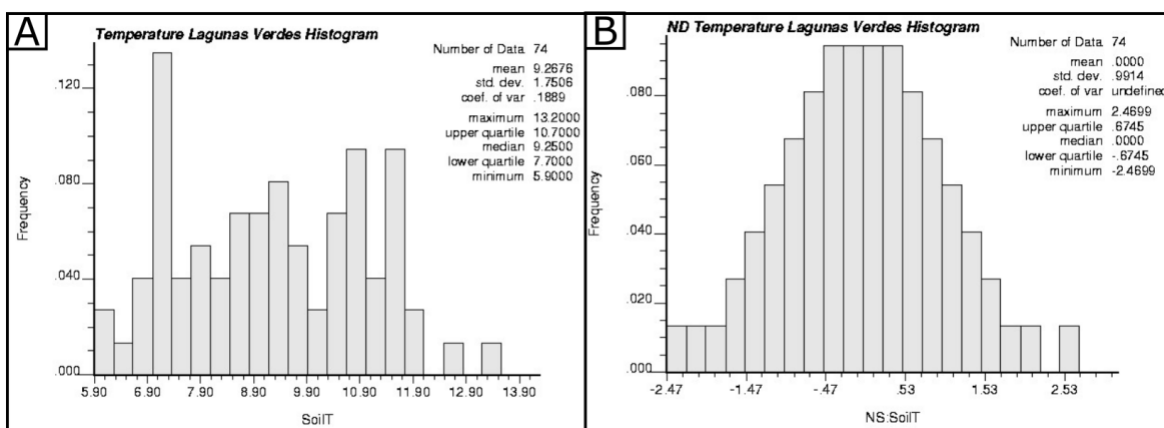


Figure 41. Histograms from the Soil Temperature ($^{\circ}\text{C}$) collected in Lagunas Verdes. A: Histogram of the collected data of Soil Temperature ($^{\circ}\text{C}$) in Lagunas Verdes. B: Histogram of the normal score transformed Soil Temperature in Lagunas Verdes.

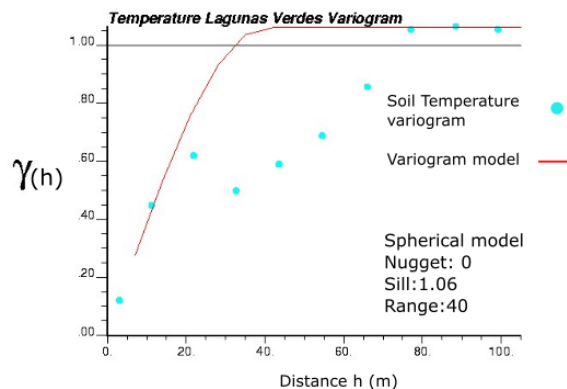


Figure 42. Experimental variogram and variogram model. The light blue dots show the variogram for the normal score transformed Lagunas Verdes Soil Temperature. The red line represents the ideal variogram model that better fits the data.

In this case, the experimental variogram was modelled with a sill at 1.06 in a range of 40 meters and nugget of 0 (Figure 42). In this case, we applied a spherical model, which was the type that best fitted the data. The E-type map of the soil Temperature distribution for the Lagunas Verdes area is presented in Figure 43. The 100 simulation average shows similarities with the distribution of the values in Figure 40. The highest values are located in the upper part, where the predominant color is yellow-reddish, representing the highest values of the data. However, we can note that there are some parts with lower values (greenish areas). The green color covers the lower part of the area, representing the lower soil temperature values.

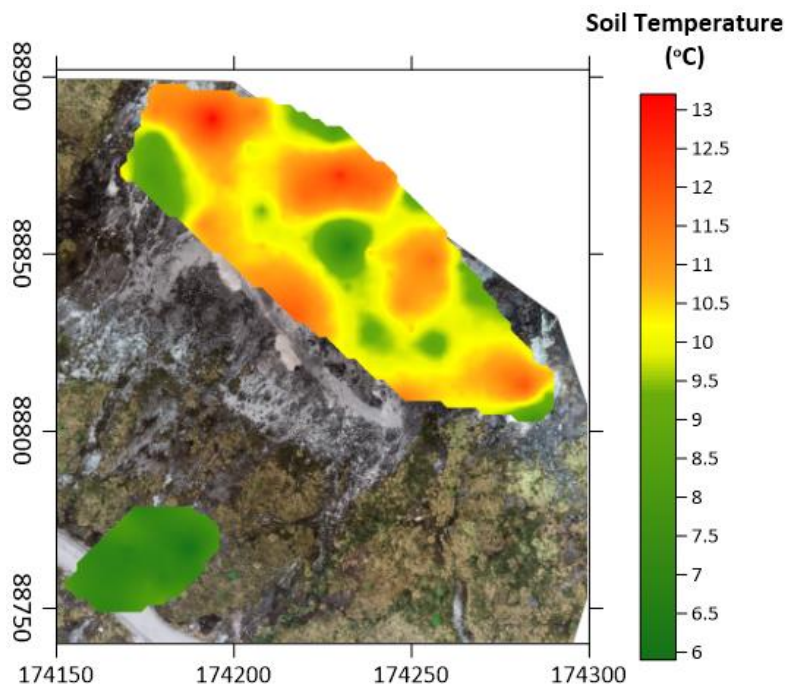


Figure 43. Map of the Soil Temperature distribution in Lagunas Verdes. E-type map of the Spatial distribution of the average of the 100 sequential Gaussian simulations. The map coordinates are in meters, UTM – WGS84 18N.

CHAPTER 5: DISCUSSION

5.1 Control points

Despite CO₂ soil emission appearing to be only influenced by biogenic and hydrothermal sources, several studies have shown that environmental factors can significantly influence CO₂ flux. Meteorological changes like air temperature, soil moisture, soil temperature, barometric pressure, and wind speed, in some instances, can be responsible for more than 50% of the flux variations (Granieri et al., 2003, 2010; Viveiros et al., 2009, 2015; Oliveira et al., 2018).

In Aguas Hediondas, we took control points in two locations in the area to recognize the flux variation and the different parameters that influence it. The first point, 'Wall Control Point,' is located on the east side of the restricted area wall near to the hydrothermal spring area. The second point is located in the southern part of the area, near the paramo forest (Figure 22). Table 6 summarizes the different measurements taken at both control points. The control points were taken at the beginning of the fieldwork (morning) and the end of the fieldwork (afternoon) each day. However, in some cases, just one measurement was taken.

Table 6. Control point measurements. Different parameters measured in the control points taken in Aguas Hediondas on different days. Detail explains if the sample point was measured during the morning (around 7:00 to 8:00 am) or in the afternoon (around 4:00 pm).

Field work day	Date	Detail	CO ₂ Flux (g m ⁻² d ⁻¹)	Air Temp (°C)	Soil Moisture (% VWC)	Soil Temp (°C)	Barometric Pressure (mbar)
Wall Control point							
2	7-Dec-20	Afternoon	4.33	10.1	32.6	10.6	662.2
3	8-Dec-20	Morning	0.00	6.4	35.9	9.6	664.7
	8-Dec-20	Afternoon	1.33	11.2	34.7	11.7	663.7
5	10-Dec-20	Morning	0.00	6.8	45.3	7.4	663.5
	10-Dec-20	Afternoon	6.50	8.6	40.8	15.4	662.2
6	11-Dec-20	Morning	0.00	8.3	44	10.6	662.9
Paramo Control point							
3	8-Dec-20	Morning	14.33	6.52	47.5	8.5	664.7
	8-Dec-20	Afternoon	12.90	11.2	38.4	9.4	662.6
5	10-Dec-20	Morning	0.00	7.12	44.9	8.3	662.8
	10-Dec-20	Afternoon	7.08	8.6	17.8	8.7	661
6	11-Dec-20	Morning	5.88	8.3	33	7.9	660.3

5.1.1 The role of barometric pressure

According to Viveiros et al. (2009), barometric pressure is one of the meteorological factors that most influences CO₂ fluxes. Table 6 and Figure 44 show the variation between the barometric pressure and the CO₂ flux. In 'Wall Control point,' we can appreciate the association between the highest CO₂ flux measurement and the lowest barometric pressure in the afternoon measurement field workday 5. The highest barometric pressures are, in turn, associated with low or null CO₂ fluxes. This inverse correlation has been observed in other studies in long time series of CO₂ flux data (Chiodini et al., 1998; Evans et al., 2001; Granieri et al., 2003; Viveiros et al., 2009). The barometric pumping effect can explain the negative relationship between barometric pressure and CO₂ flux. The pressure gradient drives this effect. In the degassing system, the pore pressure at depth is usually larger than at the surface. When the atmospheric pressure decreases, the gradient across the surface increases, allowing more CO₂ degassing from depth. On the opposite, the high atmospheric pressure forces it back into the ground (Viveiros et al., 2009; Rinaldi et al., 2012).

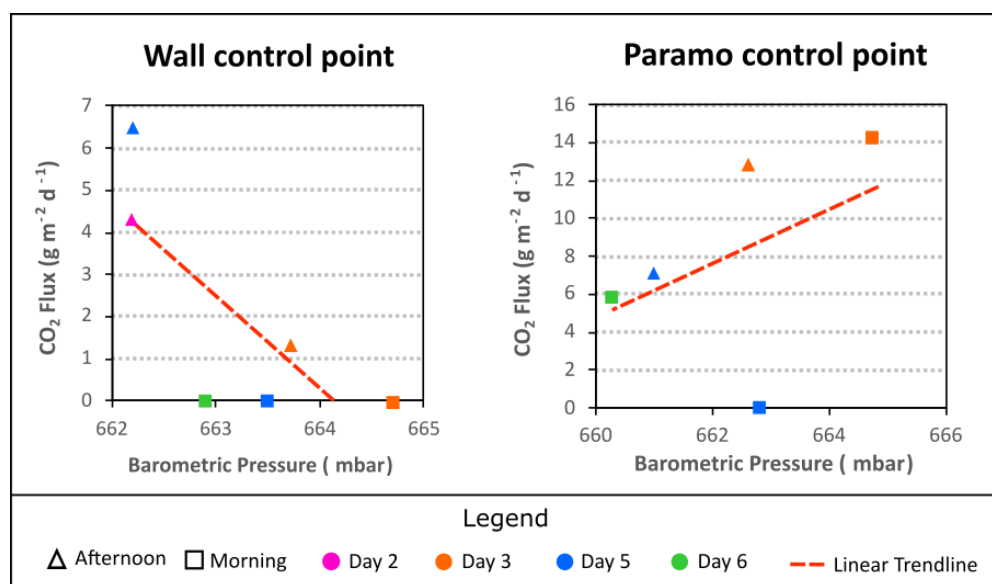


Figure 44. Atmospheric pressure (mbar) vs. CO₂ flux (g m⁻² d⁻¹) of the control points measurements.

In 'Paramo control point,' this tendency is not straightforward. The highest barometric pressure value is associated with the highest CO₂ flux, and the lowest barometric pressure is associated with the second-lowest CO₂ flux value. This could imply that another variable is more influencing in the degasification than the barometric pressure. Besides, the barometric pressure can be directly proportional to the CO₂ flux degassing if we consider that an increase in the barometric pressure can increase the contribution due to density (Rinaldi et al., 2012).

5.1.2 The role of soil moisture

Another measurement taken in the control points was soil moisture which could be related with rainfall. In Table 6 and Figure 45, we can observe that there are changes between the morning and afternoon measurements taken on the same day. In the majority of the cases, we can recognize that in the afternoon, we have greater CO₂ flux. At the same time, the soil moisture decreases in comparison with the morning measurement. Based on this, we can consider a negative relation between the soil moisture and the CO₂ flux, i.e., the CO₂ soil degassing decreases with increasing soil moisture. This effect can be explained by the water effect on the soil porosity. Water infiltration can fill the porosity of soils and create an impermeable barrier and obstruct the release of the gas to the surface dispersing it to a dry area (Granieri et al., 2003; Viveiros et al., 2015). However, this correlation can be highly influenced by other factors such as the topography, the drainage system, and the porosity of the soil (Viveiros et al., 2009).

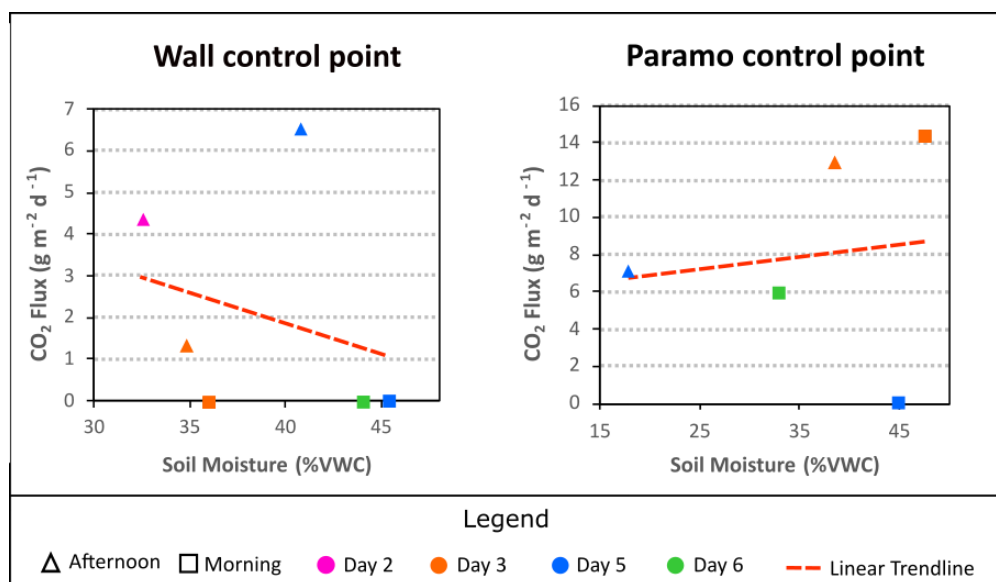


Figure 45. Soil moisture (%VWC) vs. CO₂ flux (g m⁻² d⁻¹) of the control points measurements.

5.1.3 The roll of air temperature

Air temperature is another meteorological variable measured in the control points. Our results show a positive relationship between this variable and the CO₂ fluxes in most of the measurements taken on the same day (Figure 46). Some studies have got as result an inverse correlation between these two variables (Rinaldi et al., 2012; Viveiros et al., 2014). The fluid properties could explain this relation. The air temperature changes the gas fluid mobility relating lower temperature with lower viscosity and higher CO₂ density. Thanks to buoyancy properties, higher density drives the gas upward motion, resulting in higher CO₂ fluxes (Rinaldi et al., 2012). On the other hand, in the study performed by Oliveira et al. (2018)

they observed a positive correlation between the air temperature and the CO₂ flux. They attribute this kind of relationship to a superposition of more influence environmental variables and the influence of the thermal anomalies where the control points were located. Therefore, in our study case, we cannot determine if the air temperature significantly influences by itself the CO₂ flux emission in both areas.

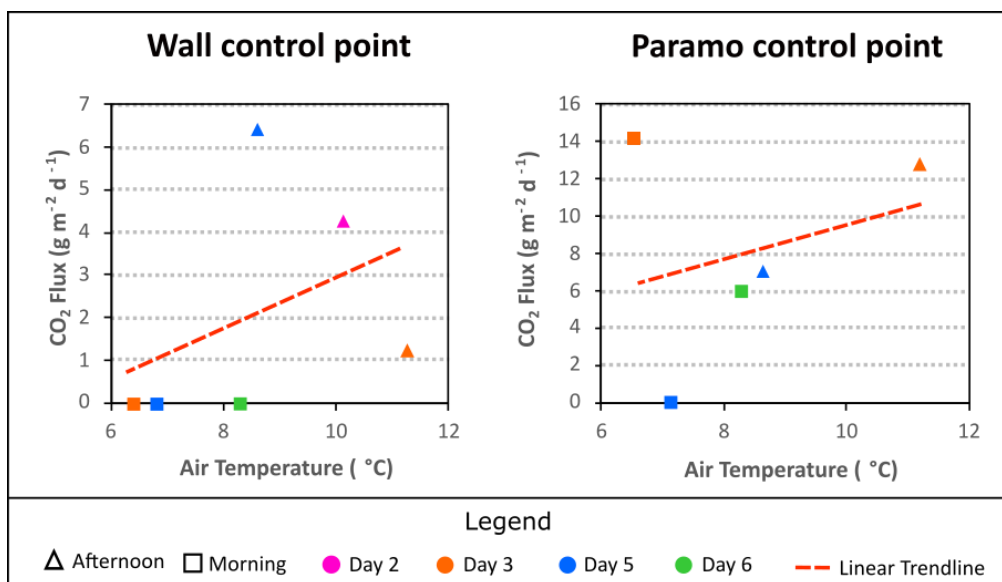


Figure 46. Air temperature (°C) vs. CO₂ flux (g m⁻² d⁻¹) of the control points measurements.

5.1.4 The roll of soil temperature

Soil temperature is the last variable measured in the control points. We can notice a variation in this variable between both control points (Figure 47). In the case of 'Wall Control Point,' in general, we got higher soil temperature values (Table 6) than in 'Paramo Control point.' Now analyzing each control point, we can appreciate that in the case of 'Wall Control Point,' the highest fluxes are associated with the highest soil temperature. On the other hand, the lowest fluxes are associated with the lowest CO₂ fluxes. In the case of the Paramo control point, the tendency is not so evident. The location of each control point plays a crucial role. The location of the hydrothermal spring near the 'Wall control point' has an influence on the soil temperature in that area. This we do not see in the 'Paramo control point' where the predominant feature of the area is the vegetation that covers the area. However, we can still see higher CO₂ fluxes associated with higher soil temperatures. The positive relation between both variables in the case of 'Wall Control Point' could be explained by the hydrothermal hot spring located in the area. The lack of vegetation in the 'Wall control point' area could also influence the afternoon/morning soil temperature variation. The direct heating from the sun could easily reach the 'Wall control point, which is directly exposed. The case for 'The Paramo control point is different, where we have a vegetation layer

that covers the control point, avoiding the soil's exposure to the sun's rays. Therefore, in the case of the 'Paramo control point, the morning/afternoon soil temperature variation is not too big compared to the 'Wall control point.' On the other hand, in Paramo Control Point, the soil temperature can be influenced more by biological oxidation because of its location. This control point is located on a paramo forest where the oxidation of vegetation can release heat, increasing the soil temperature and increasing the CO₂ flux emission (Viveiros et al., 2015).

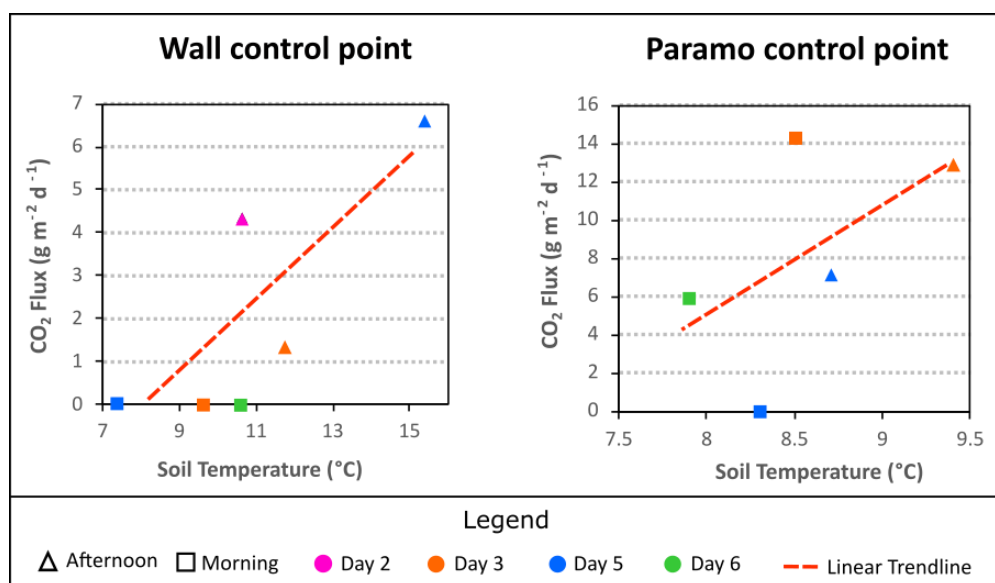


Figure 47. Soil Temperature (°C) vs. CO₂ flux (g m⁻² d⁻¹) of the control points measurements.

5.2 Soil Temperature Distribution

Soil temperature measurements were taken in both survey areas to recognize thermal anomalies and a relationship pattern between soil temperature and soil CO₂ degassing. In previous studies, a positive correlation between these two variables has been found (Fischer & Chiodini, 2015; Giammanco et al., 2016; Roulleau et al., 2017; Taussi et al., 2021). This positive correlation is explained by the ascent of deeper hot hydrothermal fluids. Hot hydrothermal fluids release steam, which condenses near the surface and heats surrounding soil thanks to the thermal energy released. The CO₂, instead, is not a condensable gas; therefore, it is released by diffuse degassing through the soil (Stix, 2015).

Aguas Hediondas is the survey area with more data density. Figure 30 and Figure 39 are the soil CO₂ flux emission map and the soil temperature distribution, respectively. If we compare both maps, we can see some similar patterns. The most remarkable pattern is located inside the walls, 'the restricted area' on the north-east side of the area. As we mentioned in the results, in this area, we got the highest CO₂ flux

emissions in the area. In the same region, we can observe the predominance of red color, which implies that the highest soil temperature follows the hot spring channel. The hydrothermal spring in the area can be the primary driver for this positive correlation for the same reasons as the influence of soil temperature on CO₂ fluxes. Therefore, this area is dominated the diffusive – advective fluxes, where the hydrothermal hot springs play the role of the pressure-driven viscous flow that transports the hydrothermal gases to the surface and heats the soil at the same time (Taussi et al., 2021). Furthermore, the $\delta^{13}\text{C}$ ‰ values from the samples taken in this area are high, implying a more significant influence of the deep hydrothermal CO₂ source than other sources such as the biogenic CO₂.

The rest of the area follows the same pattern in both maps, with low CO₂ fluxes areas associated with low soil temperature. The areas with medium Soil CO₂ fluxes are associated with medium soil temperature. The deep hydrothermal CO₂ source can drive this relation between the CO₂ flux emission and soil temperature, as was explained before. However, in this case, it is necessary to consider another source of CO₂ and heat which is the biogenic influence. In this area, there is the presence of vegetation which was not the case in the ‘restricted area’ where the vegetation was absent. As explained before, the vegetation can contribute to CO₂ emissions through the respiration process and, besides, heating the soil thanks to the oxidation of organic matter (Viveiros et al., 2015). However, the heat source from the vegetation is cooler compared with the hydrothermal origin source. The contribution of biogenic sources in this area agrees with our isotopic data. In this area, we obtained the lowest $\delta^{13}\text{C}$ ‰ values. Low $\delta^{13}\text{C}$ ‰ values are not associated with deep CO₂ hydrothermal, but with a biogenic CO₂ contribution.

Lagunas Verdes area follows a different pattern between soil CO₂ diffuse degassing and soil temperature. Firstly, we can notice that the maximum soil temperature is lower than the maximum soil temperature in Aguas Hediondas. When we compare Figure 34 and Figure 43, the map of soil CO₂ diffuse degassing map and soil temperature map, we can see some tendencies. The upper area has a positive relationship with the CO₂ emissions. In the majority of the areas where we have high fluxes, we have high soil temperatures. One exception to this tendency is in the location of the higher soil temperature (northwestern corner of the area), which is associated with low CO₂ fluxes. Contrastingly, the soil temperature was the minimum in the lower part, where we measured the highest CO₂ fluxes. This effect suggests a negative correlation between the soil temperature and the soil CO₂ flux in this area.

This relationship can be explained by cold degassing. This effect implies removing the steam component that heats the soil in thermal areas and just having a source of CO₂ flux high enough to create a high CO₂ diffuse degassing at the surface (Rahilly & Fischer, 2021). One process to remove the steam component

could be the mix of deep hydrothermal water and meteoric water. The deep hydrothermal water contributes with hydrothermal gases such as CO₂. The meteoric water cools enough the hydrothermal water to avoid the creation of hot water vapor at depth (Bergfeld et al., 2012).

Last but not least is essential to mention that the vegetation in the area is very little, being much less than in Aguas Hediondas. Besides, considering that the two $\delta^{13}\text{C}$ ‰ values from the CO₂ gas samples in this area are high, it implies a more significant contribution from deep hydrothermal CO₂ compared to its biogenic counterpart. Therefore, we can expect less biogenic influence in both measurements, CO₂ flux, and soil temperature.

5.3 Volcanic CO₂ contribution to the Diffuse Degassing

5.3.1 Mixing model with isotopes

Discriminating between the different sources of CO₂ is one of the main objectives of this study. We decided to use the isotopic composition of the CO₂ gas samples ($\delta^{13}\text{C}_{\text{CO}_2}$) to differentiate between biogenic and hydrothermal CO₂ contributions. The results that we obtained for the isotopic analysis in both sites (Table 4) have shown mainly that in areas without vegetation, the samples have higher isotopic values (-7 to -8 ‰). The values are lower in areas with vegetation (-11 to -14 ‰) (Figure 35). Here we can remember the isotopic signature; we can see that the highest values of $\delta^{13}\text{C}_{\text{CO}_2}$ usually correspond to volcanic hydrothermal emissions and the lowest to biogenic CO₂ emissions. Therefore, we realized that variations of $\delta^{13}\text{C}_{\text{CO}_2}$ values could suggest the presence of three different populations: deep hydrothermal CO₂, biogenic CO₂, and a mixture of the two.

We can estimate the isotopic ¹³C signature of hydrothermal and biogenic CO₂ from the literature. There is no fumarolic data for Chiles, but data from Cumbal (less than 10 km away) and Galeras (70 km away), two close-by volcanoes (Figure 5A), indicate a deep CO₂ source with $\delta^{13}\text{C}_{\text{CO}_2}$ values of around -7 ‰ (Fischer et al., 1997; Sano et al., 1997; Lewicki et al., 2000). For the biogenic, plants have varying values according to the plant type, but a study of paramo soils in Ecuador, in a similar environment, gave a value of -24 ‰ (Chapela et al., 2001). We applied a mixing model (Figure 48) to determine the biogenic flux, i.e., how much CO₂ is produced from biogenic processes only. It was modeled using an isotopic ¹³C composition for the hydrothermal source of -7 ‰ and for the biogenic source of -24 ‰, the values between these two would represent a mixture of both sources. The mixing curve lines for the biogenic flux were modeled based on this. A biogenic flux of 7 g m⁻² d⁻¹ does not explain some of the values measured, with two sample points outside the curve. With a flux of 50 g m⁻² d⁻¹, the mixing curve is too far from the sample points. A

flux of $15 \text{ g m}^{-2} \text{ d}^{-1}$ best fits the data. As a result, we estimate that the biogenic flux has a maximum value of $15 \text{ g m}^{-2} \text{ d}^{-1}$.

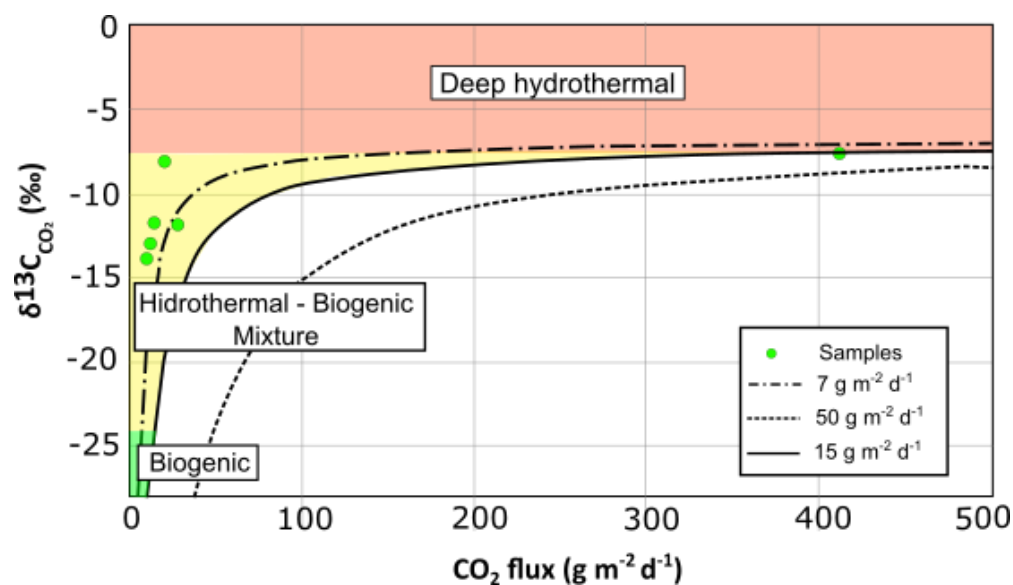


Figure 48. Diagram plotting $\delta^{13}\text{C}_{\text{CO}_2}$ ‰ isotopic composition vs. CO_2 flux ($\text{g m}^{-2} \text{ d}^{-1}$) of each gas sample taken in the field. The different lines represent theoretical flux rates based on a mixing model. The plot represents the corresponding ranges from the different CO_2 sources: Biogenic, deep hydrothermal, and a mixture.

5.3.2 Probability maps for soil CO_2 flux

Probability maps are excellent for estimating the deep hydrothermal CO_2 contribution to an area soil CO_2 diffuse degassing. Besides, they are helpful to identify DDS (Viveiros et al., 2010). The probability map requires a cut-off value to estimate the probability that, at a certain point, the CO_2 flux exceeds this threshold. We used as a cut-off value $30 \text{ g m}^{-2} \text{ d}^{-1}$, twice the maximum biogenic flux estimated before ($15 \text{ g m}^{-2} \text{ d}^{-1}$). Viveiros et al. (2010) recommend using two times higher the estimated maximum biogenic flux to decrease the uncertainty caused by the variability of the biogenic CO_2 fluxes. As a result, probability maps highlight areas where the soil CO_2 diffuse degassing is strongly influenced by deep hydrothermal CO_2 . Thus, we can estimate the CO_2 from a volcanic origin emitted in an area.

Figure 49 shows the resulting probability maps for Aguas Hediondas (A) and Lagunas Verdes (B). In Aguas Hediondas, we can observe 16 locations in the vicinity of the hot spring with a probability of 1 to present a deep CO_2 hydrothermal contribution. This result agrees with the distribution of the CO_2 flux emission, which highest values were located in the same area. The rest of the area presents a low probability of being fed by volcanic origin CO_2 solely. Therefore, we can conclude that in this part of the area, the

biogenic CO₂ source predominates. The conclusion agrees with the fact that the area is covered by more vegetation than in the hot spring area, and it has low CO₂ flux values associated.

Lagunas Verdes in general shows more influence of deep hydrothermal CO₂ than Aguas Hediondas (Figure 49B). The presence of an active fumarole could determine the predominance of direct degassing in the area of Aguas Hediondas. In the case of Lagunas Verdes, the area corresponds to an old fumarolic field; however, there is no evidence of some direct degassing structure in the area. This characteristic implies a predominance of soil CO₂ diffuse degassing in the area, having several points with a probability of 1 of having a contribution of volcanic CO₂ origin. In the lower part of the area, the high probabilistic values are concentrated in one closed circular area, which could represent a DDS. We have less high probabilistic values in the upper area than in the lower part. Nevertheless, some areas have a probability of more than the 50%. The high contribution of deep hydrothermal CO₂ in Lagunas Verdes agrees with our isotopic data obtained there and with the fact that the vegetation is very little in the zone where what prevails is the hydrothermal alteration. Due to the nature of the zone, a good explanation of the high volcanic CO₂ degassing in this area is the presence of a hidden tectonic structure in the area and a significant influence of a deep hydrothermal source that cutcrosses the area beneath the surface.

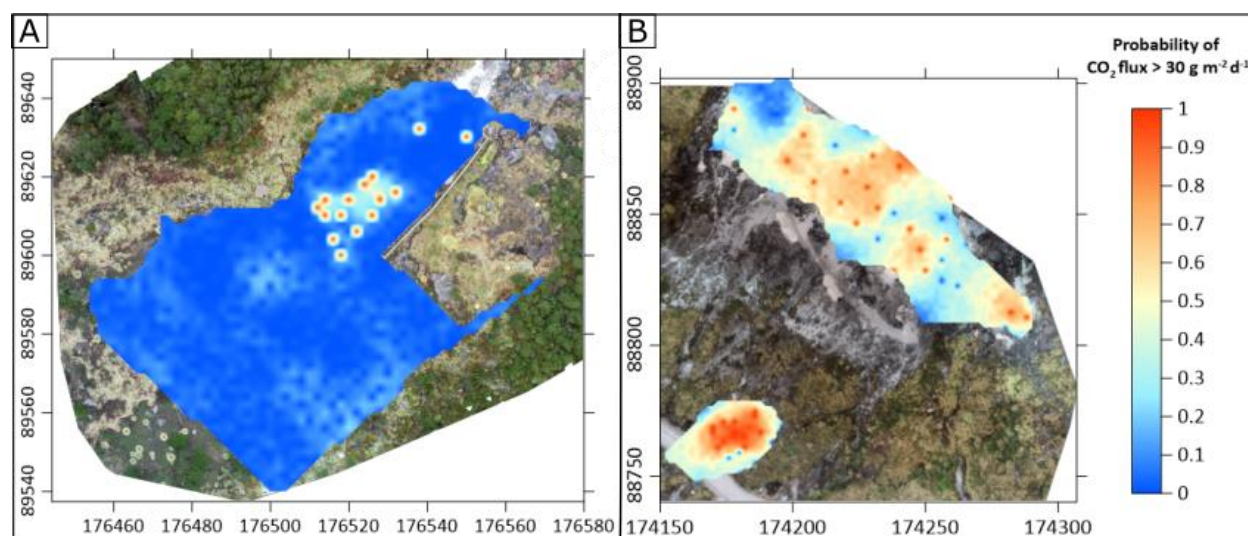


Figure 49. Probability maps for soil CO₂ diffuse degassing at A: Aguas Hediondas and B: Lagunas Verdes. The color scale shows the probability of soil CO₂ flux exceeding the cut-off value (30 g m⁻² d⁻¹). The maps coordinates are in meters, UTM – WGS84 18N.

5.3.3 CO₂ total emission

Finally, following the assumption that the contribution of deep hydrothermal CO₂ source starts with fluxes higher than 30 g m⁻² d⁻¹ we can estimate the total volcanic CO₂ origin emitted per day (Table 7). As we expected, in Lagunas Verdes, the contribution of deep hydrothermal CO₂ emission is more than 80% of

the total CO₂ diffuse degasification of the area (Table 7, column 7). At Aguas Hediondas, instead, it seems to be divided in half between the volcanic CO₂ origin and another source of CO₂ that, in this case, could be a biological source. These total emission values can be helpful as baseline values for further studies in the area, to see variations in the degasification and as a tool for the Chiles volcano activity monitoring.

Table 7. Total CO₂ diffuse degassing output at Aguas Hediondas and Lagunas Verdes. Estimation based on the realization of the 100 Sequential Gaussian Simulation (sGs).

Site	Area (km ²)	Number of points	Total CO ₂ diffuse degassing (t d ⁻¹)	Total CO ₂ emission per area (t d ⁻¹ km ⁻²)	Total deep hydrothermal CO ₂ diffuse degassing	
					(t d ⁻¹)	(%)
Aguas Hediondas	0.006	339	0.11 ± 0.01	18.33 ± 2	0.06±0.02	54.55
Lagunas Verdes	0.005	76	1.66 ± 0.08	332 ± 16	1.49±0.08	89.76

5.3.4 CO₂ diffuse degassing around the world

Soil CO₂ diffuse degassing has been researched worldwide in different degassing areas. Table 8 summarizes some places where the total diffuse degassing was estimated. Comparing this data with our results, we realize that the total CO₂ diffuse degassing estimated in our area is low. However, it is essential to take into account some variables that influence total emissions. The first factor is the survey area extension. In most cases, the survey area covers several kilometers. In our case study, we covered a few meters. Besides, geological factors that also influence the geological framework of the area, tectonic setting, the last volcano eruption, or the current volcano activity state. Besides, environmental factors could influence too, as it was discussed previously in the control points section.

For the purpose of making a good comparison, the CO₂ flux emissions were standardized to obtain the CO₂ emission per unit of area (t d⁻¹ km⁻²). As we can observe in Table 8 in column 5, the emissions are similar to or lower than the resulting CO₂ flux emission per unit of area in Chiles volcano obtained in this research (Table 7, column 5). In Lagunas Verdes, we got an emission of 332 t d⁻¹ km⁻², which result be much higher than the other places in Ecuador, like Cuicocha, and Pululahua calderas. Besides, the value is pretty significant, comparable with places with great volcanic activity, such as Furnas volcano in the Azores

archipelago. This implies tremendous importance in the CO₂ emission in this area, not only on a regional level but on a world scale.

According to Ritchie et al. (2020), the total CO₂ emission in Ecuador correspond to 30.93 million tons just in 2020. This value implies the emission per day is 84 744.55 tons of CO₂. The primary anthropogenic sectors that emit CO₂ in the country are land-use change and forestry, transport, agriculture, waste, and electricity and heat. Comparing this value with the deep hydrothermal CO₂ emission found in this research related to the Chiles volcano, the CO₂ hydrothermal-related input corresponds to 0.002% of the total CO₂ emission in the country. Besides, compared with a significant anthropogenic source such as the transport CO₂ emission, it represents 0.004%. The percentage could appear to be insignificant. However, it is essential to consider that these values just represent the emission of a small area near just one volcano out of the many volcanoes in the country. If we had more data about the CO₂ diffuse emission coming from all active/dormant volcanoes in the country, the percentage would be higher.

Table 8. CO₂ diffuse degassing emitted by degassing areas in different countries.

Study Area	CO₂ Flux (t d⁻¹)	Area (km²)	Number of Points	Total CO₂ emission per area (t d⁻¹ km⁻²)	Reference
Cuicocha Caldera, Ecuador	106	13.30	172	7.97	Padrón et al., 2008
Pululahua caldera, Ecuador	270	27.60	217	9.78	Padrón et al., 2008
Complejo Volcánico Copahue – Caviahue, Argentina	208.5	9	2380	23.16	Lamberti et al., 2020
Peteroa volcano, Argentina	6.5	0.07	125	92.80	Lamberti et al., 2020
Solfatarra volcano, Italy	1500	1	333	1500	Chiodini et al., 2001
Vulcano island, Italy	75	1.90	423	39.47	Chiodini et al., 1996
Furnas volcano, Azores archipelago	968	4.8	2605	201.16	Viveiros et al., 2010
Furnas do Enxofre, Azores archipelago	2.54	0.02	281	127	Viveiros et al., 2020

5.3.5 Diffuse Degassing Structures

Using probabilistic maps, we can recognize diffuse degassing structures (DDS). The locations that show a probability greater than 50% of emitting a CO₂ flux higher than the threshold could be considered a DDS (Viveiros et al., 2010). Following this, we can recognize DDS in Aguas Hediondas and Lagunas Verdes. In Aguas Hediondas, the DDS is located inside the walls in the ‘restricted area.’ They are highly connected with the presence of the hydrothermal spring. On the other hand, in Lagunas Verdes there is the presence of more DDS in different parts of the area. One is located in the lower part of the area, where we got the highest fluxes. Another DDS in the upper part is distributed along the area without following a linear pattern.

Usually, DDS are connected with tectonic structures such as lineaments, fractures and faults. In order to visualize some relationship between tectonic structures and DDS, we map the faults and lineaments in Chiles volcano Area (Figure 50A). In Figure 50A, we can observe that the two surveyed areas are located in areas near faults and lineaments. Lagunas Verdes is near two faults, but not precisely on them; therefore, a relationship between the DDS and one of these faults could be dismissed. However, a hidden tectonic structure could be the main driver for the degassing in this zone. Therefore, it is necessary a deeper understanding of the tectonic setting of the area to understand the degassing pattern found in the area.

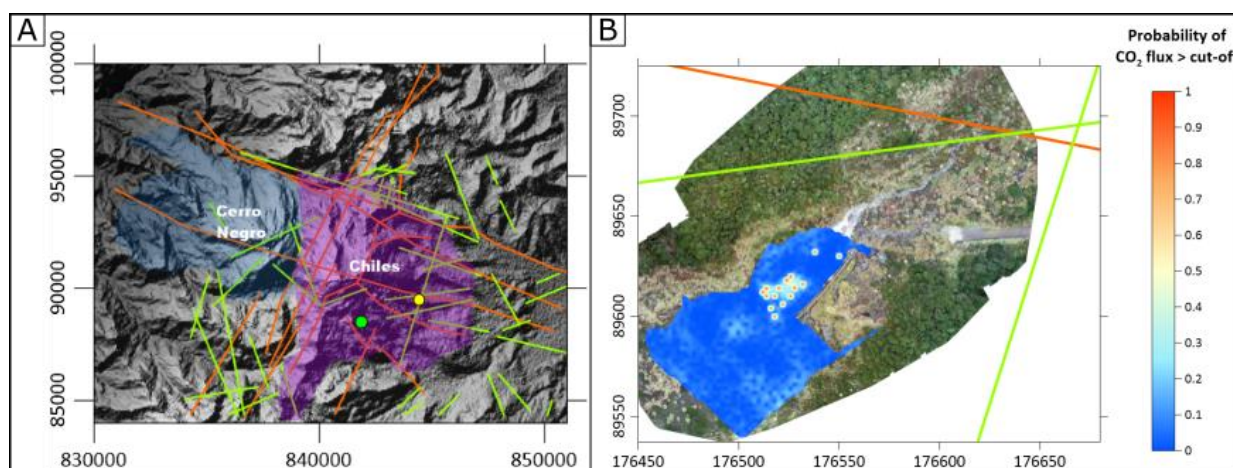


Figure 50. Lineaments (green) and Faults (Orange) that are located in Chiles volcano. A: Chiles volcano general view with the faults and lineaments and the location of the two surveyed areas, Aguas Hediondas (Yellow) and Lagunas Verdes (Green). B: Aguas Hediondas probability map with the lineaments and faults near the area. The maps coordinates are in meters, UTM – WGS84 18N.

Now in the case of Aguas Hediondas, it is located near one fault and two lineaments (Figure 50B). However, it is not located precisely above them. Therefore, we can conclude that the DDS is more related

to the presence of the hydrothermal spring than to a tectonic structure in the area. Besides, these tectonic structures near the area could influence the minor deep hydrothermal CO₂ contribution that we found in the rest of the Aguas Hediondas area. As faults and lineaments represent weak zones, they are good paths for rising CO₂ to the surface. Therefore, further studies near these tectonic structures are crucial to better understand the diffuse degassing of the area.

CHAPTER 6: CONCLUSIONS AND FUTURE WORK

The main conclusions of this research are:

1. Chiles volcano is an area with a geothermal potential that shows superficial expression of the internal heat. It does this not only through hydrothermal springs and active fumaroles but, also by diffuse degassing in the surrounding areas.
2. We can recognize soil CO₂ degasification and thermal anomalies in two areas: Aguas Hediondas and Lagunas Verdes.
3. The isotopic data reveals three populations: deep hydrothermal CO₂, biogenic CO₂ and a mixture of the two. The mixed population is a mix between a deep source with isotopic values of ¹³C ~ -7 ‰, and a biogenic source with isotopic values of ~ -24 ‰ and a flux of 15 g m⁻² d⁻¹.
4. In Aguas Hediondas in general, it seems that most gases are degassing through direct degassing, while diffuse degassing is restricted. It is an area where the soil CO₂ diffuse degassing is dominated by the hydrothermal spring located in the area. The total diffuse degassing in an area of 6 000 m² approx. was about 0.11 t d⁻¹ of which 0.6 t d⁻¹ are contributed by a deep hydrothermal CO₂ source. Moreover, in this area we can appreciate the influence of biogenic CO₂ source due to the presence of abundant vegetation.
5. Lagunas Verdes shows a higher CO₂ flux. It is an area where the deep hydrothermal CO₂ source is predominant along the area. In an area of 5 000 m² covered, the total CO₂ flux degasification corresponds to 1.66 t d⁻¹, of which more than the 80% shows the contribution of a volcanic CO₂ source, 1.49 t d⁻¹. The lack of abundant vegetation in this area just proves the predominance of the volcanic CO₂ source. The DDS in this area could be associated more with a hidden tectonic structure and a deep hydrothermal reservoir which contributes to the area with the hydrothermal gases.
6. The total diffuse CO₂ emissions in the surveyed areas apparently seem lower than in the other studied areas in Ecuador and worldwide. However, comparing the CO₂ emission per day per unit of the area, we can notice a tremendous CO₂ emission rate compared with other diffuse degassing active areas, predominantly what regards Lagunas Verdes. This fact only reinforces the evidence of the geothermal potential of the Chiles volcano.
7. The CO₂ flux emitted in the surveyed areas in Chiles volcano represents 0.002% of the total CO₂ emission in Ecuador in 2020. Besides, it represents 0.004% of a significant anthropogenic source such as the vehicle CO₂ emission. This information can help to refine the global carbon budget where the natural CO₂ inputs need to be better estimated.

For future work a more rigorous survey at Lagunas Verdes could be implemented. Lagunas Verdes is where we got the highest CO₂ fluxes and the more volcanic-related CO₂ δ¹³C ‰ values. Therefore, performing a survey with a regular measurement grid covering a larger area and collecting more isotopic samples for analysis could help us better understand and estimate the CO₂ diffuse degassing capacity in the area.

Besides, a regular CO₂ diffuse degassing in both areas could help understand the Chiles volcano's internal activity. Using the results obtained in this research as a baseline, we can notice variations in the CO₂ diffuse degassing over long periods of time. The results got in this research denote a significant diffuse degassing in the area predominantly regards Lagunas Verdes, which is worthy of regular monitoring.

Extending the survey area would be a good idea, knowing that there is evidence of places such as Lagunas Verdes with high CO₂ diffuse degassing. Performing the same methodology in other hydrothermal areas or other locations around the Chiles volcano can help us better estimate the total CO₂ emission related to the volcano.

The faults and lineaments in the area play a crucial role in diffuse degassing. Therefore, performing a new field mapping campaign to improve the map faults and widen the knowledge about the tectonic structures of the area would help with the understanding and interpretation of the CO₂ diffuse degassing of the area.

Finally, as Chiles volcano is very known for its geothermal potential, research to estimate the thermal energy release and quantify the area's geothermal potential would benefit future geothermal projects. The thermal energy released can be estimated using H₂O/ CO₂ ratio. Therefore, the estimation of CO₂ diffuse degassing of the area is fundamental for this study. As a result, we could see the thermal energy released by the geothermal area in megawatts (MW), which is crucial for implementing geothermal power plants.

REFERENCES

- Agehara, S., & Warncke, D. (2005). Soil alternate wetting and drying pure and temperature effects on nitrogen release from organic nitrogen sources. *Soil Sci Soc Am J*, *69*, 1844–1855.
- Allard, P. (1992). Diffuse degassing of carbon dioxide through volcanic systems.; Observed facts and implications. *Chishitsu Chosajo Hokoku (Report, Geological Survey of Japan);(Japan)*, *279*.
- Angermann, D., Klotz, J., & Reigber, C. (1999). Space-geodetic estimation of the Nazca-South America Euler vector. *Earth and Planetary Science Letters*, *171*(3), 329–334.
- Aspden, J. A., McCourt, W. J., & Brook, M. (1987). Geometrical control of subduction-related magmatism: the Mesozoic and Cenozoic plutonic history of Western Colombia. *Journal of the Geological Society*, *144*(6), 893–905. <https://doi.org/10.1144/GSJGS.144.6.0893>
- Bergfeld, D., Evans, W. C., Lowenstern, J. B., & Hurwitz, S. (2012). Carbon dioxide and hydrogen sulfide degassing and cryptic thermal input to Brimstone Basin, Yellowstone National Park, Wyoming. *Chemical Geology*, *330*, 233–243.
- Bernard, B., & Andrade, D. (2011). Mapa de volcanes cuaternarios del Ecuador continental. *Quito, Ecuador. IGEPN/IRD Poster Informativo*.
- Berner, R., & Lasaga, A. (1989). Modeling the Geochemical Carbon Cycle. *Scientific American*, *222*, 74–82. <https://doi.org/10.1038/scientificamerican0389-74>
- Bezyk, Y., Sówka, I., & Górka, M. (2021). Assessment of urban CO2 budget: Anthropogenic and biogenic inputs. *Urban Climate*, *39*, 100949.
- Blong RJ. (1984). *Volcanic hazards. A sourcebook on the effects of eruptions*. Academic Press.
- Bocanegra, L. C., & Sánchez, J. J. (2017). Mapa de fallas de los volcanes Chiles-Cerro Negro (Nariño) a partir de minería de datos y confirmación de campo. *Boletín de Geología*, *39*(3). <https://doi.org/10.18273/revbol.v39n3-2017005>
- Branney, M., & Acocella, V. (2015). Calderas. In *The encyclopedia of volcanoes* (pp. 299–315). Elsevier.
- Bunt, J. S., & Rovira, A. D. (1954). Oxygen uptake and carbon dioxide evolution of heat-sterilized soil [16]. *Nature*, *173*(4417), 1242. <https://doi.org/10.1038/1731242a0>
- Cardellini, C., Chiodini, G., & Frondini, F. (2003). Application of stochastic simulation to CO2 flux from soil: Mapping and quantification of gas release. *Journal of Geophysical Research: Solid Earth*, *108*(B9). <https://doi.org/10.1029/2002JB002165>
- CELEC, & ISAGEN. (2015). *Informe Geológico Parcial del Proyecto Geotérmico Binacional Tufiño-Chiles-Cerro Negro*. <https://www2.sgc.gov.co/Noticias/boletinesDocumentos/INFORME ESPECIAL CHILES-CERRO NEGRO - 2019 - N1.pdf>
- Chapela, I. H., Osher, L. J., Horton, T. R., & Henn, M. R. (2001). Ectomycorrhizal fungi introduced with exotic pine plantations induce soil carbon depletion. *Soil Biology and Biochemistry*, *33*(12), 1733–1740. [https://doi.org/https://doi.org/10.1016/S0038-0717\(01\)00098-0](https://doi.org/https://doi.org/10.1016/S0038-0717(01)00098-0)
- Chimbolema, S., Suárez, D., Peñafiel, M., Acurio, C., & Paredes, T. (2013). Guía de plantas de la Reserva ecológica el Angel. *Quito: DCG IMPRESORES*.

- Chiodini, G., Caliro, S., Cardellini, C., Avino, R., Granieri, D., & Schmidt, A. (2008). Carbon isotopic composition of soil CO₂ efflux, a powerful method to discriminate different sources feeding soil CO₂ degassing in volcanic-hydrothermal areas. *Earth and Planetary Science Letters*, 274(3–4). <https://doi.org/10.1016/j.epsl.2008.07.051>
- Chiodini, G., Cioni, R., Guidi, M., Raco, B., & Marini, L. (1998). Soil CO₂ flux measurements in volcanic and geothermal areas. *Applied Geochemistry*, 13(5), 543–552. [https://doi.org/10.1016/S0883-2927\(97\)00076-0](https://doi.org/10.1016/S0883-2927(97)00076-0)
- Chiodini, G., Frondini, F., Cardellini, C., Granieri, D., Marini, L., & Ventura, G. (2001). CO₂ degassing and energy release at Solfatara volcano, Campi Flegrei, Italy. *Journal of Geophysical Research: Solid Earth*, 106(B8), 16213–16221. <https://doi.org/https://doi.org/10.1029/2001JB000246>
- Chiodini, G., Frondini, F., & Raco, B. (1996). Diffuse emission of CO₂ from the Fossa crater, Vulcano Island (Italy). *Bulletin of Volcanology*, 58(1), 41–50. <https://doi.org/10.1007/S004450050124>
- Coplen, T. B. (1996). New guidelines for reporting stable hydrogen, carbon, and oxygen isotope-ratio data. *Geochimica et Cosmochimica Acta*, 60(17), 3359–3360.
- Cortés, G., & Calvache, M. (1997). Informe sobre la evaluación de la amenaza volcánica del Chiles y Cerro Negro. *IGEOMINAS*.
- Delmelle, P., & Stix, J. (2000). *Encyclopedia of volcanoes*. Academic Press: San Diego.
- Deutsch, C., & Journel, A. (1998). *GSLIB Geostatistical Software Library and user's guide*. <http://www.sidalc.net/cgi-bin/wxis.exe/?IsisScript=orton.xis&method=post&formato=2&cantidad=1&expresion=mfn=072548>
- Ebmeier, S. K., Elliott, J. R., Nocquet, J.-M., Biggs, J., Mothes, P., Jarrín, P., Yépez, M., Aguaiza, S., Lundgren, P., & Samsonov, S. V. (2016). Shallow earthquake inhibits unrest near Chiles–Cerro Negro volcanoes, Ecuador–Colombian border. *Earth and Planetary Science Letters*, 450, 283–291.
- Edwards, N. T. (1975). Effects of Temperature and Moisture on Carbon Dioxide Evolution in a Mixed Deciduous Forest Floor. *Soil Science Society of America Journal*, 39(2), 361–365. <https://doi.org/10.2136/sssaj1975.03615995003900020034x>
- Evans, W. C., Sorey, M. L., Kennedy, B. M., Stonestrom, D. A., Rogie, J. D., & Shuster, D. L. (2001). High CO₂ emissions through porous media: transport mechanisms and implications for flux measurement and fractionation. *Chemical Geology*, 177(1–2), 15–29. [https://doi.org/10.1016/S0009-2541\(00\)00379-X](https://doi.org/10.1016/S0009-2541(00)00379-X)
- Fischer, T. P., & Chiodini, G. (2015). Volcanic, magmatic and hydrothermal gases. In *The encyclopedia of volcanoes* (pp. 779–797). Elsevier.
- Fischer, T. P., Sturchio, N. C., Stix, J., Arehart, G. B., Counce, D., & Williams, S. N. (1997). The chemical and isotopic composition of fumarolic gases and spring discharges from Galeras Volcano, Colombia. *Journal of Volcanology and Geothermal Research*, 77(1–4), 229–253.
- Franck, S., Kossacki, K., & Bounama, C. (1999). Modelling the global carbon cycle for the past and future evolution of the earth system. *Chemical Geology*, 159(1–4), 305–317.
- Frondini, F., Chiodini, G., Caliro, S., ... C. C.-B. of, & 2004, undefined. (2004). Diffuse CO₂ degassing at Vesuvio, Italy. *Springer*, 66(7), 642–651. <https://doi.org/10.1007/s00445-004-0346-x>

- Gansser, A. (1973). Facts and theories on the Andes: twenty-sixth William Smith Lecture. *Journal of the Geological Society*, 129(2), 93–131.
- Giammanco, S., Melián, G., Neri, M., Hernández, P. A., Sortino, F., Barrancos, J., Lopez, M., Pecoraino, G., & Perez, N. M. (2016). Active tectonic features and structural dynamics of the summit area of Mt. Etna (Italy) revealed by soil CO₂ and soil temperature surveying. *Journal of Volcanology and Geothermal Research*, 311, 79–98.
- Goossens, P. J., Le, D., & Superieur, C. (1970). The geology of Ecuador Explanatory note for the geological map of the Republic of Ecuador (1:500.000). <https://Popups.Ullege.Be/0037-9395>, 255–263.
- Goovaerts, P. (1999). Geostatistics in soil science: state-of-the-art and perspectives. *Geoderma*, 89(1–2), 1–45. [https://doi.org/10.1016/S0016-7061\(98\)00078-0](https://doi.org/10.1016/S0016-7061(98)00078-0)
- Granieri, D., Avino, R., & Chiodini, G. (2010). Carbon dioxide diffuse emission from the soil: ten years of observations at Vesuvio and Campi Flegrei (Pozzuoli), and linkages with volcanic activity. *Bulletin of Volcanology*, 72(1), 103–118.
- Granieri, D., Chiodini, G., Marzocchi, W., & Avino, R. (2003). Continuous monitoring of CO₂ soil diffuse degassing at Phlegraean Fields (Italy): influence of environmental and volcanic parameters. *Earth and Planetary Science Letters*, 212(1–2), 167–179.
- Guillier, B., Chatelain, J.-L., Jaillard, E., Yepes, H., Poupinet, G., & Fels, J.-F. (2001). Seismological evidence on the geometry of the orogenic system in central-northern Ecuador (South America). *Wiley Online Library*, 28(19), 3749–3752. <https://doi.org/10.1029/2001GL013257>
- Hall, M. L., & Beate, B. (1991). El volcanismo plio-cuaternario en los Andes del Ecuador. *Estudios Geograficos*, 4, 5–38.
- Hoefs, J. (1980). *Stable Isotope Geochemistry*. Springer Berlin Heidelberg. <https://doi.org/10.1007/978-3-662-09998-8>
- Hoefs, J. (2004). Isotope fractionation mechanisms of selected elements. In *Stable isotope geochemistry* (pp. 31–76). Springer.
- IG-EPN. (2015). *Triptych Chiles Cerro Negro Volcanic Complex*. <https://www.igepn.edu.ec/publicaciones-para-la-comunidad/comunidad-eng/19269-triptych-chiles-cerro-negro-volcanic-complex/file>
- IG-EPN. (2020). *Reporte de los trabajos efectuados en el Complejo Volcánico Chiles - Cerro Negro (MultiGAS, Parámetros físico - químicos)*. <https://webcam.igepn.edu.ec/servicios/noticias/1781-reporte-de-los-trabajos-efectuados-en-el-complejo-volcanico-chiles-cerro-negro-multigas-parametros-fisico-quimicos>
- IG - EPN. (2014). *Informe del volcán Chiles - Cerro Negro No.23 -20 Octubre 2014*. <https://www.igepn.edu.ec/servicios/noticias/916-informe-del-volcan-chiles-cerro-negro-n-23-20-octubre-2014>
- IG - EPN, & SGC - OSVP. (2019). *Informe volcánico Chiles - Cerro Negro Negro – 2019 - N° 1 “Actualización del estado de actividad.”* <https://duckduckgo.com/?q=informe+volcanico+CHiles++Cerro+Negro&t=brave&ia=web>
- INAMHI. (1994). *Anuario Meteorológico 1994*.

- https://www.inamhi.gob.ec/docum_institucion/anuarios/meteorologicos/Am_1994.pdf
- Instituto Geofísico - EPN. (2014, June 7). *CHILES - CERRO NEGRO*. <https://igepn.edu.ec/chiles-cerro-negro>
- Isaaks, E. H., Isaaks, D. A. E. S. E. H., Srivastava, R. M., & (Firm), K. (1989). *Applied Geostatistics*. Oxford University Press. <https://books.google.com.ec/books?id=vC2dcXFLI3YC>
- Jaillard, E., Hérail, G., Monfret, T., Díaz-Martínez, E., Baby, P., Lavenu, A., & Dumont, J. F. (2000). Tectonic evolution of the Andes of Ecuador, Peru, Bolivia and northernmost Chile. *Tectonic Evolution of South America*, 31, 481–559.
- James, D. E. (1971). Plate tectonic model for the evolution of the Central Andes. *Geological Society of America Bulletin*, 82(12), 3325–3346.
- Javoy, M., Pineau, F., & Delorme, H. (1986). Carbon and nitrogen isotopes in the mantle. *Chemical Geology*, 57(1), 41–62. [https://doi.org/https://doi.org/10.1016/0009-2541\(86\)90093-8](https://doi.org/https://doi.org/10.1016/0009-2541(86)90093-8)
- Johansson, L., Zahirovic, S., & Müller, R. D. (2018). The interplay between the eruption and weathering of large igneous provinces and the deep-time carbon cycle. *Geophysical Research Letters*, 45(11), 5380–5389.
- Jong, E. de, Schappert, H. J. V., & MacDonald, K. B. (1974). Carbon dioxide evolution from virgin and cultivated soil as affected by management practices and climate. *Canadian Journal of Soil Science*, 54(3), 299–307. <https://doi.org/10.4141/cjss74-039>
- Kerrick, D. M. (2001). Present and past nonanthropogenic CO₂ degassing from the solid earth. In *Wiley Online Library* (Vol. 39, Issue 4). Blackwell Publishing Ltd. <https://doi.org/10.1029/2001RG000105>
- Lamberti, M., Llano, J., Massenzio, A., Yiries, J., Nogues, V., & Agosto, M. (2020). *Emisiones Difusas De Dióxido De Carbono Como Herramienta Para El Cálculo De La Potencia Térmica De Un Sistema Geotermal*.
- Larson, K. M., Freymueller, J. T., & Philipson, S. (1997). Global plate velocities from the Global Positioning System. *Journal of Geophysical Research: Solid Earth*, 102(B5), 9961–9981.
- Lee, J., Six, J., King, A. P., van Kessel, C., & Rolston, D. E. (2006). Tillage and field scale controls on greenhouse gas emissions. *Journal of Environmental Quality*, 35(3), 714–725. <https://doi.org/10.2134/jeq2005.0337>
- Lewicki, J. L., Fischer, T., & Williams, S. N. (2000). Chemical and isotopic compositions of fluids at Cumbal Volcano, Colombia: evidence for magmatic contribution. *Bulletin of Volcanology*, 62(4), 347–361.
- Marty, B., & Tolstikhin, I. N. (1998). CO₂ fluxes from mid-ocean ridges, arcs and plumes. *Chemical Geology*, 145(3), 233–248. [https://doi.org/https://doi.org/10.1016/S0009-2541\(97\)00145-9](https://doi.org/https://doi.org/10.1016/S0009-2541(97)00145-9)
- Mégard, F. (1987). Cordilleran Andes and Marginal Andes: a Review of Andean Geology North of the Arica Elbow (18 S). *Circum-Pacific Orogenic Belts and Evolution of the Pacific Ocean Basin*, 18, 71–95.
- NIOSH/OSHA. (1981). Occupational Health Guidelines for Chemical Hazards, DHHS (NIOSH). U.S. Government Printing Office.
- Norabuena, E., Leffler-Griffin, L., Mao, A., Dixon, T., Stein, S., Sacks, I. S., Ocola, L., & Ellis, M. (1998).

- Space geodetic observations of Nazca-South America convergence across the central Andes. *Science*, 279(5349), 358–362.
- O’Leary, M. H. (1988). Carbon Isotopes in Photosynthesis: Fractionation techniques may reveal new aspects of carbon dynamics in plants. *BioScience*, 38(5), 328–336.
<https://doi.org/10.2307/1310735>
- Oliveira, S., Viveiros, F., Silva, C., & Pacheco, J. E. (2018). Automatic filtering of soil CO₂ flux data: different statistical approaches applied to long time series. *Frontiers in Earth Science*, 208.
- Padrón, E., Hernández, P. A., Toulkeridis, T., Pérez, N. M., Marrero, R., Melián, G., Virgili, G., & Notsu, K. (2008). Diffuse CO₂ emission rate from Pululahua and the lake-filled Cuicocha calderas, Ecuador. *Journal of Volcanology and Geothermal Research*, 176(1).
<https://doi.org/10.1016/j.jvolgeores.2007.11.023>
- Parkinson, K. J. (1981). An Improved Method for Measuring Soil Respiration in the Field. *The Journal of Applied Ecology*, 18(1), 221. <https://doi.org/10.2307/2402491>
- Perdomo, G., Ardila, R., & Meneses, L. (1986). Estudio geológico para prospección de azufre en el área de Cumbal-Chiles-Mayasquer (Nariño). *Trabajo de Grado, Universidad Nacional de Colombia, Bogotá, Colombia*. 145p.
- Pineau, F., & Javoy, M. (1983). Carbon isotopes and concentrations in mid-oceanic ridge basalts. *Earth and Planetary Science Letters*, 62(2), 239–257. [https://doi.org/10.1016/0012-821X\(83\)90087-0](https://doi.org/10.1016/0012-821X(83)90087-0)
- Rahilly, K. E., & Fischer, T. P. (2021). Total diffuse CO₂ flux from Yellowstone caldera incorporating high CO₂ emissions from cold degassing sites. *Journal of Volcanology and Geothermal Research*, 419, 107383.
- Rahman, M. M. (2013). Carbon Dioxide Emission from Soil. *Agricultural Research*, 2(2), 132–139.
<https://doi.org/10.1007/s40003-013-0061-y>
- Ramsay, P. (2001). *The ecology of Volcán Chiles: high-altitude ecosystems on the Ecuador-Colombia border* (1st ed.). Pebble & Shell.
- Rastogi, M., Singh, S., & Pathak, H. (2002). Emission of carbon dioxide from soil. *Current Science*, 82(5).
<https://doi.org/http://www.jstor.org/stable/24105957>
- Rinaldi, A. P., Vandemeulebrouck, J., Todesco, M., & Viveiros, F. (2012). Effects of atmospheric conditions on surface diffuse degassing. *Journal of Geophysical Research: Solid Earth*, 117(B11).
- Rogie, J. D., Kerrick, D. M., Sorey, M. L., Chiodini, G., & Galloway, D. L. (2001). Dynamics of carbon dioxide emission at Mammoth Mountain, California. *Earth and Planetary Science Letters*, 188(3), 535–541. [https://doi.org/https://doi.org/10.1016/S0012-821X\(01\)00344-2](https://doi.org/https://doi.org/10.1016/S0012-821X(01)00344-2)
- Rosman, K. J. R., & Taylor, P. D. P. (1998). Isotopic compositions of the elements 1997 (Technical Report). *Pure and Applied Chemistry*, 70(1), 217–235.
- Rouilleau, E., Bravo, F., Pinti, D. L., Barde-Cabusson, S., Pizarro, M., Tardani, D., Muñoz, C., Sanchez, J., Sano, Y., & Takahata, N. (2017). Structural controls on fluid circulation at the Cavihue-Copahue Volcanic Complex (CCVC) geothermal area (Chile-Argentina), revealed by soil CO₂ and temperature, self-potential, and helium isotopes. *Journal of Volcanology and Geothermal Research*, 341, 104–118.

- Sano, Y., Gamo, T., & Williams, S. N. (1997). Secular variations of helium and carbon isotopes at Galeras volcano, Colombia. *Journal of Volcanology and Geothermal Research*, 77(1–4), 255–265.
- Schidlowski, M., & Aharon, P. (1992). *Carbon Cycle and Carbon Isotope Record: Geochemical Impact of Life over 3.8 Ga of Earth History BT - Early Organic Evolution: Implications for Mineral and Energy Resources* (M. Schidlowski, S. Golubic, M. M. Kimberley, D. M. McKirdy, & P. A. Trudinger (eds.); pp. 147–175). Springer Berlin Heidelberg. https://doi.org/10.1007/978-3-642-76884-2_11
- SGC. (2021). *Redes de monitoreo Volcán Cerro Negro*. <https://www2.sgc.gov.co/sgc/volcanes/VolcanCerroNegro/Paginas/redes-monitoreo-Cerro-Negro.aspx>
- Smith, B. N., & Epstein, S. (1971). Two Categories of $^{13}\text{C}/^{12}\text{C}$ Ratios for Higher Plants. *Physiology*, 47(3), 380–384.
- Smith, Rochette, P., Monreal, C., Desjardins, R., Pattey, E., & Jaques, A. (1997). The rate of carbon change in agricultural soils in Canada at the landscape level. *Canadian Journal of Soil Science*, 77, 219–229.
- Still, C. J., Berry, J. A., Ribas-Carbo, M., & Helliker, B. R. (2003). The contribution of C_3 and C_4 plants to the carbon cycle of a tallgrass prairie: an isotopic approach. *Oecologia*, 136(3), 347–359. <https://doi.org/10.1007/s00442-003-1274-8>
- Stix, J. (2015). Part VI Volcanic Interactions. In H. Sigurdsson (Ed.), *The Encyclopedia of Volcanoes (Second Edition)* (Second Edi, pp. 777–778). Academic Press. <https://doi.org/https://doi.org/10.1016/B978-0-12-385938-9.02008-3>
- Taussi, M., Nisi, B., Vaselli, O., Maza, S., Morata, D., & Renzulli, A. (2021). Soil CO_2 flux and temperature from a new geothermal area in the Cordón de Inacaliri Volcanic Complex (northern Chile). *Geothermics*, 89, 101961.
- Telenchana, E. (2017). *Estudio Geovulcanológico del volcán Chiles - Provincia del Carchi*. Escuela Politécnica Nacional.
- U.S. DOE. (2012). *Hydrothermal Resources Factsheet*. <http://pubs.usgs.gov/fs/2008/3082/>.
- Van Geldern, R., Nowak, M. E., Zimmer, M., Szzybalski, A., Myrtilinen, A., Barth, J. A. C., & Jost, H. J. (2014). Field-Based Stable Isotope Analysis of Carbon Dioxide by Mid-Infrared Laser Spectroscopy for Carbon Capture and Storage Monitoring. *Analytical Chemistry*, 86(24), 12191–12198. <https://doi.org/10.1021/AC5031732>
- Viveiros, F., Cardellini, C., Ferreira, T., Caliro, S., Chiodini, G., & Silva, C. (2010). Soil CO_2 emissions at Furnas volcano, São Miguel Island, Azores archipelago: Volcano monitoring perspectives, geomorphologic studies, and land use planning application. *Journal of Geophysical Research: Solid Earth*, 115(12). <https://doi.org/10.1029/2010JB007555>
- Viveiros, F., Chiodini, G., Cardellini, C., Caliro, S., Zanon, V., Silva, C., Rizzo, A. L., Hipólito, A., & Moreno, L. (2020). Deep CO_2 emitted at Furnas do Enxofre geothermal area (Terceira Island, Azores archipelago). An approach for determining CO_2 sources and total emissions using carbon isotopic data. *Journal of Volcanology and Geothermal Research*, 401. <https://doi.org/10.1016/j.jvolgeores.2020.106968>
- Viveiros, F., Ferreira, T., Silva, C., & Gaspar, J. L. (2009). Meteorological factors controlling soil gases and

- indoor CO₂ concentration: a permanent risk in degassing areas. *The Science of the Total Environment*, 407(4), 1362–1372. <https://doi.org/10.1016/j.scitotenv.2008.10.009>
- Viveiros, F., Ferreira, T., Silva, C., Vieira, J. C., Gaspar, J. L., Virgili, G., & Amaral, P. (2015). Permanent monitoring of soil CO₂ degassing at Furnas and Fogo volcanoes (São Miguel Island, Azores). *Geological Society, London, Memoirs*, 44(1), 271–288.
- Viveiros, F., Vandemeulebrouck, J., Rinaldi, A. P., Ferreira, T., Silva, C., & Cruz, J. V. (2014). Periodic behavior of soil CO₂ emissions in diffuse degassing areas of the Azores archipelago: Application to seismovolcanic monitoring. *Journal of Geophysical Research: Solid Earth*, 119(10), 7578–7597.
- Wagner, T., Magill, C. R., & Herrle, J. O. (2018). Carbon Isotopes. In W. M. White (Ed.), *Encyclopedia of Geochemistry: A Comprehensive Reference Source on the Chemistry of the Earth* (pp. 194–204). Springer International Publishing. https://doi.org/10.1007/978-3-319-39312-4_176
- Wefer, G., & Berger, W. H. (1991). Isotope paleontology: growth and composition of extant calcareous species. *Marine Geology*, 100(1), 207–248. [https://doi.org/https://doi.org/10.1016/0025-3227\(91\)90234-U](https://doi.org/https://doi.org/10.1016/0025-3227(91)90234-U)
- Werner, C., & Cardellini, C. (2006). Comparison of carbon dioxide emissions with fluid upflow, chemistry, and geologic structures at the Rotorua geothermal system, New Zealand. *Geothermics*, 35(3), 221–238. <https://doi.org/https://doi.org/10.1016/j.geothermics.2006.02.006>